

**FABRICATION AND CHARACTERISATION OF SUPERSTRATE COPPER  
ZINC TIN SULPHIDE ( $\text{Cu}_2\text{ZnSnS}_4$ ) THIN FILMS SOLAR CELLS**

**BY**

**MUTEEU ABAYOMI OLOPADE**

**B.Sc. (Ibadan), M.Sc. (Ibadan)**

**MATRIC No. 79343**

**A THESIS IN THE DEPARTMENT OF PHYSICS**

**SUBMITTED TO THE**

**FACULTY OF SCIENCE IN PARTIAL FULFILMENT OF THE  
REQUIREMENTS FOR THE AWARD OF THE DEGREE OF**

**DOCTOR OF PHILOSOPHY**

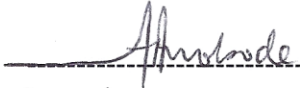
**OF THE**

**UNIVERSITY OF IBADAN, IBADAN**

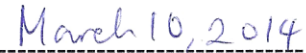
**DECEMBER, 2013**

## CERTIFICATION

This is to certify that this research work was carried out under our supervision by Mr. Muteeu Abayomi Olopade in the Department of Physics, University of Ibadan, Nigeria.



Supervisor  
**A. M. Awobode,**  
B.Sc., M.Sc. (Ibadan), Ph.D. (Cantab)  
Research Physicist, Department of Physics,  
University of Massachusetts, Boston, U.S.A.



DATE

-----  
Supervisor  
**O. E. Awe,**  
B.Sc., M.Sc., Ph.D. (Ibadan)  
Senior Lecturer, Department of Physics,  
University of Ibadan

-----  
DATE

UNIVERSITY

## ACKNOWLEDGEMENTS

All glorifications are due to Almighty Allah who out of His infinite mercies has once again assisted me in embarking on and finishing another stage of my professional pursuit in the Department of Physics, University of Ibadan.

I am deeply indebted to Dr. A. M. Awobode and Dr. O. E. Awe. They guided and motivated me throughout the period of carrying out this research. Many thanks to Dr. A. A. Oberafor and Dr. M. N. Zebaze-Kana of the Sheda Science and Technology Complex (SHESTCO), Sheda, Abuja, who made available to me the facilities at the Physics Advanced Laboratory (PAL) of the complex under the STEP-B Programme. Also, my profound gratitude goes to Dr. U. I. Kasim and Dr. A. Ahmed of the Federal University of Technology, Minna and Federal University of Technology, Yola, respectively, who taught me a lot about thin film technology, solar cells and vacuum systems. Special thanks to my teachers at the Department of Physics, University of Ibadan, for their constructive criticisms which saw me through a fulfilling research programme.

I am grateful to the many co-workers and graduate students I have had the pleasure of working with at the Sheda Science and Technology Complex, Abuja. Special thanks to Mr. N. Alu, Mr. I. Thomas, Mrs. K. Onogu, Miss. D. Olalekan and Miss. B. O. Akogwu for making my research project a truly enriching experience. I wish to acknowledge with gratitude the invaluable contribution of Dr. M. T. Lamidi of the Department of English, University of Ibadan for proof reading this thesis.

I am able to achieve my research goals because of my family and friends throughout the years. To talk about repaying them is an insult to their unconditional love, affection, and friendship. I will say I consider myself the luckiest person alive.

## **DEDICATION**

I dedicate this thesis to ALLAH (the Creator of Heaven and Earth). Also to my mum (Mrs. R. A. OLOPADE), my dad (Mr. A. A. OLOPADE), my lovely wife and children for their major role in what I have accomplished in life.

UNIVERSITY OF IBADAN LIBRARY

## TABLE OF CONTENTS

<b>Content</b>	<b>Pages</b>
CERTIFICATION .....	2
ACKNOWLEDGEMENTS.....	3
DEDICATION.....	4
TABLE OF CONTENTS.....	5
LIST OF FIGURES .....	7
LIST OF TABLES.....	9
ABSTRACT.....	10
CHAPTER ONE: INTRODUCTION.....	12
1.1. Global warming crisis and solar cells .....	12
1.2 Electric power consumption .....	14
1.3 Traditional electricity generation technologies.....	17
1.4 Renewable electricity generation technologies.....	17
1.5 Objectives of the study.....	20
CHAPTER TWO: LITERATURE REVIEW.....	21
2.1. Theoretical background .....	21
2.1.1. Solar cells.....	21
2.1.2. A P-N Junction in the dark.....	22
2.1.3 Interaction with light.....	23
2.1.4. I-V characteristics .....	25
2.1.5. Heterojunctions.....	31
2.2. Historical background of photovoltaics.....	37
2.3. Thin film photovoltaics.....	40
2.4. $\text{Cu}_2\text{ZnSnS}_4$ -family-based thin film photovoltaics.....	41
2.4.1. $\text{Cu}_2\text{ZnSnS}_4$ (CZTS) family and device issues.....	41
CHAPTER THREE: MATERIALS AND METHODS .....	46
3.1. The device structure.....	46
3.2. Materials .....	46
3.2.1. Thin film depositing equipment.....	46
3.2.2. Thin film characterising equipment.....	49

3.3. Methods.....	62
3.3.1. Preparation of substrate.....	62
3.3.2. Preparation of SnO <sub>2</sub> :F thin film (Window layer).....	62
3.3.2. Preparation of the heterojunction partner (buffer layer).....	68
3.3.3. Preparation of the absorber layer.....	69
3.3.4. Contacts deposition.....	71
CHAPTER FOUR: RESULTS AND DISCUSSION.....	75
4.1 The Window layer (SnO <sub>2</sub> :F) optimization results:.....	75
4.1.1. Effects of time of deposition on the light transmission and sheet resistance of films.....	75
4.1.2. Effects of deposition (substrate) temperature on the light transmission and sheet resistance of films.....	75
4.2. The Buffer layer (CdS) optimization results:.....	76
4.3. The Absorber layer (Cu <sub>2</sub> ZnSnS <sub>4</sub> ) optimization results:.....	84
4.4. The solar cells:.....	90
CHAPTER FIVE: CONCLUSION AND RECOMMENDATIONS.....	100
5.1 Conclusion.....	100
5.2 Recommendations.....	101
REFERENCES.....	102
APPENDIX A: PUBLICATIONS.....	108

## LIST OF FIGURES

Figure 1.1.	Schematic diagram of the work principle of solar cells	13
Figure 1.2.	Solar irradiation spectrum of AM1.5G and energy utilization spectrum by a single junction solar cell with an energy bandgap of 1.4 eV	15
Figure 1.3.	Nigeria- electricity demand projection	16
Figure 1.4.	The alarming increase in the concentration of atmospheric CO <sub>2</sub>	19
Figure 2.1.	Formation of a homojunction p-n diode	24
Figure 2.2.	Photocurrent generation in a p-n homojunction solar cell	27
Figure 2.3.	I-V characteristic of an ideal p- n junction solar cell	28
Figure 2.4.	An equivalent circuit of a solar cell	29
Figure 2.5(a)	Effect of a non-zero series resistance on the I-V characteristic	32
Figure 2.5(b)	Effect of a finite shunt resistance on the I-V characteristic	33
Figure 2.6.	Two materials, before heterojunction formation	35
Figure 2.7.	Heterojunction formation	36
Figure 2.8.	Band diagram of the CuIn(Ga)Se <sub>2</sub> /CdS/ZnO solar cell	38
Figure 2.9.	Mineral kesterite	43
Figure 3.1.	Structure of the fabricated solar cell device	47
Figure 3.2.	Precursor section of the APCVD set up at the Sheda Science and Technology Complex	50
Figure 3.3.	The entire APCVD set-up at the Physics Advanced Laboratory of the Sheda Science and Technology Complex, Abuja	51
Figure 3.4.	Spin coating process	52
Figure 3.5.	Spin-coating machine at the Physics Advanced Laboratory of the Sheda Science and Technology Complex, Abuja	53
Figure 3.6.	Thermal evaporation process	54
Figure 3.7.	Heating sources for thermal evaporation process	55
Figure 3.8.	Schematic representation of the fundamental operating principles of Scanning electron microscope	58
Figure 3.9.	A modern x-ray diffractometer	59
Figure 3.10.	Use of four point probe to measure the sheet resistivity of a solar cell	65

Figure 3.11.	Working principle of one lamp solar simulator	66
Figure 3.12.	Sulphur vaporization section of the annealing process at the Physics Advanced Laboratory of the Sheda Science and Technology Complex, Abuja	72
Figure 3.13.	Cooling section of the furnace during the annealing process at the Physics Advanced Laboratory of the Sheda Science and Technology Complex, Abuja	73
Figure 4.1(a)	Dependence of sheet resistance of FTO film on deposition time	77
Figure 4.1(b)	Dependence of Transmittance of FTO film on deposition time	78
Figure 4.2	UV-Visual light transmission of FTO films prepared at different deposition time	79
Figure 4.3	Dependence of sheet resistance and transmittance of FTO film on deposition temperature	80
Figure 4.4.	UV-Visual light transmission of FTO films prepared at different substrate temperature	81
Figure 4.5(a)	X-ray diffraction pattern of CdS film (10 cycles)	83
Figure 4.5(b)	SEM micrograph of CdS thin film (10 cycles)	85
Figure 4.6(a)	$(\alpha hv)^2$ as a function of photon energy ( $hv$ ) for films deposited at 1600 rpm	86
Figure 4.6(b)	$(\alpha hv)^2$ as a function of photon energy ( $hv$ ) for films deposited at 1800 rpm	87
Figure 4.6(c)	$(\alpha hv)^2$ as a function of photon energy ( $hv$ ) for films deposited at 2000 rpm	88
Figure 4.6(d)	$(\alpha hv)^2$ as a function of photon energy ( $hv$ ) for films deposited at 2200 rpm	89
Figure 4.7	X-ray diffraction pattern of CZTS films grown on soda lime glass	91
Figure 4.8	Surface morphology (SEM) image of the CZTS thin film	92
Figure 4.9.	EDX spectrogram of CZTS film deposited at 1200 rpm	93
Figure 4.10.	Absorption spectrum of CZTS thin film	95
Figure 4.11(a)	J-V characteristics of a typical CZTS photovoltaic cell with an active area of $2.25 \text{ cm}^2$	97
Figure 4.11(b)	J-V characteristics of a typical CZTS photovoltaic cell with an active area of $2.25 \text{ cm}^2$	98



## LIST OF TABLES

<b>Tables</b>		<b>Page</b>
Table 3.1	ASTM spectral irradiance for three standard spectra	64
Table 4.1	Chemical compositions of CZTS thin films	94

UNIVERSITY OF IBADAN LIBRARY

## ABSTRACT

Greenhouse gases emitted from burnt fossil fuels are major contributors to global warming which currently threatens existence of life. Hence, the global campaign for the replacement of fossil fuels with solar energy. The  $\text{Cu}_2\text{ZnSnS}_4$  (CZTS) thin film has emerged as a promising material for photovoltaic absorption layer in the fabrication of solar cells. Various methods of deposition have been used to fabricate superstrate CZTS thin film solar cells. However, there is limited information on the use of sol-gel method which is known to perfectly control chemical composition for the fabrication of this type of solar cells. In this study, a superstrate structured CZTS thin film solar cell was fabricated using the sol-gel method and thereafter characterised. The possibility of using paper tape during the fabrication process instead of photomask which is not always readily available was also investigated.

Superstrate structured CZTS thin film solar cells were fabricated using atmospheric pressure chemical vapour to deposit  $\text{SnO}_2:\text{F}$  thin film (as window layer). Also, spin coating method was used to deposit CdS thin film (as buffer layer) from the sol-gel of cadmium acetate, 2-methoxy ethanol, thiourea and polyethylene glycol. Sol-gel sulphurising method was used to deposit  $\text{Cu}_2\text{ZnSnS}_4$  thin film (as absorber layer) from  $\text{CuCl}_2$ ,  $\text{ZnCl}_2$ ,  $\text{SnCl}_4$  and thiourea (as sulphur source). Layers of the film were masked using paper tape, optimised and characterised following standard procedures before being used in the fabrication of (SLG)/FTO ( $\text{SnO}_2:\text{F}$ )/Ag/CdS/CZTS/Al solar cell. The deposited films were characterised using scanning electron microscope for surface morphology, Jandel universal four point probe for sheet resistance, MD-10 X-ray Diffractometer for crystallography and AvaSpec-2048 UV-VIS spectrophotometer for optical properties. The CZTS thin film solar cells of active area  $2.25\text{cm}^2$  were examined for their efficiencies using the Newport solar simulator under irradiation of  $100\text{mW}/\text{cm}^2$ . The mean of the efficiencies of CZTS solar cells from sol-gel method were compared with previous work on screen printing and doctor-blade methods.

The  $\text{SnO}_2:\text{F}$  thin film obtained had a transmittance of 80% in the UV-Visible region of the electromagnetic spectrum and a sheet resistance of  $15\ \Omega/\text{sq}$  which is within acceptable values for a window layer. The calculated energy band gap of the CdS and CZTS films from the transmittance and reflectance data were 2.40 eV and 1.51 eV respectively. This value for CZTS is closest to near-optimal direct band gap value (1.50eV) when compared with those obtained via screen printing (1.40eV) and doctor blade (1.41eV) methods. The X-ray diffraction pattern of the

CdS film exhibit hexagonal structure with (002) orientation while CZTS film had kesterite structure with (112) orientation. The absorption co-efficient of CZTS film in the visible region was  $10^4 \text{ cm}^{-1}$ . The X-ray diffraction pattern showed sharp peaks whereas broadened peaks were observed in the X-ray diffraction pattern obtained via doctor blade method. The fabricated solar cells with buffer layer thicknesses of 40 nm and 60 nm had efficiencies of  $0.28 \pm 0.01\%$  and  $0.13 \pm 0.01\%$  respectively when compared with screen printing (0.53%) and doctor-blade (0.55%).

Superstrate  $\text{Cu}_2\text{ZnSnS}_4$  solar cells have been successfully fabricated using sol-gel spin coating method and paper tape in lieu of photomask.

**Keywords:**  $\text{Cu}_2\text{ZnSnS}_4$ , Photomask, Solar cells, Superstrate thin film.

**Word Count:** 500

UNIVERSITY OF IBADAN LIBRARY

## CHAPTER ONE

### INTRODUCTION

#### 1.1. Global warming crisis and solar cells

The world's current consumption of electrical energy is about 12-13 TW and the earth receives more solar energy in 1 hour than the energy used in 1 year globally, considering the solar constant  $1.7 \times 10^5$  TW at the top of the earth's atmosphere (Nozik, 2005). However the solar energy incidence, around  $1 \text{ kW/m}^2$ , is quite dilute and requires vast area of energy converters to meet the world's energy consumption. Therefore high efficiency solar energy conversion is crucial. Solar cells, also called photovoltaics, are devices that convert the energy of the sunlight into electricity by the photovoltaic effect discovered by the French scientist Henri Becquerel in 1839. Electron-hole pairs are generated by the energy of the incident photons overcoming the energy bandgap of the photovoltaic material to make a current flow according to the built-in potential slope, typically with a p-n junction of semiconductor, in the material, as schematically depicted in Fig. 1.1. Solar cells have been recognized as an important alternative power source especially since the 1970s oil crises. Solar cells are also promising as a carbon-free energy source to suppress global warming.

The energy conversion efficiency of a solar cell is defined as the ratio of the electric power generated by the solar cell to the incident sunlight energy into the solar cell per time. Currently the highest reported cell efficiencies in laboratories are around 40% while the energy conversion efficiencies for thermal power generation can exceed 50%. This fact however never means the superiority of thermal generation since its resources such as fossil fuels are limited while the solar energy is essentially unlimited. The incident energy flux spectrum of sunlight for reported solar cell efficiencies is standardized as some specifically defined spectra such as Air Mass 0 (AM0), Air Mass 1.5 Global and Direct (AM1.5G and AM1.5D) (Emery, 2003). Figure 1.2 shows the AM1.5G spectrum, most commonly referred for terrestrial-use solar cells under non-concentrated sunlight spectrum measurements. The solar spectrum widely ranges through 300 nm to 2000 nm with its peak around 500-600 nm and a large fraction stems from the visible range. The dips prominently observed around 1100 nm, 1400 nm and so on are due to the absorption mainly by  $\text{CO}_2$  and  $\text{H}_2\text{O}$  in the atmosphere. The energy fraction of the solar spectrum utilized by an ideal single-junction solar cell with an energy bandgap of 1.4eV is determined by

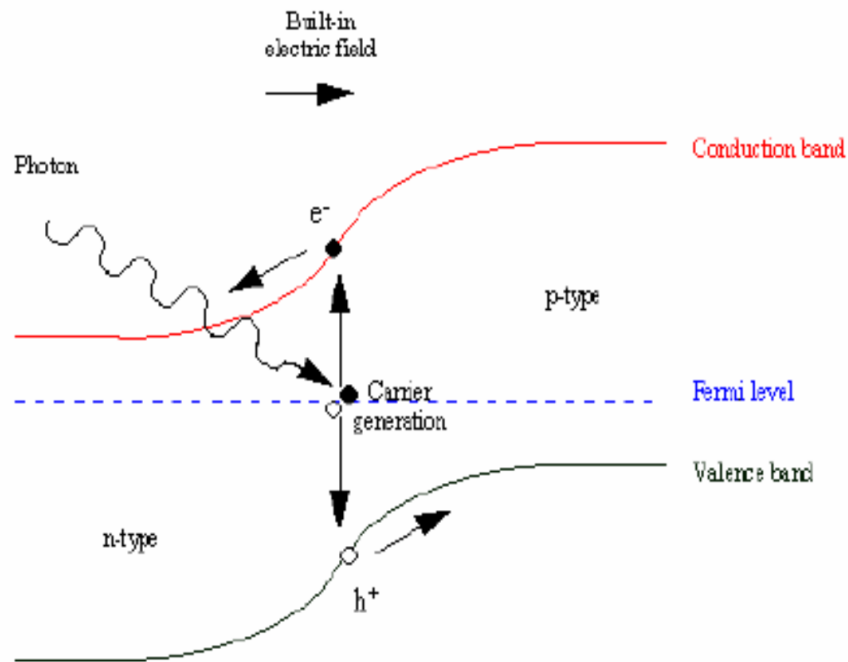


**Figure 1.1: Schematic diagram of the work principle of photovoltaic devices or solar cells (Electrical current is generated from charge carriers (electrons and holes) excited by incident light flowing directed by the potential slope built by a p-n junction in a semiconductor)**

the detailed balance calculation based on thermodynamics, considering recombination loss of carriers (electron-hole pairs) proposed by Shockley and Queisser (1961) as shown in Fig. 1.2. The area ratio of this energy generation spectrum by the solar cell to the solar irradiation spectrum corresponds to the energy conversion efficiency and is 31% in this case.

Concentration of sunlight into smaller incident area using lenses has two advantages for solar cell applications. The first is the material cost reduction with smaller area of cells required to generate the same amount of energy. The second is the efficiency enhancement with the higher open-circuit voltage determined by the ratio of the photocurrent to the recombination current. However, too much sunlight concentration would rather reduce the open-circuit voltage with increased temperature and also induce significant power loss by the series resistance. There is therefore an optimized concentration factor for each solar cell.

## **1.2 Electric power consumption**

Electric power has now become the fundamental platform that supports most of our physical needs. Indeed, it was only a couple of centuries ago that there was no electricity. Today, it is so difficult to imagine ourselves without it. No wonder the Nigeria power crisis has scared many a folk, and is making the headlines of media reports every day. Even scarier is the fact that there is a possibility that the whole power situation is going to be worse than it is now.

Several factors contribute to the immense increase in electricity usage in the world in recent times. The first is the world's population growth which will result into increase in power consumption. The second factor is the growing industrialization of the developing and underdeveloped countries. The third factor is the gradual spread of the so-called modern style of living, where extended families are often broken into nuclear ones. In this case, houses and workplaces are not shared anymore, and total power usage is consequently increased. The United States is a country with an increasing demand for electricity. In the US alone, electricity sales increased by about 80% from 1975 to 1997 (Mcveigh *et al.*, 2000). The electricity demand in Nigeria has been on the increase (Sambo, 2008). Sambo explains that the demand projections will rise from 5,746MW in the base year of 2005 to 297,900MW in the year 2030, which translates to the injection of 11,686MW every year to meet the demand as shown in Fig. 1.3.

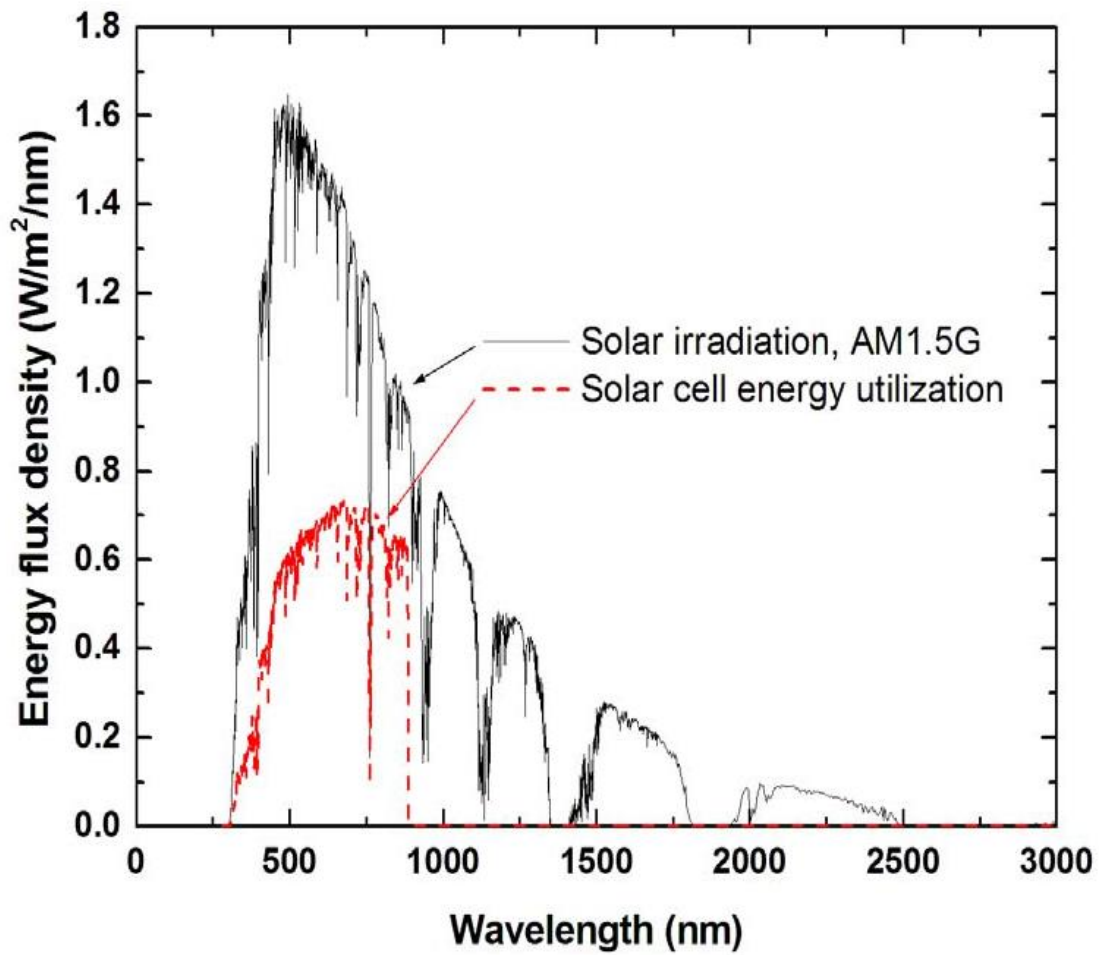
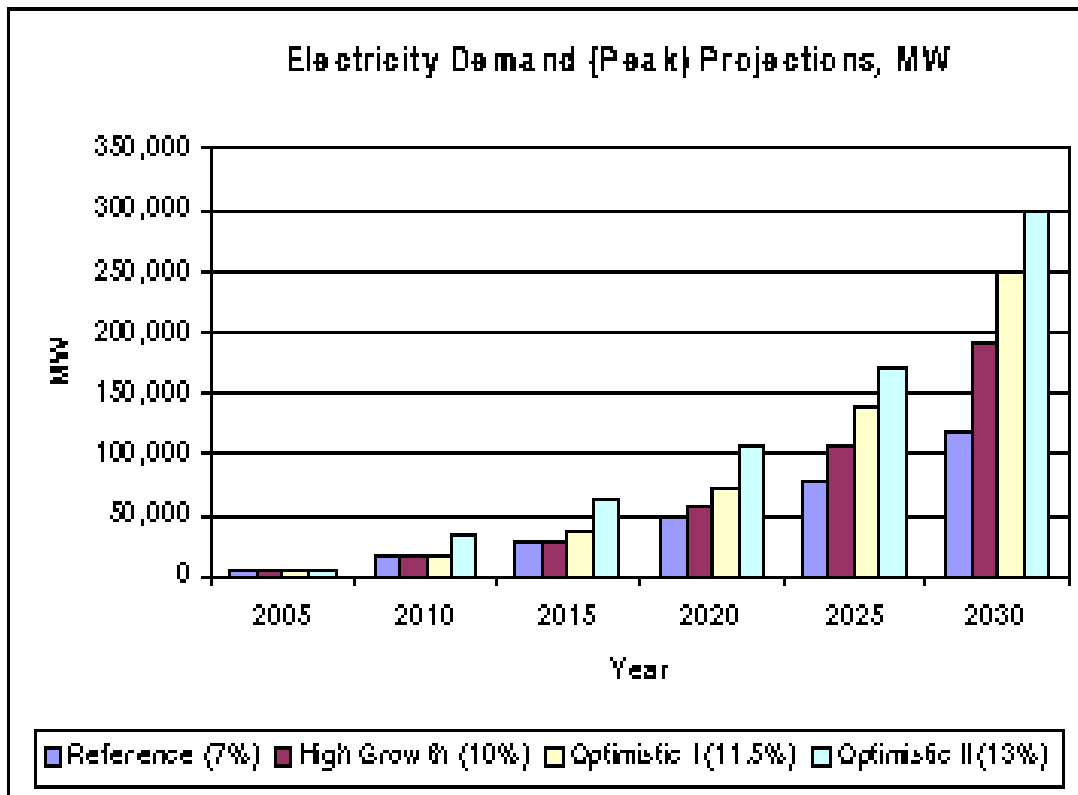


Fig. 1.2 Solar irradiation spectrum of AM1.5G and energy utilization spectrum by a single junction solar cell with an energy bandgap of 1.4 eV



**Fig. 1.3 Nigeria- electricity demand projection**

(Source: Bulletin on National Workshop on the Participation of State Governments in the Power Sector)



Several technologies have been and are being used to generate this power. These can vaguely be divided into two types: traditional and non-traditional (renewable) technologies. These are reviewed below.

### **1.3 Traditional electricity generation technologies**

Traditionally, much of the electricity has been generated using the following three technologies:

- (i) Power from Fossil Fuels: These fuels include oil, coal and natural gas,
- (ii) Nuclear Power, and
- (iii) Hydro-electric Power.

The first one, fossil fuels technology, can be categorized as a non-renewable technology, meaning that the sources used for this technology cannot be recycled. The other two can be classified as renewable. Currently 70% of power is, in fact, generated using fossil fuel (Sweet, 2001). This is not at all surprising, for fossil fuels are abundant at present, and so the resulting power is at a low cost to the consumers. However, there are few important aspects of this technology that show up as distinct disadvantages when one considers the future of electricity generation.

There are serious environmental concerns associated with the use of fossil fuels as the source of electric power. These fuels—coal, oil and natural gas—were created chiefly by the decay of plants that flourished millions of years ago. Burning these fuels unlock the carbon stored by these plants and release it to the air as carbon IV oxide. For instance, burning one gallon of gasoline generates 22 pounds of carbon IV oxide. For every pound of coal burnt, nearly three pounds of carbon IV oxide would go into the atmosphere. Since 1750, carbon IV oxide in the air has risen by more than 30%. This atmospheric CO<sub>2</sub> rises over the years is depicted in Fig. 1.4. A solution to this problem is to start using renewable energy sources to generate electricity.

### **1.4 Renewable electricity generation technologies**

Two traditional renewable energy sources which minimizes the emission of green house gases are the nuclear power and the hydro-electric power.

The nuclear power alternative, although being used quite extensively, has drawn serious concerns regarding safety. Accidents such as Chernobyl are still fresh on our minds. Moreover, the radioactive waste that is created in a nuclear plant has to go through an expensive and

elaborate disposal. Such disposal practices have been proven to be quite controversial, and the public is becoming more and more aware of the uncertainties involved (Nathan, 2001).

Hydroelectric power has also been developed extensively, taking up a major share of the electricity generation in developing countries. However, this, too, comes at the expense of the environment, essentially destroying the river ecosystems that the hydroelectric plants are built on. Therefore, a significant expansion of this resource faces severe opposition from environmentalists (Kelsi *et al.*, 2013).

Sequel to these reasons, nuclear and hydroelectric power cannot be considered environment-friendly. This, then, leaves us with the five renewable technologies that can be considered environmentally clean. These are:

- (i) Wind: Wind spins blades, which turn a generator to produce power.
- (ii) Solar Photovoltaics: Sunlight is converted directly to electricity using appropriate semiconductor materials.
- (iii) Solar Thermal: Sunlight is reflected with mirrors to boil water which runs a turbine.
- (iv) Geothermal: This makes use of natural heat (steam) present inside the earth to run turbines.
- (v) Biomass: This is burning/extracting fuels from organic matter (plants or animal manure) for power generation.

One promising way to make solar electricity affordable for the layman is to employ the various thin film technologies which uses materials such as Copper Indium Diselenide ( $\text{CuInSe}_2$ ), Copper Indium Disulphide ( $\text{CuInS}_2$ ), Cadmium Telluride ( $\text{CdTe}$ ), Copper Gallium Diselenide ( $\text{CuGaSe}_2$ ), and Copper Zinc Tin Sulphide ( $\text{Cu}_2\text{ZnSnS}_4$ ). The material  $\text{Cu}_2\text{ZnSnS}_4$  has the potential to be used as solar cell material, and also, to be used as a material for multi-structured tandem solar cell systems.  $\text{Cu}_2\text{ZnSnS}_4$  (CZTS) is a semiconductor with a direct band gap of about 1.5 eV, an absorption coefficient of  $10^4 \text{ cm}^{-1}$ , and its constituents have high relative abundance in the earth crust. The afore-mentioned reasons give it a potential for thin film solar cell material.

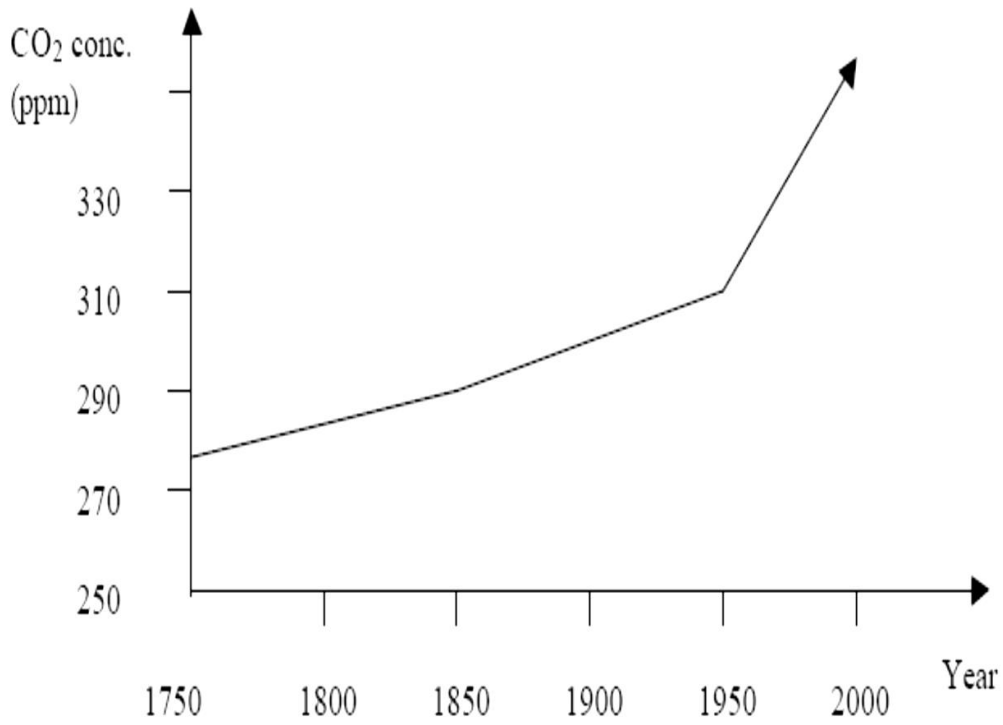


**Fig. 1.4 The alarming increase in the concentration of atmospheric CO<sub>2</sub>**  
(source: [www.enviroweb.org](http://www.enviroweb.org))

The aim of this study was to grow and characterise CZTS films and evaluate their performance in complete solar cells. For the growth of CZTS thin film, we employed the sol-gel method and subsequent sulphurization by heating at 500°C in sulphur atmosphere, using a three zone furnace. The sol-gel method was selected because it allows synthesis of pure materials from the liquid phase.

This thesis has been divided into five chapters. Following this introductory chapter is the literature review, where details of the theoretical background and review on solar cells as well as thin film  $\text{Cu}_2\text{ZnSnS}_4$  solar cells are discussed. Chapter Three provides a comprehensive discussion on the growing of thin films of FTO, CdS, and CZTS and the fabrication of CZTS solar cells. Also, the characterisation technique involved in determining the properties of these thin films and solar cells were discussed. In Chapter Four, the results of the characterisation of our films and solar cells were discussed. Finally, chapter Five provides a summary of this dissertation and sets the course for possible future research.

### **1.5 Objectives of the study**

The objectives of the study are:

1. To fabricate superstrate  $\text{Cu}_2\text{ZnSnS}_4$  thin film solar cells using simple methods of deposition (sol-gel spin coating method).
2. To explore the possibility of using paper tape in masking the different layers of the cell in lieu of photomask.
3. To characterise the fabricated solar cells for their performance characteristics such as fill factor, open circuit voltage, short circuit current and efficiency.

## CHAPTER TWO

### LITERATURE REVIEW

#### 2.1. Theoretical background

The conversion of sunlight directly into electricity using the electronic properties of suitable materials appears to be an elegant energy conversion process and an ideal alternative to conventional energy sources. Sequel to the simplicity of this process, and the abundance of the source that it uses, it appears to be one of the most promising ways of meeting the increasing energy demands of our planet.

##### 2.1.1. Solar cells

One of the most promising techniques is solar cells, which combine several advantages. They can be used more or less in any dimension, from the small one in a calculator up to solar power plants in the GW range. This also makes solar cells an autonomous source of energy. It is possible to cover the energy demand of small villages or street lamps at bus stops, which is especially interesting if it is not possible or too expensive to connect them to the grid. Moreover, it is a technology that is quiet, has no emissions and has no moving parts, which makes it a technology with a quite long lifetime. Producers give guaranties of 20–25 years, but in principle much longer lifetimes are possible (Neuberger, 2009).

The semiconductors used in the fabrication of a solar cell are chosen in such a way that, when light is shone on the device, one of them will absorb a significant portion of the light. Absorption of the light creates mobile carriers, both negative (electrons) as well as positive (holes) in the material. Thereafter, the generated carriers recombine in a semiconductor. However, a good solar cell is designed in such a way that most of these generated carriers, after they are swept across the junction, are collected by the metallic contacts. Such carriers are then made to flow in an external circuit, and their energy can be utilized. The phenomenon of solar energy conversion thus involves the processes of absorption of radiation, generation of carriers, transportation of these carriers to the junction, separation of the carriers at the junction, collection of the separated carriers, and finally the utilization of the power generated.

A brief survey of the basic properties of p-n junctions, and the electronic processes involved when light interacts with a solar cell is discussed in subsequent sections of this chapter.

### 2.1.2. A P-N Junction in the dark

An n-type semiconductor material has a large concentration of electrons, and a few holes, whereas a p-type semiconductor has a lot of holes, and few electrons. When two such materials are appropriately joined together, diffusion of carriers takes place because of the large concentration gradients at the junction. Each electron leaving the n-side leaves behind an uncompensated positively charged donor ion, and every hole going across the junction leaves a negatively charged acceptor ion. These ionized donors and acceptors, present in the region depleted of carriers (called the depletion region), build up an electric field. This field is set up such that it creates a drift component of current that opposes the diffusion of carriers. At thermodynamic equilibrium, when there is no net flow of charge across the junction, an equilibrium contact potential, also called a built-in potential,  $V_0$  is thus set up across the depletion region. This potential difference produces a bending of the energy bands of the semiconductors. Such a band bending is shown in Fig. 2.1, for the case of a homojunction p-n diode (made by using p- and n-doped parts of a single semiconductor).

When an external voltage is applied to the p-n junction diode, one of two things can happen. If the bias is forward, that is a positive voltage  $V_f$  is applied to the p-side, the height of the potential barrier is reduced from  $V_0$  to  $V_0 - V_f$ , thereby reducing the band-bending. This increases the diffusion current of majority carrier electrons from the n-side surmounting the barrier to diffuse to the p-side, and holes surmounting the barrier from p to n. A large current, directed from the p- to the n-side, hence, flows in the forward bias. On the other hand, if a reverse bias is applied to the junction (p-side negative with respect to the n-side), the band-bending increases, and this decreases the diffusion current from p to n to negligible values. The other current component that flows in a p-n junction is the so-called generation current, which is directed from n to p (opposite to the diffusion current).

This is the drift component, composed of minority carriers from both sides of the junction, and is relatively insensitive to the height of the potential barrier. These minority carriers are generated by thermal excitation of electron-hole pairs (EHP's), at or near the junction, and are swept to the other side of the junction because of the electric field. In reverse bias, this is the only current present (because the diffusion current is negligible), and hence this current component is sometimes referred to as the reverse saturation current,  $I_0$ , with the corresponding current density denoted by  $J_0$ . Note that the letters I and J, refer to the currents and the

corresponding current densities, respectively. The total current density in a p-n junction in the dark can be written as in equation (2.1) (Sze, 1981):

$$J = J_0 \left[ \exp\left(\frac{qV}{kT}\right) - 1 \right] \quad (2.1)$$

Where the  $J$  and  $J_0$  designate the total and the reverse current densities, respectively,  $V$  is the applied voltage,  $k$  is the Boltzmann constant,  $q$  is the electronic charge, and  $T$  is the absolute temperature. As can be easily seen, at equilibrium ( $V = 0$ ), the net current is zero. The above equation defines the I-V characteristic of the junction diode, which is shown graphically in the next section.

### 2.1.3 Interaction with light

#### 2.1.3.1. Photocurrent

When light is shone on the junction, the photons that have energies greater than the band gap of the semiconductor have a high probability of being absorbed. The absorption of light can be described by relating the radiation intensity  $I_0$  falling on a semiconductor surface to the intensity  $I$  that remains after the light has penetrated a distance  $x$  (Pillai, 2010):

$$I(\lambda) = I_0 \exp[-\alpha(\lambda)x] \quad (2.2)$$

The parameter  $\alpha$ , which is a function of the wavelength of the light, is a characteristic of the material, and is known as the absorption coefficient. The value of the absorption coefficient must be high for the absorber material used in a solar cell device, so that most of the light is absorbed in a useful way.

Each photon that is absorbed in the absorber material generates an EHP. Such minority carriers, if generated within a certain distance of the junction (called a diffusion length), can diffuse to the junction, be swept to the other side, and be collected by appropriate contacts.

When a monochromatic light of wavelength  $\lambda$  is incident on the surface of a solar cell, the photocurrent and spectral response, that is, the number of carriers collected per incident photon at each wavelength, can be derived as follows:

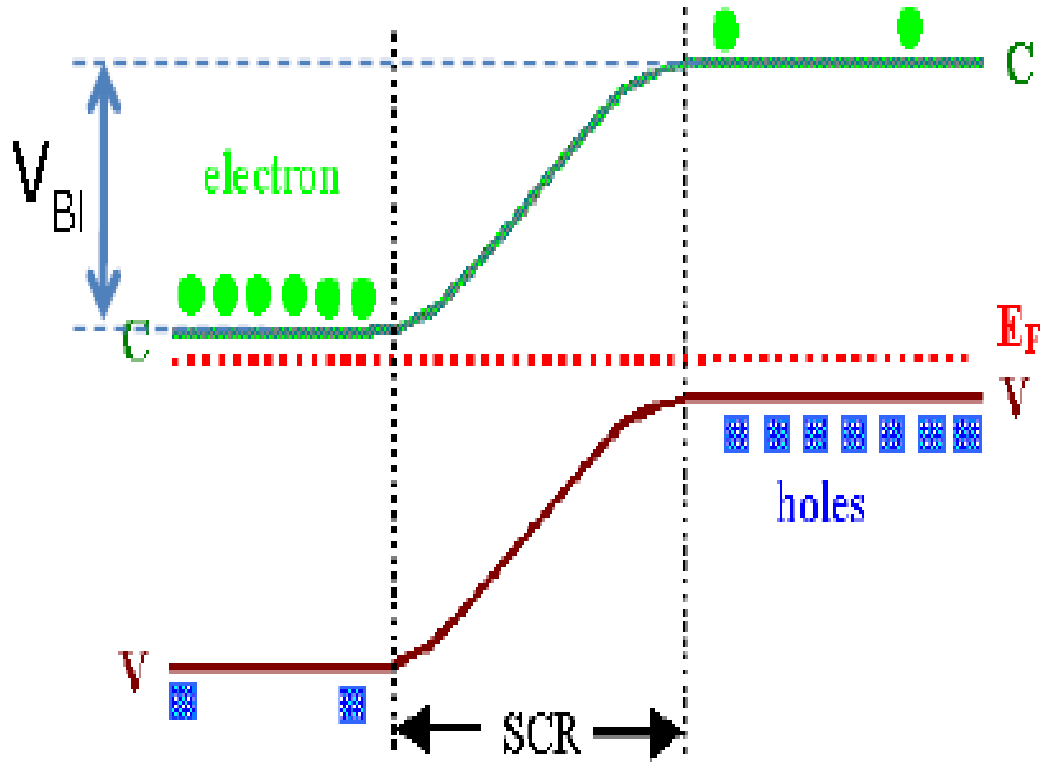


Figure 2.1. Formation of a homojunction p-n diode

UNIVERSITY



The generation rate of electron- hole pairs at a distance  $x$  from the semiconductor surface is given by:

$$G(\lambda, x) = \alpha(\lambda)F(\lambda)[1 - R(\lambda)]exp[-\alpha(\lambda)x] \quad (2.3)$$

Where  $F(\lambda)$  is the number of incident photons per  $cm^2$  per unit bandwidth, and  $R(\lambda)$  the fraction of these photons reflected from the surface. Using the appropriate boundary conditions, and assuming low- injection conditions, the internal spectral response (SR) is given by:

$$SR(\lambda) = \frac{1}{qF(\lambda)[1-R(\lambda)]} [J_p(\lambda) + J_n(\lambda) + J_{dr}(\lambda)] \quad (2.4)$$

Where  $J_p(\lambda), J_n(\lambda),$  and  $J_{dr}(\lambda)$  are the photocurrent contributions from the p-region, the n-region, and the depletion region, respectively (Sze, 1981).

Once the SR is known, the total photocurrent density obtained from the solar spectrum distribution  $F(\lambda)$  is given by

$$J_L = q \int_0^{\lambda_m} F(\lambda) [1 - R(\lambda)]SR(\lambda)d\lambda \quad (2.5)$$

The generation of EHPs because of light gives rise to an added generation rate  $g_{op}$ , given in EHP/ $cm^3.s$ , which produces a current from the n- to the p-side (opposite to the dark forward diffusion current). If  $L_p$  and  $L_N$  are the diffusion lengths for the minority carrier holes and electrons, respectively, then the resulting optically generated current for a junction of area,  $A$   $cm^2$  and depletion region width  $w$  can be written as (Neaman, 2003):

$$J_L = qAg_{op}(L_p + L_N + w) \quad (2.6)$$

Figure 2.2 depicts the current generation in the p-n junction under illumination.

#### 2.1.4. I-V characteristics

The resulting I-V characteristic of the diode, in dark as well as in light, is shown in figure 2.3. Depending on the intended application, the diode can be operated either in the third or the

fourth quadrants of the I-V characteristic. Power is delivered to the device from the external circuit when the current and junction voltage are both positive and both negative. If operated in the fourth quadrant, however, power is delivered from the junction to the external circuit, and this is the principle of operation of a solar cell device. Figure 2.4 shows an equivalent circuit of a solar cell. The generation of the photocurrent  $I_L$  is represented by a current generator, in parallel with a diode that represents the p-n junction. There are two resistances shown in the figure 2.4., where  $R_s$  is the series resistance, which should ideally be zero, but always exists, in a practical solar cell. It comprises the bulk resistance of the absorber semiconductor, as well as any other resistance in the device such as those coming from the contact materials used. The parallel (or shunt) resistance  $R_p$  represents any parallel paths for the junction current to flow (an example is metal particulates shunting the junction). Ideally, such parallel paths should not exist, making  $R_p$  infinite. For simplicity, let us assume that the current generated by light can be added to the current flowing in the dark (superposition), and also that  $R_s = 0$ , and  $R_p = \infty$  (ideal case). Then, the current density  $J$  flowing in the device in the presence of light can be expressed as:

$$J = J_0 \left[ \exp\left(\frac{qV}{AkT}\right) - 1 \right] - J_L \quad (2.7)$$

Here, the first term on the right is the forward current driven by the voltage  $V$ , and the second term is the (reverse) light generated counterpart.  $J_0$  is often referred to as the reverse saturation current.

Terms that are commonly used as measures of solar cell performance are the short circuit current ( $J_{sc}$ ) and open circuit voltage ( $V_{oc}$ ). The short-circuit current density  $J_{sc}$  is simply the light generated current  $J_L$ . The open-circuit voltage can be obtained by setting  $J = 0$ .

$$J_{sc} = J_L \quad (2.8)$$

$$V_{oc} = \frac{kT}{q} \ln\left(\frac{J_L}{J_0}\right) + 1 \quad (2.9)$$

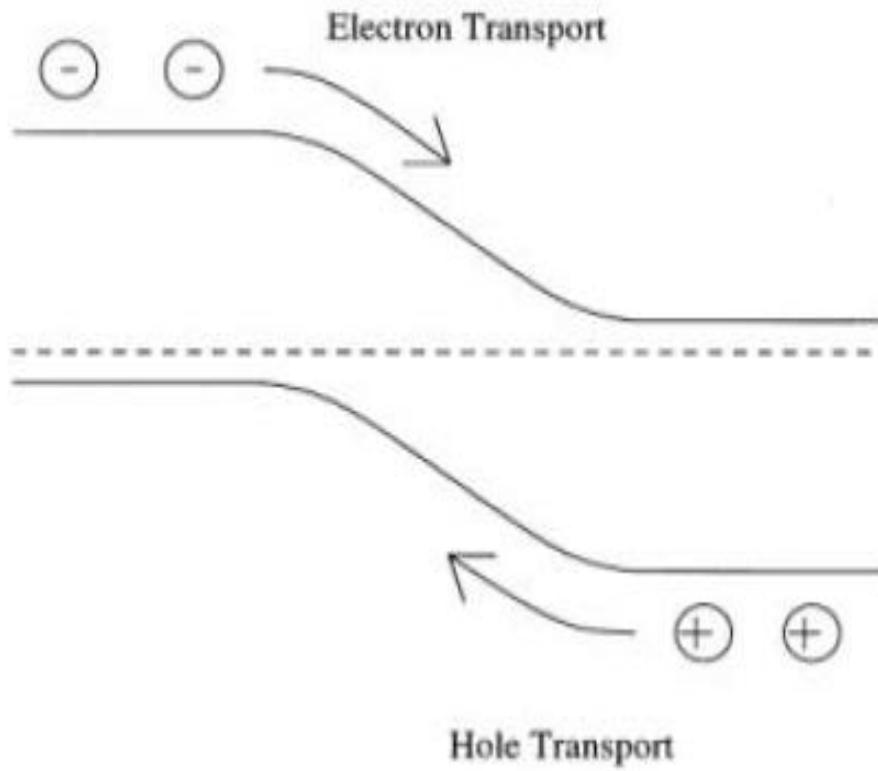
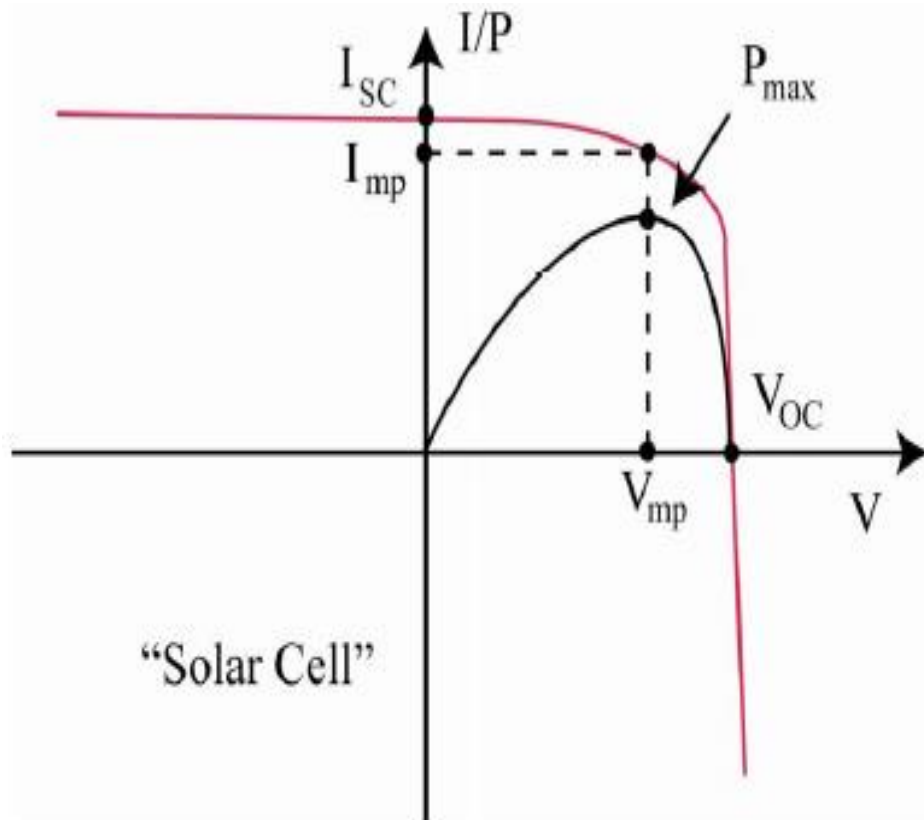


Figure 2.2. Photocurrent generation in a p-n homojunction solar cell

UNIVERSI



**Figure 2.3. I-V characteristic of an ideal p-n junction solar cell**

(Source : Solar Electric Systems University of Delaware, ECE Spring 2009, page 5)

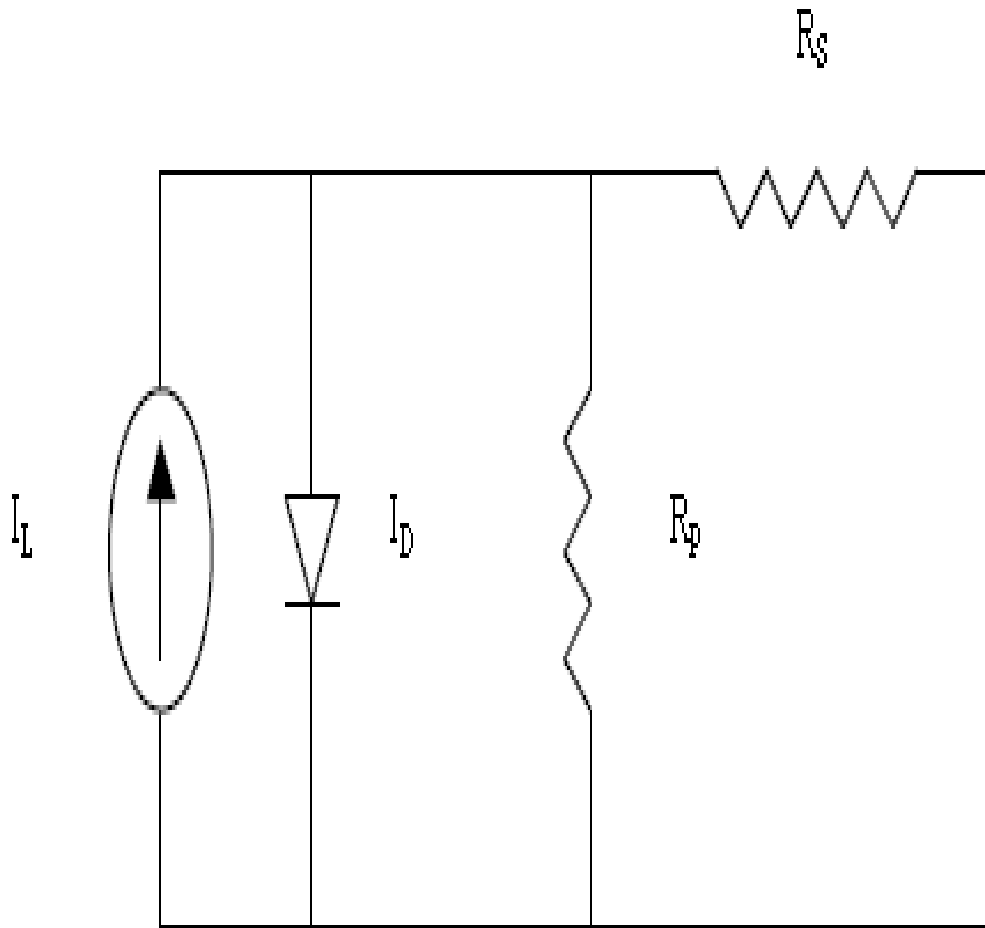


**Figure 2.4. An equivalent circuit of a solar cell**

It can be easily seen that, while the  $J_{sc}$  depends only on the light-assisted generation, the  $V_{oc}$  depends on the current generation-recombination processes as well as on the nature of the junction transport ( $A$  and  $J_0$ ). Both  $I_{sc}$  and  $V_{oc}$  are shown in Fig. 2.3 above.

No power can be generated under short or open circuit. The maximum power  $P_{MAX}$  produced by a device is reached at a point on the characteristic where the product  $IV$  is maximum, that is, when the area covered by the power rectangle shown in Figure 2.3 is maximum. The Fill Factor ( $ff$ ) is defined as:

$$Fill\ Factor(ff) = \frac{I_{MAX}V_{MAX}}{I_{SC}V_{OC}} \quad (2.10)$$

The  $ff$ , therefore, is a measure of the *squareness* of the characteristic. The efficiency  $\eta$  of a solar cell is defined as:

$$\eta = \frac{P_{MAX}}{P_{RAD}} \quad (2.11)$$

Eq. 2.11 in terms of  $V_{oc}$ ,  $J_{sc}$  and  $ff$ , becomes:

$$\eta = \frac{J_{sc}V_{oc}ff}{P_{RAD}} \quad (2.12)$$

Where  $P_{RAD}$  is the power of the radiation incident upon the cell. The standard conditions used to calculate the solar cell efficiency are: an irradiance of  $100\text{mW}/\text{cm}^2$ , standard reference AM1.5 spectrum, and a temperature of  $25^\circ\text{C}$ .

When we consider a practical solar cell, the above equation for the current transport has to be modified. Real cells usually have a non-zero series resistance  $R_s$ , and a finite shunt resistance  $R_p$ . The equation for the current  $I$  ( $= J * \text{Area}$ ) then becomes:

$$I = I_0\{exp[q(V - IR_s)/AkT] - 1\} + (V - IR_s)/R_p \quad (2.13)$$

The factor  $A$ , in the denominator of the exponential, is the so-called *ideality factor*, which relates to the mechanism of the junction transport in a practical device. The value of  $A$  usually varies between 1 and 2. A value of 1 usually means that the junction transport is by diffusion, whereas a value of 2 signifies that the transport is controlled by recombination in the depletion region.

If the values of  $R_s$  and  $1/R_p$  are significant, then the I-V characteristic of the device gets affected, as shown in Figures 2.5(a) & (b).  $V_{oc}$  is unchanged by a reasonably low  $R_s$ , whereas  $I_{sc}$  decreases slightly. On the other hand, a finite  $R_p$  usually decreases  $V_{oc}$ , while  $I_{sc}$  is unaffected.

The most common types of junction that are used to form solar cells are:

- (i) Homojunction: p-n junction within the same semiconductor material.
- (ii) Heteroface structure: similar to a homojunction, but with an added window layer made of a larger band-gap semiconductor.
- (iii) Heterojunction: p- n junction between two different semiconductor materials.
- (iv) Schottky barrier: metal-semiconductor junction.

### 2.1.5. Heterojunctions

When semiconductors of different bandgaps and electron affinities are brought together to form a junction, as in a heterojunction, discontinuities are produced in the energy bands, as the Fermi level of the different materials line up at equilibrium. The discontinuities in the valence ( $\Delta E_v$ ) and the conduction bands ( $\Delta E_c$ ) accommodate the difference in the bandgaps. Figure 2.6 (on the next page) shows an example of such a heterojunction system, and the important parameters, before the two semiconductors are joined together. The band bending that occurs after the two are joined together is depicted in Figure 2.7. It can be seen, from the resulting band-bending that a spike has appeared in the conduction band, where the two materials meet. Such a spike is the result of properties specific to the materials used, such as the electron affinities  $\chi$ 's. A discontinuity such as this limits the electron current that flows from the p-side to the n-side when the solar cell is placed in light, and hence should be avoided by proper selection of the semiconductor materials, and by appropriate processing

It should be noted that, in heterojunctions, the light can either be incident on the larger band- gap material (back wall-type) or on a thin layer of the smaller band-gap material (front wall type). Similarly, in Schottky barriers, it is possible to have the light incident on either of the semitransparent metal forming the barrier (front wall), or through the

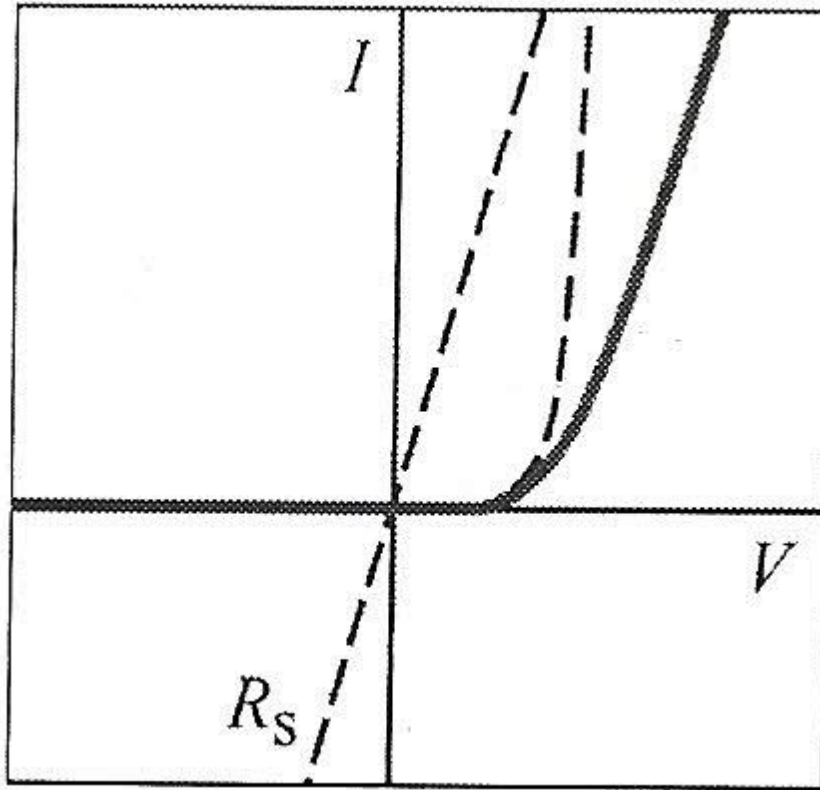


Figure 2.5(a) Effect of a non-zero series resistance on the I-V characteristic



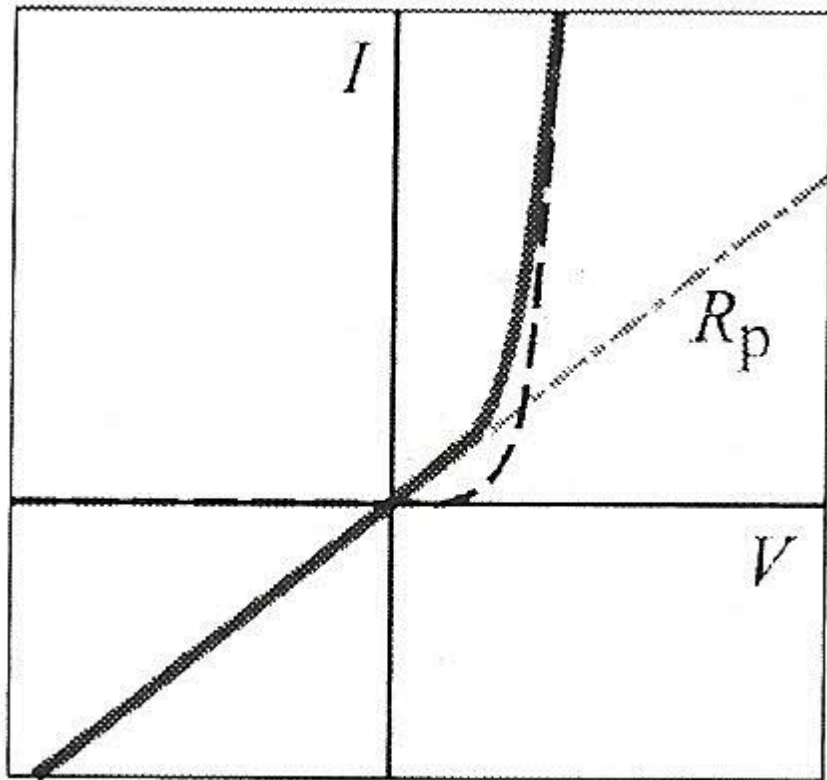


Figure 2.5(b) Effect of a finite shunt resistance on the I-V characteristic

semiconductor (back wall) (Bube, 1974).

The solar cells examined in this research work are the front wall type heterojunction solar cells. A heterojunction can either be isotype (where both the semiconductors have the same type of conductivity) or anisotype (where the conductivities are different). Again, the  $\text{Cu}_2\text{ZnSnS}_4/\text{CdS}$  junction used in this research belongs to the latter type, viz. anisotype.

The principal advantage of using a direct bandgap heterojunction system for a solar cell, such as the one used in this research can be seen as follows. Consider the case of an indirect bandgap homojunction solar cell, an example of which is a Silicon solar cell. Here, because of the low absorption coefficient associated with the indirect bandgap, a large thickness of the material is needed to absorb enough light. If we consider replacing this system by a direct bandgap homojunction system, another problem arises. Because the light needs to be absorbed as close to the junction as possible (so that the generated carriers are easily collected by the junction), the top layer (say, n-layer) needs to be fairly thin, with a thicker p- layer underneath it. In such a structure, the carriers generated in the n- layer have a high probability of diffusing away from the junction, towards the front contact, and eventually getting lost because of the high surface recombination velocity at the contact surface. Now, if the system is a direct bandgap heterojunction, then it can be designed in such a way that the top n- layer is made of a wider bandgap material which will absorb little light in the spectrum of interest. Most of the light hence will reach the junction and the underlying p-type absorber, thereby significantly reducing the likelihood of surface recombination at the front contact.

The p-CuIn(Ga)Se<sub>2</sub>/n-CdS solar cell structure has been optimized in this way, and the resulting band diagram is shown (Figure 2.8), along with the n-type ZnO which acts as the front contact. The CuGaSe<sub>2</sub>/CdS and CuInS<sub>2</sub>/CdS cells have similar structures, except that the conduction band of the absorber is raised further above.

For heterojunction solar cell structures, an added complication is the increased defect states at the interface. These mainly arise because of the lattice mismatch between the two semiconductors. However, processing conditions may also have a strong effect. Therefore, unlike in homojunctions, the carrier transport properties in heterojunctions are usually dominated by phenomena in the interface region. The current transport in the depletion layer has been attributed to either the recombination, or the tunnelling, or a combination of both.

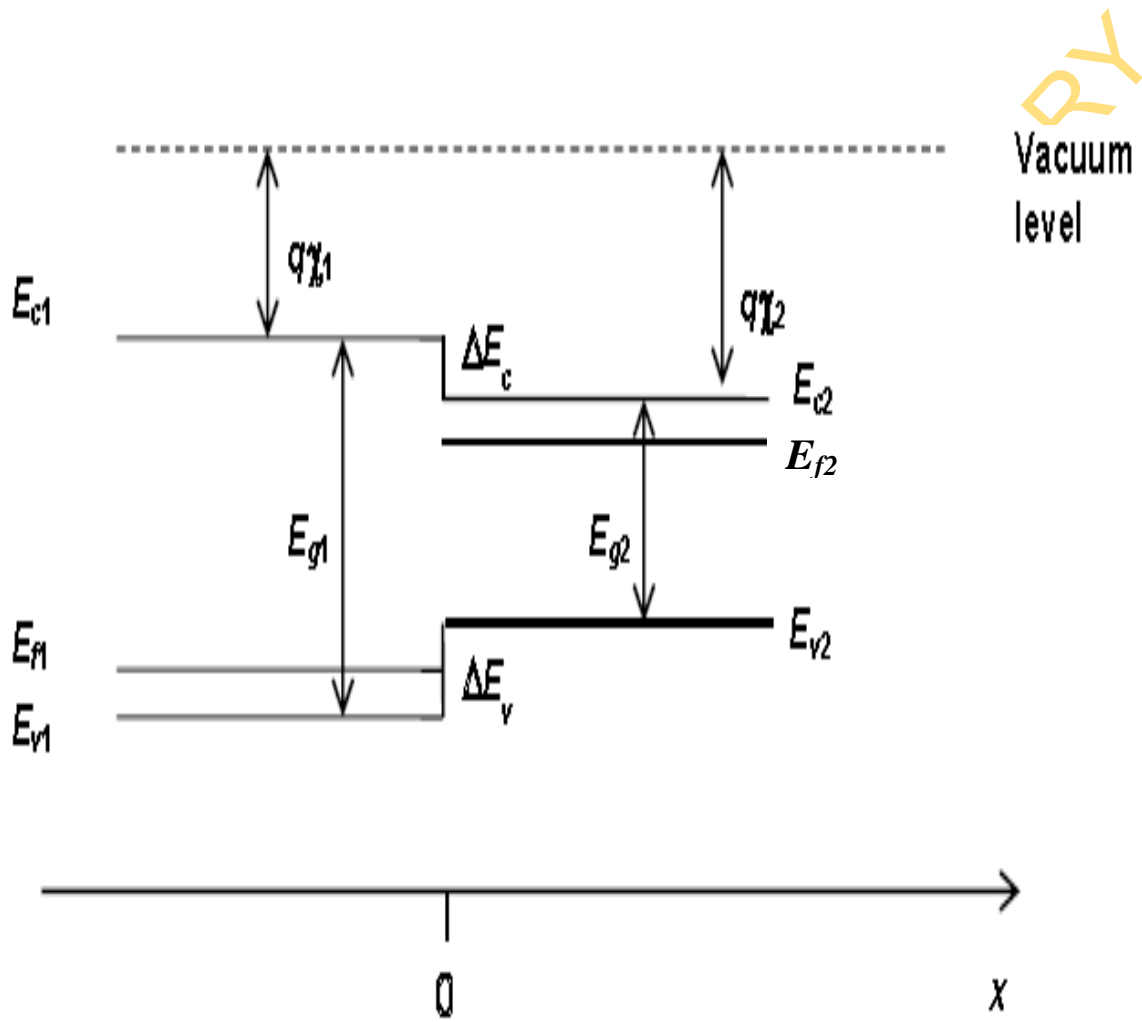


Figure 2.6. Band structure of two materials before heterojunction formation

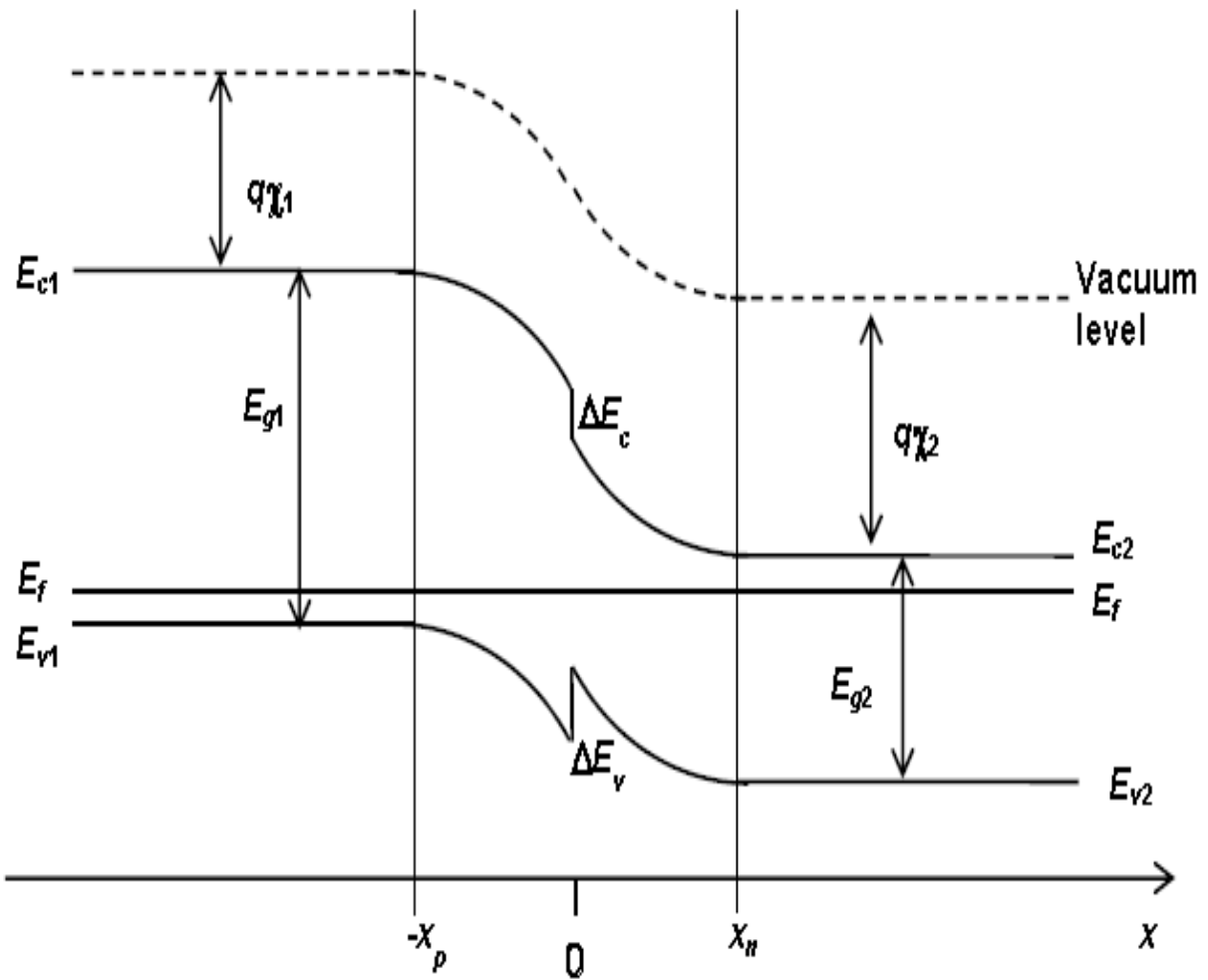


Figure 2.7. Heterojunction formation

- (i) The charge stored in these states distorts the band profile, and
- (ii) The states give rise to a high density of recombination centres, thereby producing high forward current ( $J_0$ ) values.

In some cases, the extremely high density of charged states at specific energy levels at the interface is sufficient to pin the surface (or interface) Fermi level at that energy.

## 2.2. Historical background of photovoltaics

Becquerel reported the photovoltaic effect in 1839, when he found that a light dependent voltage developed between electrodes immersed in an electrolyte (Becquerel, 1839). In 1876, this effect was observed in an all-solid-state Selenium system. Subsequent work on the PV effects in selenium and cuprous oxide led to the development of the selenium PV cell that was widely used in photographic exposure meters (Adams & Day, 1876). The modern era of PV began in 1954 at the Bell laboratories, where silicon single crystal solar cell was successfully developed. This device represented a major development because it was the first photovoltaic structure that converted light to electricity with a reasonable efficiency of 6% (Chapin *et al.*, 1954).

Until the 1960's, the main interest in the development of solar cells was their application as power sources in spacecraft. The early 1970s saw a growing interest in the development of PV technologies for terrestrial use. More recently, the focus has shifted from single-crystal technology to the low-cost alternative of thin film technology. Before going into the specifics of PV technologies, it will be worthwhile to outline the general requirements for such a technology. The most important of these are as listed below:

- (i) Conversion efficiency should be high for laboratory cells as well as for modules (as the cost decreases, this requirement becomes less important. However, to keep the area-related costs down, module level efficiencies of at least 10% are necessary).
- (ii) Constituent materials (semiconductors, metals) should be readily available, and should be inexpensive.
- (iii) A simple but reproducible deposition method that is suitable for large area production should be available.
- (iv) The cells/modules should be stable over long periods of time.

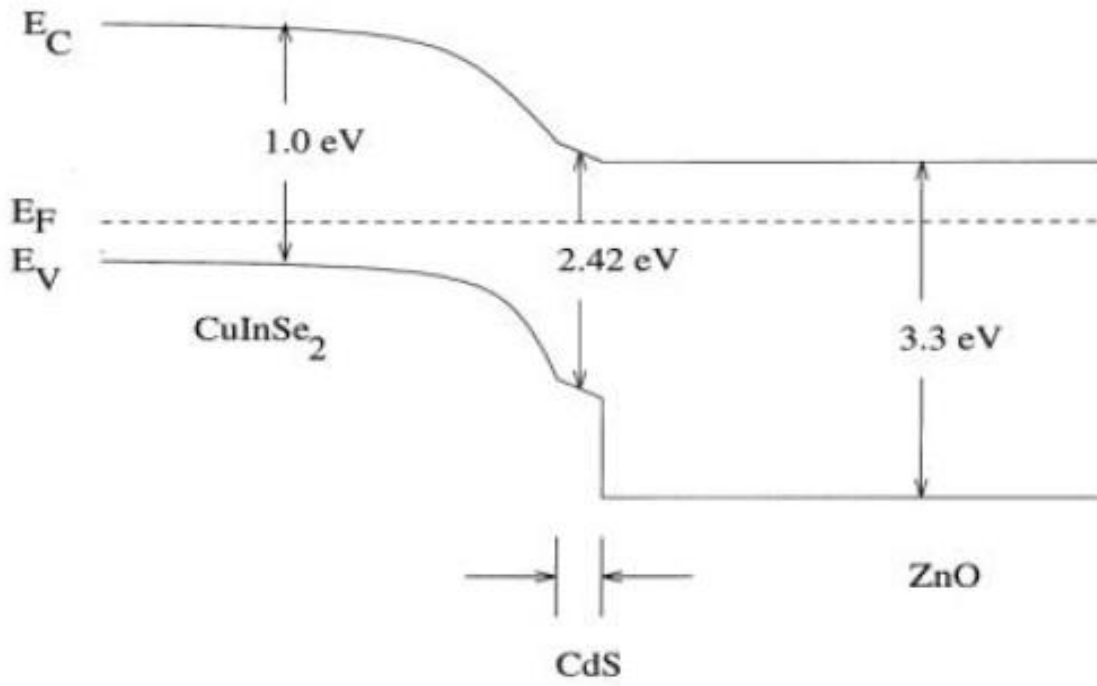


Figure 2.8. Band diagram of the CuIn(Ga)Se<sub>2</sub>/CdS/ZnO solar cell

(v) Total (capital + maintenance) cost should be low.

(vi) Constituent materials should be non-toxic/environmentally friendly.

Currently, the most widely used PV technologies are the single-crystal silicon technology and the polycrystalline silicon technology. Together, these two forms of silicon constitute about 86% of the solar cell market today (Goetzberger, 2000). However, there are distinct disadvantages of using silicon as the absorber material for solar cells. These notable disadvantages are that silicon is an indirect bandgap semiconductor, with a relatively low absorption coefficient for absorbing sunlight. Consequently, a considerable thickness (about 100 microns) of silicon is needed to absorb light, thereby increasing the material cost. This, in turn, means that the photogenerated carriers have to traverse long distances to reach the junction, which is near the front surface. The diffusion length of the minority carriers has to be very high, which can happen only when the material is of very high purity and of high crystalline perfection. This, then, increases the processing costs. Moreover, the single-crystal or polycrystalline silicon wafers are cut from ingots grown by the Czochralski method, or by controlled solidification in a crucible or mould. Sawing of these wafers results in material loss, adding to the total material cost.

Although the laboratory efficiencies of these cells have exceeded 24%, the commercially available module efficiencies are usually limited to less than 16%. It is surprising that, in spite of these shortcomings, silicon is the dominant solar cell technology. At least a major part of the reason lies with the fact that this technology has benefitted tremendously from the high standard of silicon technology that was originally developed for transistors, and later for integrated circuits. The resulting silicon-based solar cells have exhibited high efficiency and good stability. The best laboratory efficiency for a single-crystal silicon solar cell is 24.5% (Green, 1999), while the best production cells have efficiencies of 15-16%. However, the resulting electricity costs are still relatively high, when compared to the cost of conventional electricity, making it necessary to look for new materials and technologies to replace silicon.

One alternative to the silicon technology that has been extensively investigated is the gallium arsenide (GaAs) technology. GaAs is a direct bandgap semiconductor with a high absorption coefficient, with the bandgap of 1.43 eV that is well suited to the solar spectrum. The effect of the direct bandgap is easily appreciated when it is recognized that for a 90% light absorption, it takes only 1  $\mu\text{m}$  of GaAs versus 100  $\mu\text{m}$  of silicon. This technology, however, is

quite expensive, and, as a result, more scientists and researchers are getting interested in the development of the low-cost alternative which is thin film photovoltaics (Silverman *et al.*, 2013).

### 2.3. Thin film photovoltaics

The thin film technologies that hold the greatest promise are Amorphous Silicon (a-Si), Cadmium Telluride (CdTe) and Copper Indium Diselenide (CuInSe<sub>2</sub>). The a-Si technology, which uses a silicon-hydrogen alloy (containing 20-30% hydrogen) as the absorber material, has been around for a couple of decades. The first amorphous solar cells were prepared in 1976 (Carlson, 1976). The a-Si technology currently dominates the thin film photovoltaics market. (The dominance of silicon in its crystalline and amorphous forms is an overwhelming 99% of the total photovoltaics market. Most of the remaining 1% is taken up by CdTe, with CuInSe<sub>2</sub> only recently beginning to show up on the commercial scene.)

The cuprous sulfide/cadmium sulfide heterojunction was the first all-thin-film photovoltaic system developed. Currently, two of the most promising thin film polycrystalline technologies are Cadmium Telluride (CdTe) and Copper Indium Diselenide (CuInSe<sub>2</sub>), both of which use Cadmium Sulfide (CdS) as the (n-type) heterojunction partner. Both CuInSe<sub>2</sub> as well as CdTe are direct bandgap materials. Such polycrystalline thin film PV technologies offer several advantages, which can be weighed against the shortcomings of single-crystal and poly silicon cells that are listed above. These are:

- (i) Thin film technologies often involve semiconductor materials that have direct bandgaps, and hence have very high absorption coefficients for the wavelengths of interest. Therefore, only a small thickness, usually a few micrometers, is enough to absorb the entire sunlight incident on the absorber layer. This provides for significant savings in the material costs.
- (ii) Because of the low consumption of the active solar cell material, rare and expensive materials can be considered.
- (iii) A variety of relatively inexpensive vacuum deposition techniques can be employed for the processing of thin film solar cells, thereby reducing the processing costs. These techniques include physical processes such as RF and DC magnetron sputtering, thermal vacuum evaporation, close-space sublimation, electron beam evaporation, etc. Wet chemical processes such as Spray pyrolysis, Dip-coating, Spin coating, chemical bath deposition method, etc.
- (iv) There are no small wafers to wire together, while making solar cell modules. Separate cells can be monolithically integrated on the module by scribing steps between depositions (Gabor,



1994). This makes packaging and wiring easier and also allows high voltage to be produced with smaller areas (Goetzberger & Hebling, 2000).

(v) Thin films can be deposited on flexible, lightweight substrates, thereby making the cells viable for a larger variety of applications.

Based on this list of desirable properties, one might begin to think that thin film technologies are clearly the one solution that will get rid of all the hurdles that photovoltaic technology faces. However, in spite of all these advantages, these technologies have not been able to get the electricity cost down enough, due to the following shortcomings:

- (i) Most of the thin film technologies involve heterojunctions, and hence face the problem of faulty interfaces, arising because of lattice mismatches between the materials.
- (ii) Difficulty of getting different films to adhere to each other well.
- (iii) Difficulty in achieving uniformity of thickness, composition, and quality across a large substrate.
- (iv) Difficulty in achieving stability of the films over many years.
- (v) Toxicity of some constituents involved (for instance, Cd in the case of CdTe/CdS, and, to a lesser extent, CuInSe<sub>2</sub>/CdS).

Although thin film PV technology is still in its infancy, both CdTe as well as CuInSe<sub>2</sub> technologies have shown tremendous promise. Laboratory efficiency numbers have exceeded 18% for CuIn(Ga)Se<sub>2</sub>, and 15% for CdTe, whereas commercially available thin film modules have shown conversion efficiencies in the neighbourhood of 10-12% (Romeo *et al.*, 2004).

One of the main problems facing the CdTe technology is the toxicity of cadmium. This necessitates end-of-life recycling programs for CdTe modules, thus adding to the total cost. Cu<sub>2</sub>ZnSnS<sub>4</sub>, on the other hand, has consistently passed the toxicity tests, and hence can be thought of as the leader among all current thin film technologies.

## **2.4. Cu<sub>2</sub>ZnSnS<sub>4</sub>-family-based thin film photovoltaics**

### **2.4.1. Cu<sub>2</sub>ZnSnS<sub>4</sub> (CZTS) family and device issues**

CZTS is the I<sub>2</sub>-II-IV-VI<sub>4</sub> quaternary compound semiconductors made by substituting the selenium with sulfur, the rare metal indium with zinc and tin in CIS ternary compound. Each component of CZTS is abundant in the earth's crust (Cu: 50 ppm, Zn: 75 ppm, Sn: 2.2 ppm, S: 260 ppm) and they possess extremely low toxicity. On the other side, in the case of CIS

compound, the contents of indium and selenium in the earth's crust are 0.05 ppm or less (Emsley, 1998). It has a Kesterite structure as shown in figure 2.9.

The first report on the photovoltaic effect on heterodiodes consists of cadmium-tin-oxide transparent conductive film and CZTS thin film on a stainless steel substrate achieved an open-circuit voltage as 165mV (Ito & Nakazawa, 1988). In 1989, by annealing the same device in air, they achieved the open-circuit voltage of 250 mV and the short-circuit current of 0.1 mA/cm<sup>2</sup> (Ito & Nakazawa, 1989). In 1997, fabricated CZTS thin films by thermal evaporation of the elements and binary chalcogenides were carried out in high vacuum. For the heterojunction of this film with the CdS/ZnO window layer, they reported the highest conversion efficiency of 2.3% and the highest open-circuit voltage of 570 mV (Friedlmeier *et al.*, 1997). In 2003, CZTS thin films were grown by RF magnetron sputtering. The films had refractive index of 2.07, the absorption coefficient was about 10<sup>4</sup> cm<sup>-1</sup>, and the band gap energy was about 1.51 eV (Seol *et al.*, 2003). In 1996 at PVSEC-9 (9<sup>th</sup> Photovoltaic Specialist Energy Conference), it was reported, for the first time, that CZTS thin films were able to be formed successfully by vapor phase sulfurization of E-B-evaporated precursors; and the conversion efficiency was 0.66% with the device structure of ZnO:Al/CdS/CZTS/Mo/soda lime glass(SLG) substrate (Katagiri *et al.*, 1996). In 1999, the conversion efficiency was increased up to 2.63%, which was reported at PVSEC-11 (Saitoh *et al.*, 1999). Furthermore, it attained the highest conversion efficiency of 5.45% in 2003, which was reported at WCPEC-3 (Tsuchida *et al.*, 2003). The photoconductivity of CZTS thin films prepared by photo-chemical deposition (PCD) from aqueous solution containing CuSO<sub>4</sub>, SnSO<sub>4</sub>, ZnSO<sub>4</sub> and Na<sub>2</sub>S<sub>2</sub>O<sub>3</sub> were measured (Moriya *et al.*, 2005). The characterization of sprayed CZTS thin films has been neglected in most of the CZTS-related literature. Yet, in 1996, using two steps, stoichiometric CZTS films having kesterite structure and exhibiting a resistivity of about 2×10<sup>2</sup> Ω cm, using the spray deposition technique on a glass substrate as a first step and then a sulfurization at 550 °C as a second step (Nakayama & Ito, 1996). They reported that the chemical composition of the CZTS films was controlled by varying the concentration of the spray solution.

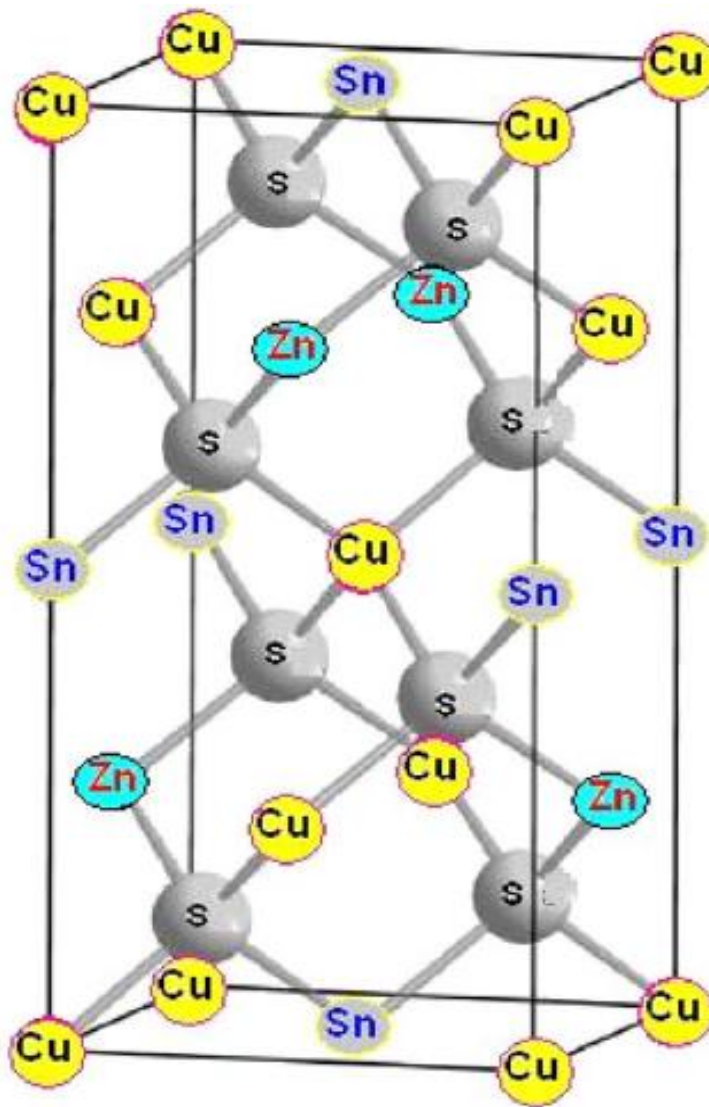


Fig.2.9. Mineral kesterite (Cu<sub>2</sub>ZnSnS<sub>4</sub>)  
(Source: Babichuk *et al.*, 2012)

In 2001, Madarasz *et al.* prepared CZTS thin films using the thermal decomposition of thiourea complexes of Cu (I), Zn (II), and Sn (II) chlorides as precursors (Madarasz *et al.*, 2001).

Apart from the physical vapour deposition methods cited above for the deposition of CZTS films (which means that all these preparations were done in vacuum, and therefore makes the deposition of this thin film quite expensive and complicated), chemical deposition methods like Photochemical depositions (Moriya *et al.*, 2006), Sol-gel (Tanaka *et al.*, 2007), Spray pyrolysis (Madarasz *et al.*, 2001) and Screen printing method (Zhihua *et al.*, 2010) have been used to deposit these films.

Tsukagoshi and his co-workers reported on the preparation of CIGS thin films under non-vacuum condition to reduce cost and to simplify the preparation process (Tsukagoshi *et al.*, 2006). The CIGS thin films were deposited by mechanochemical and screen-printing/sintering processes. The solar cell based on the CIGS films prepared under this non- vacuum condition achieved an efficiency of 2.7%.

Presently, CZTS thin films are conventionally prepared in vacuum atmosphere, rendering it rather expensive and complicated. Furthermore, there are only two reports to the best of our knowledge, on the preparation of solar cells with CZTS absorber layers deposited under non-vacuum conditions. The first cell was reported to have open circuit voltage ( $V_{oc}$ ) of 390mV, a short circuit current ( $I_{sc}$ ) density of 7.8mA/cm<sup>2</sup>, a fill factor (ff) of 0.33 and an efficiency of 1.01% under irradiation of AM1.5 and 100mW/cm<sup>2</sup> (Kunihiko *et al.*, 2009). The second cell with an active area of 0.15cm<sup>2</sup> was grown by the screen-printing method had a short-circuit current density (4.76mA/cm<sup>2</sup>), open-circuit voltage (386mV), fill-factor (0.27), and efficiency of a typical photovoltaic cell of 0.49% (Zhihua *et al.*, 2010). Qin Miao Chen *et al.*, (2011) fabricated a superstrate structure of CZTS thin film solar cell by the screen printing process and had an efficiency of 0.53%. Also, Chen Qin-Miao *et al.*, (2012) used the doctor-blade method to investigate the preparation of superstrate CZTS film for low cost solar cell and had an efficiency of 0.55%.

In this research work, superstrate CZTS-based solar cells with structure (Soda Lime Glass (SLG)/FTO:Ag/CdS/CZTS/Al) were fabricated under non- vacuum conditions. The CZTS absorber layers, the FTO (fluorine doped tin oxide) window layer and CdS buffer layers were prepared under non-vacuum conditions to simplify the preparation processes and to reduce the entire production cost.

Each of the layers of these solar cells was first optimized to know the conditions necessary for the preparation of their sol-gels and depositions. These optimizations were done through the thin film deposition of individual layers and their characterisations using the Four Point Probe, Profiler, UV-Spectrophotometer, Scanning Electron Microscope (SEM), Energy Dispersive Spectrometer (EDS).

The details of the research work and results obtained are adequately discussed in the subsequent chapters.

UNIVERSITY OF IBADAN LIBRARY

## CHAPTER THREE

### MATERIALS AND METHODS

#### 3.1. The device structure

The fabricated  $\text{Cu}_2\text{ZnSnS}_4$  solar cell is as depicted in figure 3.1. It involves a sequential deposition of the various thin films which serve specific purposes, such as the absorber material, the buffer, and the front and back contacts. The overall structure can be written as: Glass substrate/ FTO:Ag (Front contact)/ CdS (n-type Buffer)/ $\text{Cu}_2\text{ZnSnS}_4$ (Absorber material)/Al(Back contact).

#### 3.2. Materials

The materials used in this research can be categorized into the depositing and characterizing equipment. The details are discussed as follows:

##### 3.2.1. Thin film depositing equipment

###### 3.2.1.1. Soda-lime glass

Soda-lime glass (SLG) is the most common form of glass produced. It is composed of about 70 per cent silica (silicon dioxide), 15 per cent soda (sodium oxide), and 9 per cent lime (calcium oxide), with much smaller amounts of various other compounds. The soda serves as a flux to lower the temperature at which the silica melts, and the lime acts as a stabilizer for the silica. It is an inexpensive substrate material, and offers good resistance to corrosion. It is also easily available at local hardware stores. There are other advantages associated with the use of glass as the substrate; these include the fact that the substrate can be used as a packaging material. This becomes even more important when the solar cells are superstrate-type, wherein the light is shone through the glass to reach the absorber. Another benefit of using soda-lime glass is the diffusion of sodium (Na) from the glass to the deposited layers. In  $\text{CuInSe}_2$ -type cells, the  $V_{OC}$ 's have been shown to increase because of this Na reaching the absorber films (Su-Huai *et al.*, 1999). The disadvantage associated with the use of soda-lime glass is that the operating temperatures have to be limited to about  $600^\circ\text{C}$ , otherwise the glass is prone to warping or even breakage because of the stress.

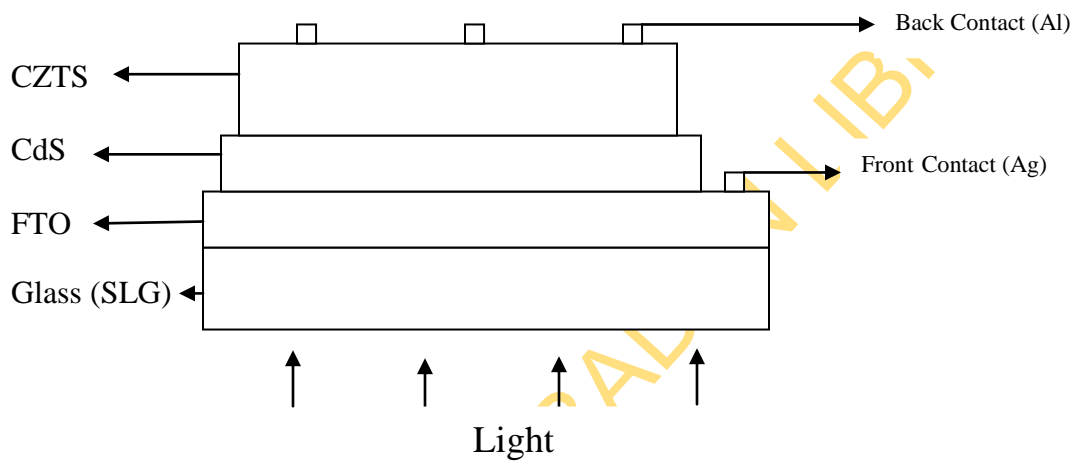


**Fig. 3.1. Structure of the fabricated solar cell device**

### **3.2.1.2. Atmospheric pressure chemical vapour deposition machine (APCVD)**

Atmospheric chemical vapor deposition (APCVD) is a chemical process used to produce high-purity, high-performance solid materials. The process is often used in the semiconductor industry to produce thin films. In typical CVD, the wafer (substrate) is exposed to one or more volatile precursors, which react and/or decompose on the substrate surface to produce the desired deposit. Frequently, volatile by-products are also produced, which are removed by gas flow through the reaction chamber. The precursor and the entire APCVD set up used for this research at the Physics Advanced Laboratory of Sheda Science and Technology Complex are as shown in figures 3.2 and 3.3 respectively. The advantages of this method include its high deposition rates as well as its simple and high throughput. This method is mainly used for thick oxides.

### **3.2.1.3. Spin coater**

The spin coater is used in depositing thin films from sol-gels. Spin coating has been used for several decades for the application of thin films. A typical process involves depositing a small puddle of a fluid resin onto the centre of a substrate and then spinning the substrate at high speed (typically around 3000 rpm) as depicted in Fig. 3.4. Centripetal acceleration will cause the resin to spread to, and eventually off, the edge of the substrate, leaving a thin film of resin on the surface. Final film thickness and other properties will depend on the nature of the resin (viscosity, drying rate, per cent solids, surface tension, etc.) and the parameters chosen for the spin process. Factors such as final rotational speed, acceleration, and fume exhaust contribute to how the properties of coated films are defined. One of the most important factors in spin coating is repeatability. Subtle variations in the parameters that define the spin process can result in drastic variations in the coated film. In general, higher spin speeds and longer spin times create thinner □films. The spin coating process involves a large number of variables that tend to cancel and average out during the spin process and it is best to allow sufficient time for this to occur. The spin coater used in this research is the WS-650-23B from Laurell Technologies Corporation as shown in Fig. 3.5.

### **3.2.1.4. Thermal vacuum evaporator**

A thermal evaporator uses an electric resistance heater to melt the material and raise its



vapour pressure to a useful range. This is done in a high vacuum, both to allow the vapour to reach the substrate without reacting with or scattering against other gas-phase atoms in the chamber, and reduce the incorporation of impurities from the residual gas in the vacuum chamber. Thermal evaporation is the simplest way of depositing material onto a substrate. One major disadvantage of this is that a lot of materials is lost in the process. The process is as represented in Fig. 3.6 while the different heating sources are shown in Fig. 3.7. The purity of the films depends on the purity of the source material and the quality of the vacuum. The thickness of the film varies due to the geometry of the chamber. The thermal evaporator used in this research is the Edward 306 thermal evaporator.

#### **3.2.1.5. Three-zone furnace**

The multiple zones enable the user to create different thermal gradients by varying the temperature of three zones. The furnace includes one fused quartz tube, one pair of vacuum sealing flanges with pressure gauge and ball valve for immediate use. Three 30 segments temperature controllers are installed with K type thermal couple. Microprocessor-based self-tuning PID control provides excellent temperature control without overshooting along with an accuracy of  $\pm 1$  °C. It is an excellent furnace for annealing, diffusing and sintering samples under various gas atmospheres.

### **3.2.2. Thin film characterising equipment**

#### **3.2.2.1. Scanning electron microscope (SEM)**

The SEM is perhaps the most widely employed thin film and coating characterisation instrument. A schematic representation of the working principle of the SEM is as shown in Fig.3.7. Electrons thermionically emitted from a tungsten or LaB<sub>6</sub> cathode filament are drawn to an anode, focused by two successive condenser lenses into a beam with a very fine spot size ( $\sim 50$  Å). Pairs of scanning coils located at the objective lens deflect the beam either linearly or in a raster fashion over a rectangular area of the specimen surface. Electron beams having energies ranging from a few thousands to 50keV (with a 30keV being the common value) are utilized. Upon impinging on the specimen, the primary electrons decelerate and in losing energy, they transfer it inelastically to other atomic electrons and to the lattice.



**Fig.3.2. Precursor section of the APCVD set up at the Sheda Science and Technology Complex**



**Fig.3.3. The entire APCVD set-up showing the arrangement of the precursor, dopant and depositing section.**

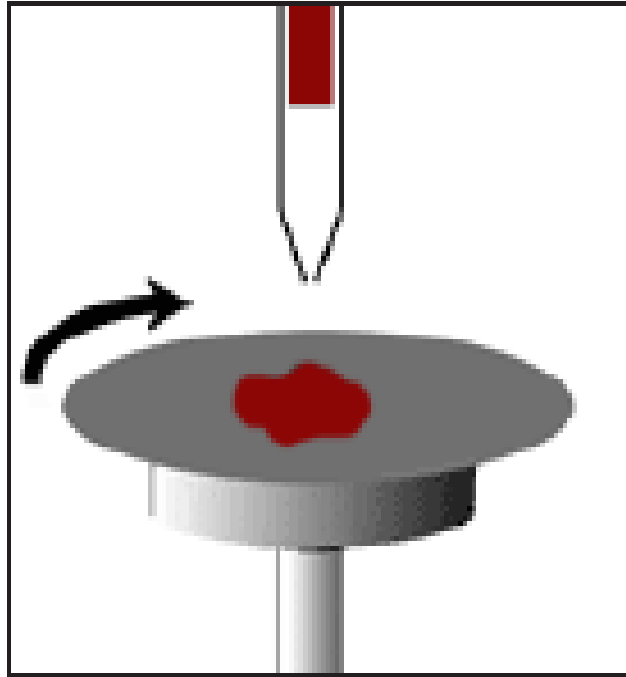


**Fig.3.4. Spin-coating process**



**Fig.3.5. Spin-coating machine at the Physics Advanced Laboratory of the Sheda Science and Technology Complex, Abuja**

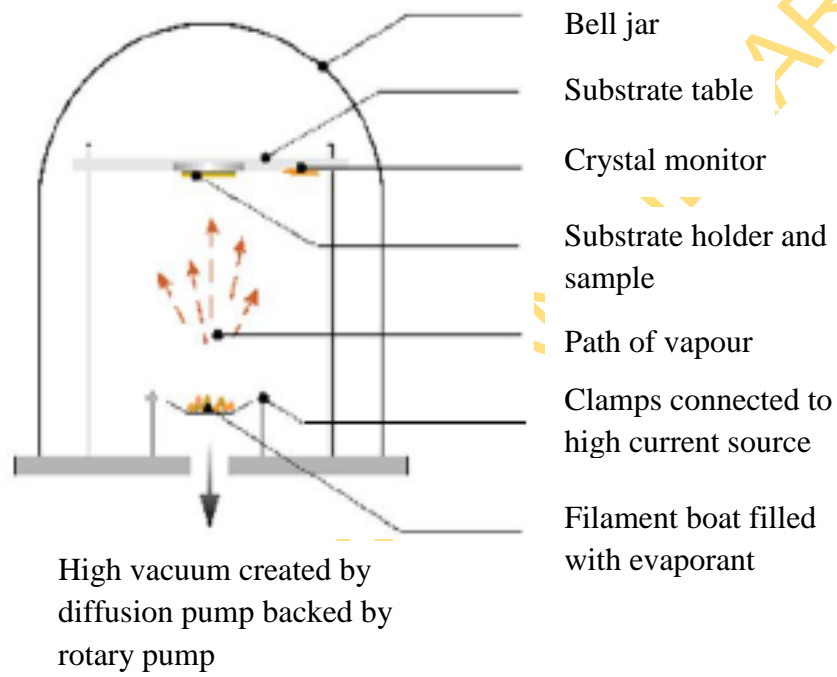


**Fig.3.6. Thermal evaporation process**

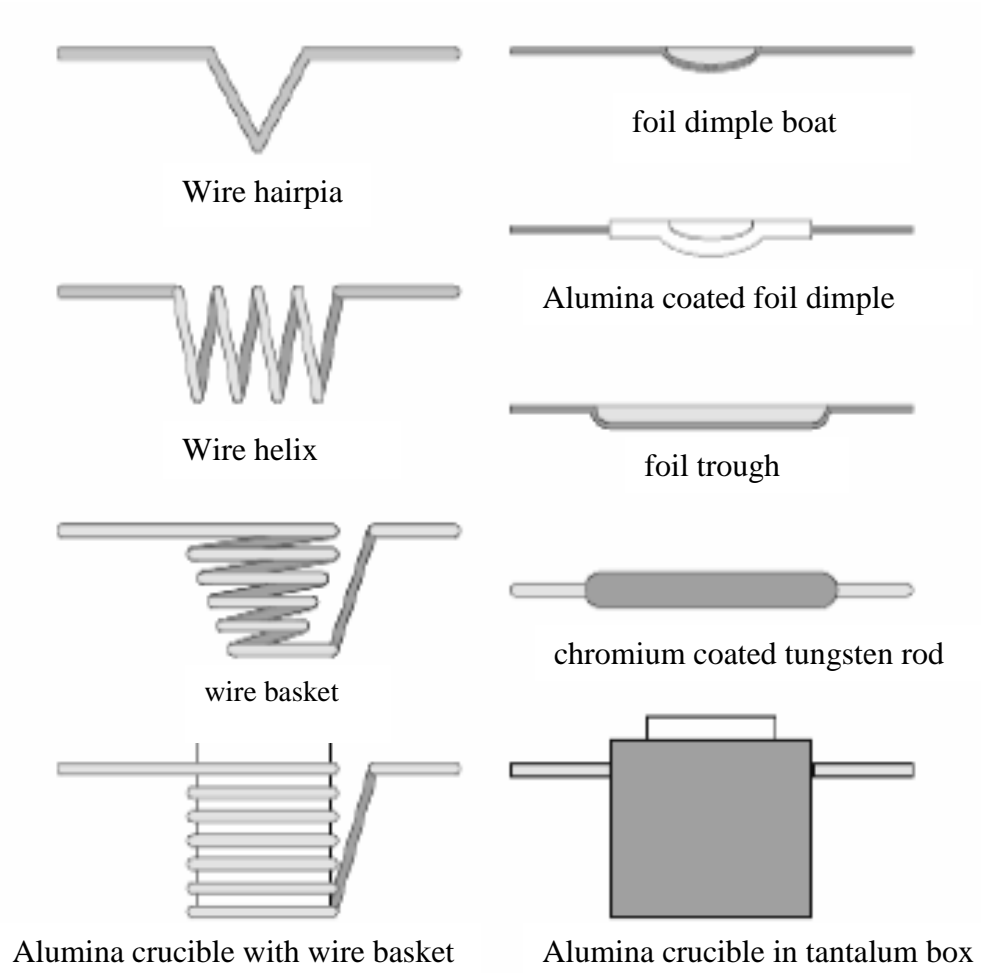


**Fig.3.7. Heating sources for thermal evaporation process**

### 3.2.2.2 Energy dispersive X-ray spectroscopy (EDS)

The stoichiometry of multinary compound semiconductor has a strong influence on their material properties. The exact control of the stoichiometry and accurate analysis of the composition of thin films are therefore a prerequisite for preparation of high quality thin film absorbers. By far the most commonly used technique for the chemical analysis of thin films is electron probe micro-analysis (EPMA), sometimes also called Energy Dispersive X-ray Spectroscopy (EDX or EDS). This method is fast, non-destructive and very high lateral resolution can be obtained. Most EDS systems are interfaced to SEM's, where the electron beam serves to excite characteristic X-rays from the area of the specimen being probed. There are two common methods to record the spectra of the emitted characteristic radiation. The first is to measure the whole energy spectrum simultaneously with an energy sensitive detector. The second option is to use a goniometer and an analyzing crystal with  $\theta$ - $2\theta$  coupling and to assign a measured intensity to a  $2\theta$  position. By means of the Bragg equation  $n\lambda=2d\sin\theta$ , the energy of a measured peak can then be determined from the  $2\theta$ -position of the detector. The first technique, the energy dispersive spectrometry, is known as EDS or EDX, while the second approach is called the wavelength dispersive spectrometry (WDS or WDX).

### 3.2.2.3 X-Ray diffractometer (XRD)

X-ray diffractometers consist of three basic elements: an X-ray tube, a sample holder, and an X-ray detector as shown in Fig.3.8. X-rays are generated in a cathode ray tube by heating a filament to produce electrons, accelerating the electrons toward a target by applying a voltage, and bombarding the target material with electrons. When electrons have sufficient energy to dislodge inner shell electrons of the target material, characteristic X-ray spectra are produced. These spectra consist of several components, the most common being  $K_{\alpha}$  and  $K_{\beta}$ .  $K_{\alpha}$  consists, in part, of  $K_{\alpha 1}$  and  $K_{\alpha 2}$ .  $K_{\alpha 1}$  has a slightly shorter wavelength and twice the intensity as  $K_{\alpha 2}$ . The specific wavelengths are characteristic of the target material (Cu, Fe, Mo, Cr). Filtering, by foils or crystal monochromators, is required to produce monochromatic X-rays needed for diffraction.  $K_{\alpha 1}$  and  $K_{\alpha 2}$  are sufficiently close in wavelength such that a weighted average of the two is used. Copper is the most common target material for single-crystal diffraction, with  $CuK_{\alpha}$  radiation =  $1.5418\text{\AA}$ . These X-rays are collimated and directed onto the sample. As the sample and detector are rotated, the intensity of the reflected X-rays is recorded. When the geometry of the incident



X-rays impinging the sample satisfies the Bragg Equation, constructive interference occurs and a peak in intensity occurs. A detector records and processes this X-ray signal and converts the signal to a count rate which is then output to a device such as a printer or computer monitor.

X-ray diffraction is a very important experimental technique that has long been used to address all issues related to the capital structure of bulk solids, including lattice constants and geometry, identification of unknown materials, orientation of single crystals, and preferred orientation of polycrystals, defects, stresses, etc. In this study a MD-10 Mini-X-ray Diffractometer system has been used to analyze the various thin films produced in this study.

#### 3.2.2.4 Four-point probe

The four-point probe method is widely used for the determination of the electrical resistivity of a semiconductor layer. When an electric field  $E$  is applied to a semiconductor material, an electric current will flow. This current density is given by:

$$J = \sigma E \quad (3.1)$$

Where the electrical conductivity of the layer is given by  $\sigma$ . When a rectangular-shaped sample with dimensions  $l \times w \times d$  (where  $l$  is the length,  $w$  the width and  $d$  the thickness of this rectangle) is considered, the resistance is given by:

$$R = \rho(l/wd) \quad (3.2)$$

If  $l = w$  then the above equation becomes:

$$R = \rho/d = R_s \quad (3.3)$$

The quantity  $R_s$  is known as the sheet resistance of one square of the film that is independent of the size of the square. The most common method of measuring this sheet resistance is with the four-point probe method. The instrument is made up of four point-probes that touch the surface of the film as shown in Fig.3.9. to measure the sheet resistivity of a solar cell. A current  $I$  is passed through the outer two probes, while a potential difference  $V$  is measured between the inner two probes.

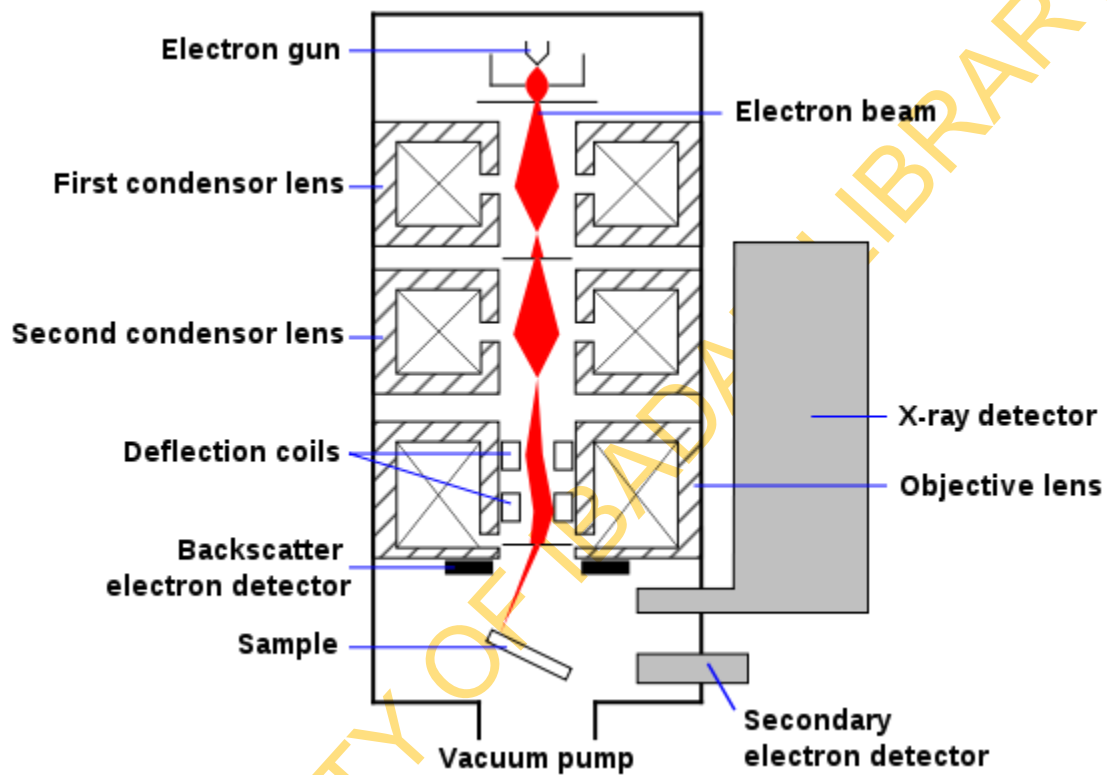


**Figure 3.8: Schematic representation of the fundamental operating principles of scanning electron microscope**

(source: [www.dur.ac.uk/resources/research/publicity/ScanningElectronMicroscopy](http://www.dur.ac.uk/resources/research/publicity/ScanningElectronMicroscopy))

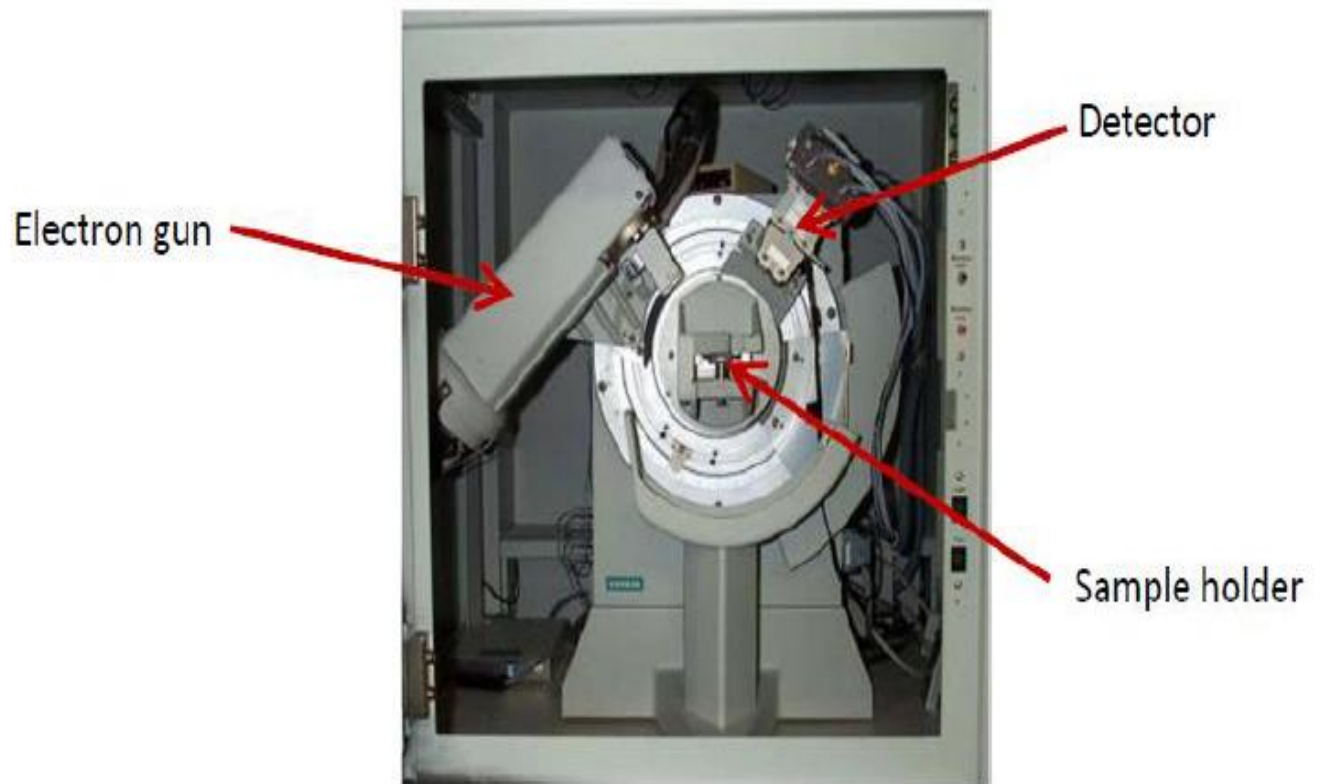


Figure 3.9: A modern x-ray diffractometer

UNIVERSI

The resistivity is given as:

$$\rho = \frac{V}{I} 2\pi x \quad (3.4)$$

Where  $x$  is the distance between the probes. If the material is in the form of an infinitely thin film resting on an insulating support then the equation can be written as:

$$\rho = \frac{V}{I} \frac{\pi d}{\ln 2} \quad (3.5)$$

or

$$\frac{\rho}{d} = R_s = 4.53 \frac{V}{I} \quad (3.6)$$

### 3.2.2.5 UV/VIS-Spectrophotometer

UV/VIS-Spectrophotometer is used to determine the absorption or transmission of UV/VIS light (180 to 820 nm) by a sample. It can also be used to measure concentrations of absorbing materials based on developed calibration curves of the material. A sample is placed in the UV/VIS beam and a graph of the transmittance, reflectance or absorbance versus the wavelength is obtained. Alternatively, samples are prepared in known concentrations and their absorbance is read by the UV/VIS-Spectrophotometer. Results are then graphed to make a calibration curve from which the unknown concentration can be determined by its absorbance.

The Avec UV/VIS-Spectrophotometer is used in this research. Transmission and reflection measurements were taken of each relevant sample at room temperature with a scan range between 300-1200nm. Following the analysis of Pankove, the optical transmission coefficient (T) of a transmitting medium is defined as the ratio of the intensity of transmitted radiation to that of the incident radiation,  $I/I_0$  (Pankove, 1971). These two intensities are related to the absorption coefficient( $\alpha$ ) and the optical path length (t) by the following expression:

$$I = I_0 e^{-\alpha t} \quad (3.7)$$

Taking reflection effects into account, for an incident intensity of  $I_0$  at a front surface of a transmitting medium, the transmitted radiation is given by  $(1 - R)I_0$  where  $R$  is the reflection coefficient. Using equation 3.7, the portion of the radiation reaching the back surface of the medium is  $(1 - R)I_0 e^{-\alpha t}$ . Only a fraction of this radiation given by  $(1 - R)(1 - R)I_0 e^{-\alpha t}$  emerges from the medium. Taking into account all the multiple internal reflections, the total transmitted radiation can be expressed as (Pankove, 1971):

$$T = \frac{I}{I_0} = \frac{(1-R)^2 \exp(-\alpha t)}{1 - R^2 \exp(-2\alpha t)} \quad (3.8)$$

Again, where  $I$  and  $I_0$  are the transmitted and incident light intensity respectively,  $t$  (or optical path length) is the film thickness, and  $\alpha$  is the absorption coefficient. For high values of  $\alpha t$ , the term  $R^2 \exp(-2\alpha t)$  in the denominator can be neglected since  $R$  is also neglected for high absorption, and  $\exp(-2\alpha t)$  is approximately zero. This leads to the simplified relation between  $\alpha$  and measured  $R$  and  $T$ ,

$$\alpha = \frac{2 \ln(1-R) - \ln(T)}{t} \quad (3.9)$$

The optical absorption coefficient  $\alpha$  varies with photon energy  $h\nu$  according to the relation

$$\alpha h\nu = A(h\nu - E_g)^n \quad (3.10)$$

where  $n$  characterises the transition process and  $E_g$  is the band gap. For semiconductors with direct band gap transition,  $n = 1/2$  while  $n = 2$  for those with indirect band gap transition.

### 3.2.2.6 Solar simulator

A solar simulator (also artificial sun) is a device that provides illumination approximating natural sunlight. The purpose of the solar simulator is to provide a controllable indoor test facility under laboratory conditions, used for the testing of solar cells, sun screen, plastics, and other materials and devices. The light from a solar simulator is controlled in three dimensions:

1. spectral content
2. spatial uniformity

### 3. temporal stability

Each dimension is classified in one of three classes: A, B, or C. A solar simulator meeting class A specifications in all three dimensions is referred to as a Class A solar simulator, or sometimes a Class AAA. The percentage of total irradiance is shown below in Table 3.1 for the standard terrestrial spectra of AM1.5G and AM1.5D, and the extraterrestrial spectrum, AM0.

Several types of lamps have been used as the light sources within solar simulators. These lamps include the Xenon arc lamp, Metal Halide arc lamp, quartz tungsten halogen lamps, and light emitting diode. A schematic diagram of the working principle of a solar simulator is shown in Fig. 3.10.

## 3.3. Methods

### 3.3.1. Preparation of substrate

The glass pieces purchased from local stores sometimes have scratches and/or spots on them, which can degrade the structure and performance of the films deposited on them. It therefore becomes important that the glasses are thoroughly cleaned before they are used.

The cleaning procedure involves a Alconox detergent/de-ionised (DI) water soak step, followed by DI water rinse. The glass pieces then go through an ultrasonic clean in chemicals (acetone then ethanol) that remove the organics from the glass. This is again followed by a DI water rinse. Lastly, the glass is blown dried with high-purity nitrogen.

### 3.3.2. Preparation of SnO<sub>2</sub>:F thin film (Window layer)

A good window layer needs to satisfy two requirements. It has to be highly conductive, so that the current generated by the photons can easily be conducted into the external circuit. The sheet resistance of this layer needs to be as low as possible, because often the external metal grid (front contact) is a set of thin metal fingers, separated by a significant distance between them. The current has to flow in a direction perpendicular to the direction of incident light. Secondly, the window layer material has to be as transparent to the incident photons as possible, so that they go through the layer unabsorbed, to reach the absorber layer. Fluorine doped Tin Oxide (SnO<sub>2</sub>:F) is used as the window material for our solar cells due to the superstrate configuration being used in this research according to Shadia and Ahmad-Bitar (2010) . SnO<sub>2</sub>:F transmits about 90% of the incident light between 400 and 1000nm. Transmission drops off at higher wavelengths due to the

free carrier absorption, which increases with increased doping. Therefore, a compromise has to be made in terms of achieving a low resistivity value and low free carrier absorption.

UNIVERSITY OF IBADAN LIBRARY

**Table 3.1: ASTM spectral irradiance for three standard spectra**

<b>Wavelength Interval [nm]</b>	<b>AM1.5D</b>	<b>AM1.5G</b>	<b>AM0</b>
300–400	no spec	no spec	8.0%
400–500	16.9%	18.4%	16.4%
500–600	19.7%	19.9%	16.3%
600–700	18.5%	18.4%	13.9%
700–800	15.2%	14.9%	11.2%
800–900	12.9%	12.5%	9.0%
900–1100	16.8%	15.9%	13.1%
1100–1400	no spec	no spec	12.2%

UNIVERSITY OF IBADAN LIBRARY



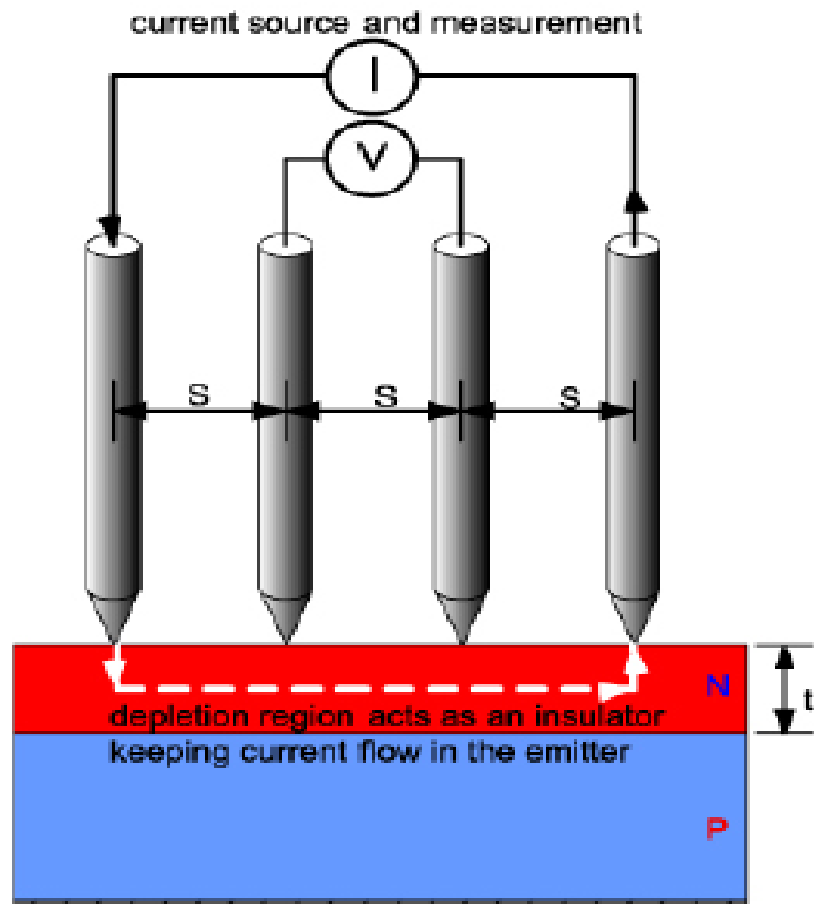


Figure 3.10: Use of a four-point probe to measure the sheet resistivity of a solar cell

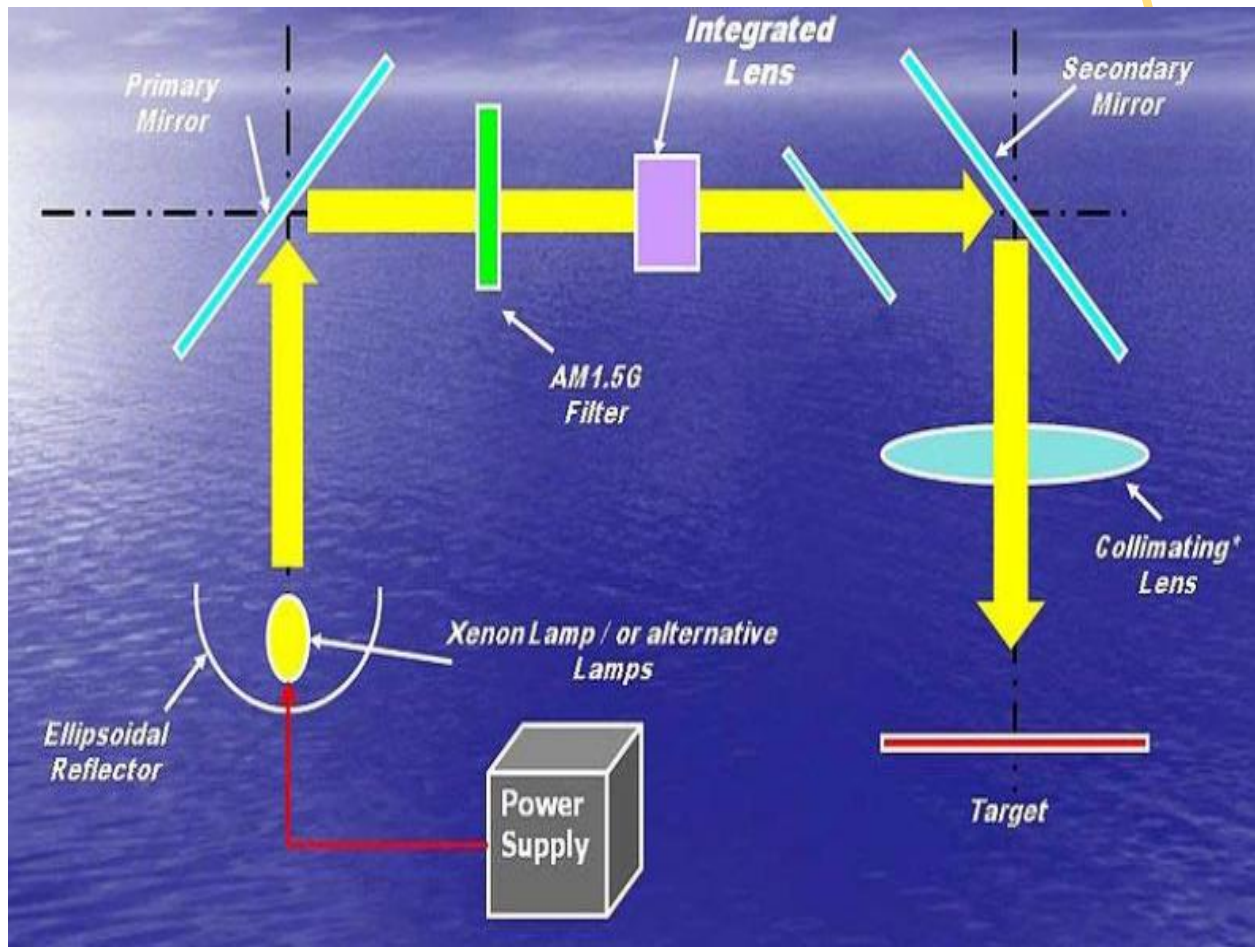


Figure 3.11: Working principle of one lamp solar simulator

Soda lime glass (SLG) was used as substrate for the deposition of FTO thin films in this research. The soda lime glass was soaked in aqua regia for 24 hours (mixture of HCl and HNO<sub>3</sub> in the ratio 3:1 respectively) to remove the sodium content of the glass because it increases the resistance of the FTO thin film when deposited on it. The Soda lime glass (SLG) was carefully removed from the aqua regia and cleaned with acetone, then ethanol and blown dry. A simple pictorial arrangement of our precursors and deposition set up is as shown in Fig.3.2 and Fig.3.3 respectively. The FTO thin films on the SLG were prepared by atmospheric pressure chemical vapour deposition (APCVD) with Tin (IV) chloride (SnCl<sub>4</sub>) and Hydrogen Fluoride (HF) as the precursor and dopant. High purity N<sub>2</sub> was used as the carrier gas and H<sub>2</sub>O was used as the activator. The machine was designed and fabricated at the Physics Advanced Laboratory of the Sheda Science and Technology Complex, Sheda, Abuja.

The experimental conditions were as follows: SnCl<sub>4</sub> (99% pure) and HF (99% pure) were gasified in volumetric flasks by bubbling with N<sub>2</sub>. Also, the HF was heated at 52<sup>0</sup>C. The flow rates were 1.05 ± 0.01 g/min for SnCl<sub>4</sub> and 0.05 ± 0.01 g/min for HF. The activator gas (H<sub>2</sub>O vapour) was carried with air and gasified at 30<sup>0</sup>C using a pump which was regulated by using a regulator. Its flow rate was 0.03 ± 0.01 g/min. The carrier gas (N<sub>2</sub>) flow rate was 1.05 ± 0.01 g/min. The susceptor of the APCVD machine can be moved, allowing multiple, or graded deposition across the same substrate. The temperature of the glass surface (substrate) during deposition was varied from 320<sup>0</sup>C-360<sup>0</sup>C while the deposition time was varied from 60s to 140s. Several runs of the experiment were carried out and films with good physical properties were characterized for their optical and electrical properties. The optical transmission spectra were obtained using UV- Visible spectrophotometer (Avantes UV-Vis-NIR) while the sheet resistances of the films were obtained using the four-point probe system (Jandel universal four-point probe) and the film thicknesses were measured using Dektak 3ST surface profiler on an etched step edge.

Some of the best characterised films were selected and used as window layers for the growth of superstrate structure of Cu<sub>2</sub>ZnSnS<sub>4</sub> thin film solar cells.

### 3.3.2. Preparation of the heterojunction partner (buffer layer)

The role of the CdS buffer layer is two-fold: it affects both the electrical properties of the junction and protects the junction against chemical reactions and mechanical damage. From the electric point of view, the CdS layer optimises the band alignment of the device (Schmid *et al.*, 1996 and Contreras *et al.*, 2002) and builds a sufficiently wide depletion layer that minimizes tunneling and establishes a higher contact potential that allows higher open circuit voltage value (Contreras *et al.*, 2002). The buffer layer also plays a very important role as a “mechanical buffer” because it protects the junction electrically and mechanically against the damage that may otherwise be caused by the oxide deposition (especially by sputtering). Moreover, in large-area devices the electric quality of the absorber layer film in a solar cell is not necessarily the same over the entire area, and recombination may be enhanced at grain boundaries or by local shunts. The thickness as well as the deposition method of the CdS layer has a large impact on device characteristics.

In order to optimise the conditions that are appropriate for the deposition of a good buffer layer, Cadmium Sulphide thin films were deposited onto glass substrates by spin-coating method. Solutions for CdS were prepared from Cadmium acetate (BDH), 2-Methoxy ethanol, Thiourea (BDH) and polyethylene glycol (PEG 200, Merck). 2-Methoxy ethanol and PEG were used as the solvent and the stabilizer respectively. 0.4ml Poly ethylene glycol was dissolved in 20ml of 2-methoxy ethanol and stirred for 1 hour. Thereafter, 0.0186M of CdAc was added and stirring continued for another 30mins. After which 0.01582M of thiourea was dissolved in 5ml of 2-Methoxy ethanol and added drop wisely to the initially stirred solution. The entire solution precipitated and 2 drops of  $\text{HNO}_3$  were added to have a clear solution. The stirring continued for another 1 hour. Thereafter, it was filtered and aged for 48hours.

SLG substrates of  $(1.5 \times 1.5) \text{ cm}^2$  were treated by ultrasonic cleaning in chemicals (acetone then ethanol) and then rinsed with deionized water. The sol solution was dropped onto the SLG substrates at speeds of 1600, 1800, 2000 and 2200 rpm for 30seconds respectively. After deposition by spin coating the film was dried in air at  $200^\circ\text{C}$  for 3 mins to remove solvent and residual organics and film densification. The coating and drying processes were repeated 10 times to obtain thick films.

The thickness of the CdS films was measured with Dektak 8 Profilometer after etching a step between film and substrate with a 10% Volume of HCl solution. The surface morphology of

deposited films was characterized using a scanning electron microscope (SEM, EVO/MA 10(ZEISS)). The crystallinity of CdS thin films were analyzed with an X-ray diffractometer (MD-10), using Cu-K $\alpha$  radiation with wavelength, 1.5418Å.

The stoichiometries of the films were determined by using 25KV in an EDS analyzer installed in the scanning electron microscope. EDS analysis was made in 150 seconds and measured peaks were compared with the database to distinguish the chemical elements. The CdS transmittance spectrums were measured in the 400-800nm range using the AVEC spectrophotometer.

### 3.3.3. Preparation of the absorber layer

Presently, CZTS thin films are conventionally prepared in a vacuum atmosphere, rendering it rather expensive and complicated. Furthermore, CZTS thin films have been deposited under non-vacuum conditions such as spray pyrolysis and sol-gel method. The depositions of thin films under non-vacuum conditions have been done by sulphurizing deposited metallic precursors; but in this work, this method was not used. Rather, the CZTS thin films were first deposited onto the soda lime glass (SLG) by spin-coating method before sulphurising in the furnace.

As mentioned earlier, our process for the deposition of the absorber layer is a two-stage sequential process, these stages being:

**(i) Sol-gel preparation and deposition:** The optimization of our absorber thin film (CZTS film) was first considered. CZTS thin films were deposited onto glass substrates by spin-coating method. Solutions for CZTS were prepared from Copper Chloride (BDH), Tin (II) chloride (BDH), Zinc Chloride (BDH), 2-Methoxy ethanol, Thiourea (BDH) and Acetic acid as the stabilizer. 2-Methoxy ethanol and Acetic acid were used as the solvent and the stabilizer respectively. 0.8ml Acetic acid was mixed in 25ml of 2-methoxy ethanol and stirred for 1 hour. Thereafter, 0.1953g of CuCl<sub>2</sub>, 0.1200g of ZnCl<sub>2</sub> and 0.1568g of SnCl<sub>2</sub> were added and stirring continued for another 30mins. After which 0.4215g of thiourea was dissolved in 5ml of 2-Methoxy ethanol and added drop-wisely to the initially stirred solution. The entire solution precipitated and 2 drops of Acetyl acetone were added to have a clear solution. The stirring continued for another 30 minutes. Thereafter, it was filtered and aged for 48 hours.

Soda lime glass (SLG) substrates of dimension (1.5X1.5) cm<sup>2</sup> were treated by ultrasonic cleaning in chemicals (acetone then ethanol) and then rinsed with deionized water. The sol solution was dropped onto the SLG substrates at speeds of 1000, 1200, 1400 and 1600 rpm for 30 seconds respectively. After deposition by spin-coating, the film was dried in air at 250°C for 3 mins to remove solvent, residual organics and for film densification. The coating and drying processes were repeated 16 times to obtain thick films.

The thickness of the CZTS films was measured with Dektak 8 Profilometer after etching a step between film and substrate with a 10% Volume HCl solution. The surface morphology of deposited films was characterised using a scanning electron microscope [SEM, EVO/MA 10(ZEISS)]. The crystallinity of CZTS thin films were analyzed with an X-ray Diffractometer (MD-10) using Cu-K $\alpha$  radiation with wavelength, 1.5418Å.

The stoichiometry of the films was determined by using 25KV in an EDS analyzer installed in the scanning electron microscope (SEM). EDS analysis was made along 150 seconds and measured peaks were compared with the database to distinguish the chemical elements. The CZTS transmittance spectrums were measured in the 400-1000 nm range, using the AvaSpec-2048 Standard Fiber Optic spectrometer. The Spin-coater set up used in this research work is as shown in Figure.3.4

**(ii) Sulphurisation:** Sulphurisation is a relatively high-temperature step where the CZTS thin film is annealed in a high flux of sulphur vapour. This is to improve on the sulphur composition of the CZTS film as observed in the EDS analysis and to improve on the crystallinity of the film, following the observations made with the SEM analysis result. The glass ware made of silica used in the annealing process was fabricated at the Scientific Equipment Development Institute (SEDI), Minna for this research work. The setup mainly consists of 3 parts:

- (a) Evaporation zone
- (b) Sulfurisation zone
- (c) Cooling zone

**(a) Evaporation zone:** Argon gas was allowed to flow for 15-20 minutes before switching on the furnace to start the sulfurisation process. A small cylindrical furnace is used in this section of the setup. The temperature of the furnace can reach 140<sup>0</sup>C in about 15 minutes. The purpose of this furnace is to evaporate the elemental sulfur- (the melting point of sulfur is 120<sup>0</sup>C). Hence, in

the smaller oven, sulfur is brought to its melting point and the vapour formed in the chamber is carried away by Argon gas to the three zone furnace through the glassware to the bigger furnace where the sulfurization takes place. The laboratory set up is as shown in Fig. 3.11.

**(b) Sulfurization zone:** The bigger furnace has three zones, namely; Right zone (RZ), Middle zone (MZ) and Left zone (LZ). The RZ and LZ are to maintain a perfect temperature in the MZ where the substrates have been neatly arranged in the silica tube for sulfurization to take place. After switching on the smaller furnace and the temperature reaches  $140^{\circ}\text{C}$ , the furnace was switched on and water was allowed to flow through it. Thereafter, we set the RZ, MZ and LZ of this furnace to  $350^{\circ}\text{C}$  and water is allowed to flow through the other end of silica tubing (Cooling zone). After an hour, the MZ begins to ramp down due to its set point. At this time the RZ and LZ are equally set to room temperature ( $25^{\circ}\text{C}$ ). When the temperatures of all zones in the furnace reached  $140^{\circ}\text{C}$ , the small furnace was switched off.

Thereafter, the whole set up was allowed to cool to room temperature, shut down and the samples were brought out for further studies.

**(c) Cooling zone:** This zone is an extension of the silica tube from the sulfurising zone which consists of a water jacket which allows for the constant flow of water during the sulfurization to cool down the sulphur vapour. The cooled sulphur vapour is then dissolved in water to prevent pollution of the environment. After sulfurization and characterisation of the films, the conditions used in depositing the best film were used in depositing the absorber layer on the buffer layer (CdS layer). The sulfurisation zone and cooling zone is shown in Figure 3.12.

After carrying out the necessary optimization for each of the layers of the solar cell, the best parameters which gave the best films were used to grow our solar cells. Two different cells (A and B) with different buffer layer thicknesses (40nm and 60nm) were then grown.

#### **3.3.4. Contacts deposition**

Thermal Evaporation was used to deposit  $1\mu\text{m}$  of Silver (Ag) and Aluminium (Al) as front and back contacts through a metal mask unto the FTO and CZTS layers respectively. Cells A and B were introduced into the chamber sequentially since there was only one single substrate holder available. The mask was designed to cover less than 10% of the total active cell area. Evaporations were carried out at  $10^{-6}$  mbar at a rate of 2 nm/sec. The areas of the solar cells grown were  $(1.5 \times 1.5) \text{ cm}^2$  each.

Three zone  
furnace



Smaller furnace

**Fig.3.12. Sulphur vaporization section of the annealing process at the Physics Advanced Laboratory of the Sheda Science and Technology Complex, Abuja**





**Fig.3.13. Cooling section of the furnace during the annealing process at the Physics Advanced Laboratory of the Sheda Science and Technology Complex, Abuja**

Finally, the fabricated solar cells were placed under the solar simulator to determine their performance characteristics.

UNIVERSITY OF IBADAN LIBRARY

## CHAPTER FOUR

### RESULTS AND DISCUSSION

The results obtained for the stage-by-stage processes of fabricating  $\text{Cu}_2\text{ZnSnS}_4$  solar cell devices are as presented in the following manner. Firstly, the characterization results obtained from the optimization of the window layer (FTO) is presented and discussed, followed by that of the buffer layer (CdS), then the absorber layer (CZTS) and finally the results obtained from the characterization of our fabricated solar cells are presented and discussed.

#### 4.1 The Window layer ( $\text{SnO}_2\text{:F}$ ) optimization results:

About 30 runs of depositions of the FTO thin films were carried out on the APCVD machine. The films showed high optical transparency and good adhesion to the glass substrate. The effect of time of deposition and substrate temperature on both the transmittance and sheet resistance of the films were examined as detailed below.

##### 4.1.1. Effects of time of deposition on the light transmission and sheet resistance of films

The changes in the sheet resistance and transmission of light through the films made at different deposition times were studied to optimize the thicknesses of the deposited FTO thin films. As shown in Figs.4.1 (a) & (b), the sheet resistance of the films prepared at the same substrate temperature ( $300^\circ\text{C}$ ) decreases with increase in deposition time. The transmittance of the films decreases with increase in deposition time as shown in Fig.4.2. These results obtained are in agreement with the results of Sheel *et al.* (2009). It shows that there is an optimization of the FTO film thickness to achieve the sufficient electrical conductivity and at the same time keep the optical absorption losses low (high transmittance). It was observed that films with large time of depositions were thicker and had milky appearances when observed in air. These reveal an improved conductivity (low sheet resistance values) but poor transmittance to light in the UV region.

##### 4.1.2. Effects of deposition (substrate) temperature on the light transmission and sheet resistance of films

As shown in Fig.4.3, the sheet resistance increased as the substrate deposition temperature increases while the transmittance of the films increased with the temperature of the

substrate (as shown in Fig.4.4). The increase in the sheet resistance and the transmittance of the films indicate that the conductivity of the films reduces with increase in substrate temperature while the transmittance increases, which shows an improvement of the passage of light in the visible region through the films. These results are in agreement with those of Sheel *et al.* (2009). Also, these observations are due to the efficient incorporation of donors at higher temperature and defect concentrations as suggested by Zdenek *et al.* (2009). In addition, these results (as shown in Fig.4.4.) confirm that the transmittance trend in Fig.4.3. is quite in order.

In conclusion, the effects of substrate temperature and deposition time on the optical and electrical properties of SnO<sub>2</sub> films grown by APCVD method were assessed. The optical transmittance and the sheet resistance of TCO films prepared under the same conditions decrease with increase in deposition time (as the thickness of the film increases with deposition time). The substrate temperature influences both the incorporation ratio of dopants into the SnO<sub>2</sub> film during the growth as well as the defect concentration. The optimized SnO<sub>2</sub> films have the sheet resistance of 15.8Ω/sq and optical transmittance of 80%.

#### **4.2. The Buffer layer (CdS) optimization results:**

The deposition speed of our films on the spin-coater was used to arrive at the appropriate speed for the deposition of good CdS thin film for the buffer layer of the solar cell. The speed considered were 1600 rpm, 1800 rpm, 2000 rpm and 2200 rpm respectively. The optical, structural and morphological characterisation results of these films are presented and discussed. It is observed that film thickness increases with increasing number of cycle for a determined spinning speed. This makes film with controlled thickness to be deposited. The average baked thickness was evaluated to be about 20 nm per coating cycle by using the Profilometer. Generally, the thickness of the coating depends on the speed at which solution level falls, concentration, and viscosity of the respective solution, temperature and relative humidity.

Fig.4.5 (a) shows typical XRD pattern for a CdS film prepared by 10 cycles spin-coating of CdS films followed by post-deposited heat treatment. The presence of small peaks in the pattern indicates that the films are nanocrystalline in nature. The X-ray diffraction pattern shows that the CdS films exhibit hexagonal structure with (002) orientation. The average size of grains has been obtained from the x-ray diffraction pattern using Scherrer's formula (Devi *et al.*, 2007).

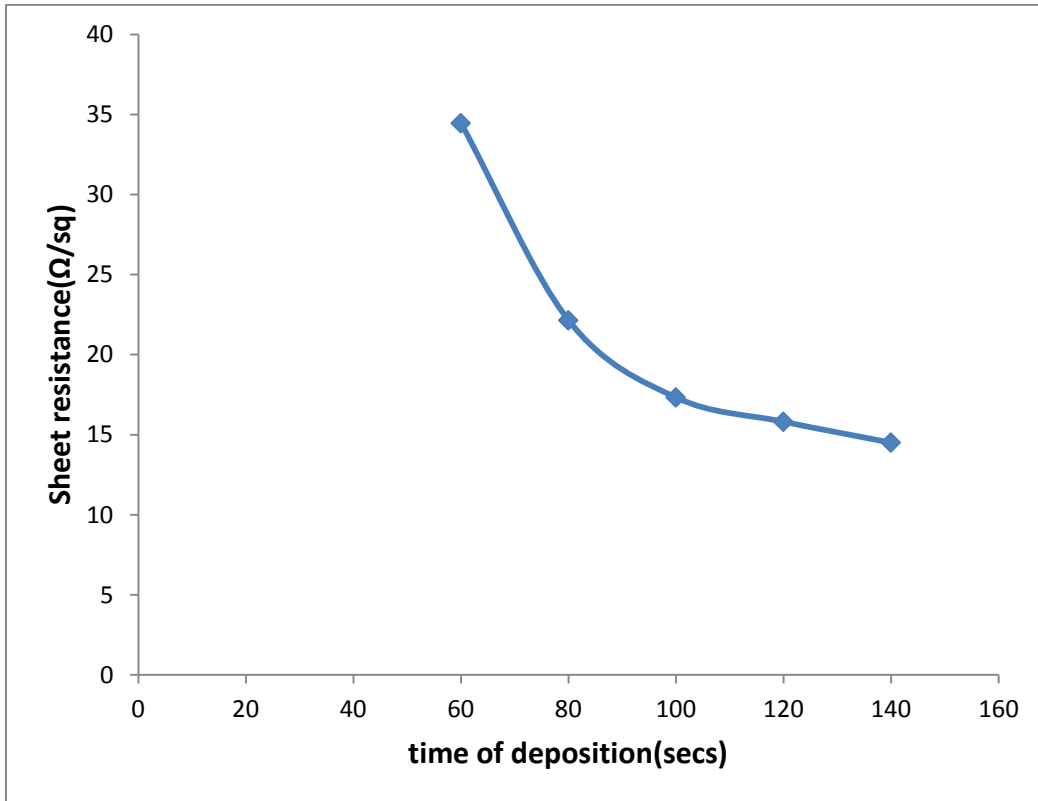


**Fig.4.1. (a) Dependence of sheet resistance of FTO film on deposition time**

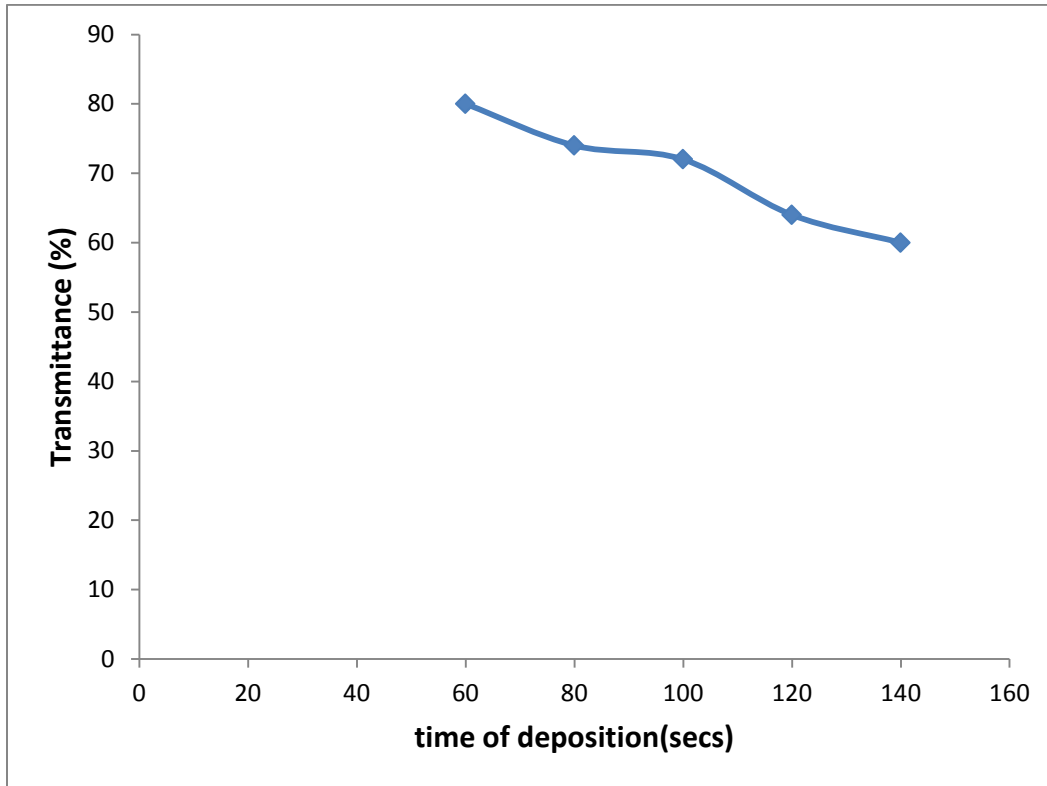


**Fig.4.1. (b) Dependence of transmittance of FTO film on deposition time**

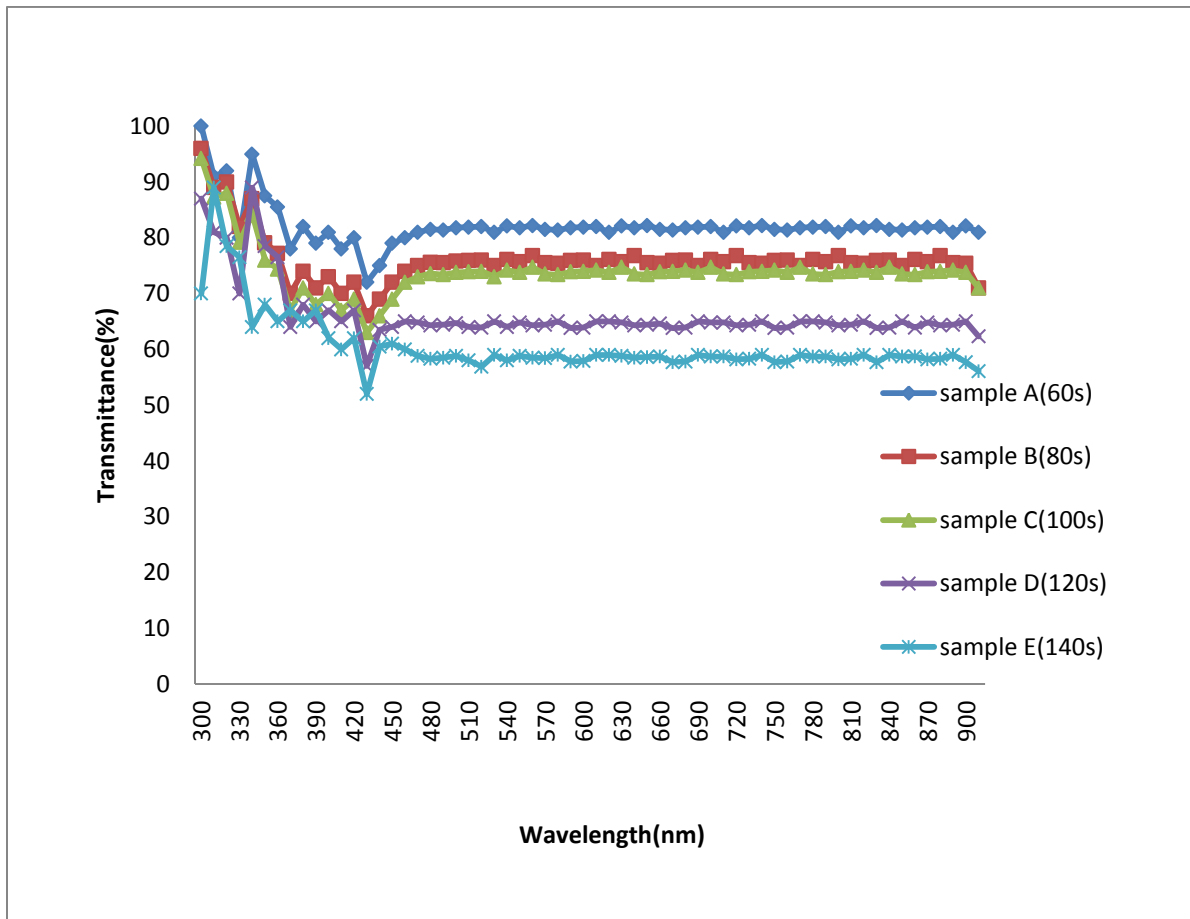


**Fig.4.2. UV-Visual light transmission of FTO films prepared at different deposition times**

UNIVERSITY

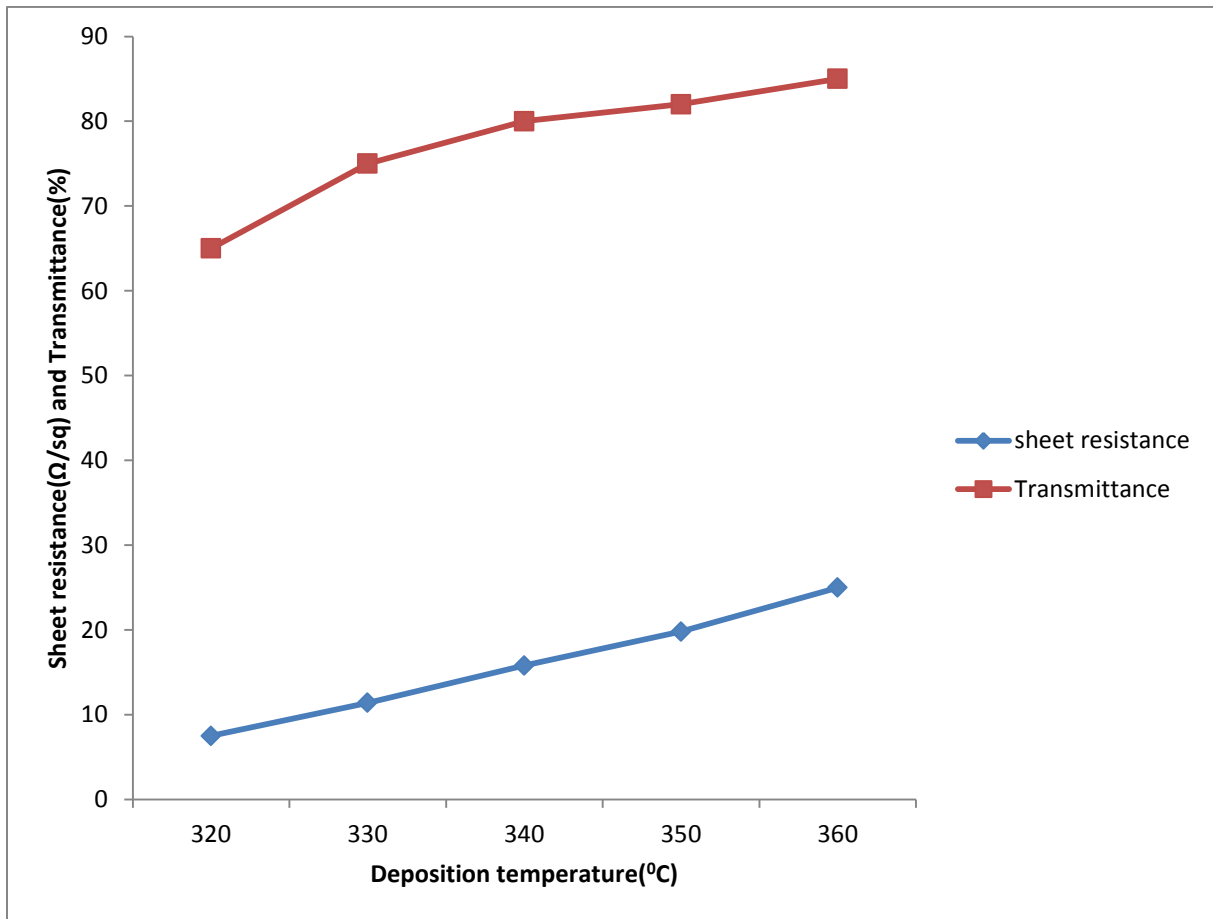


**Fig.4.3. Dependence of sheet resistance and transmittance of FTO film on deposition temperature**

UNIVERSITY



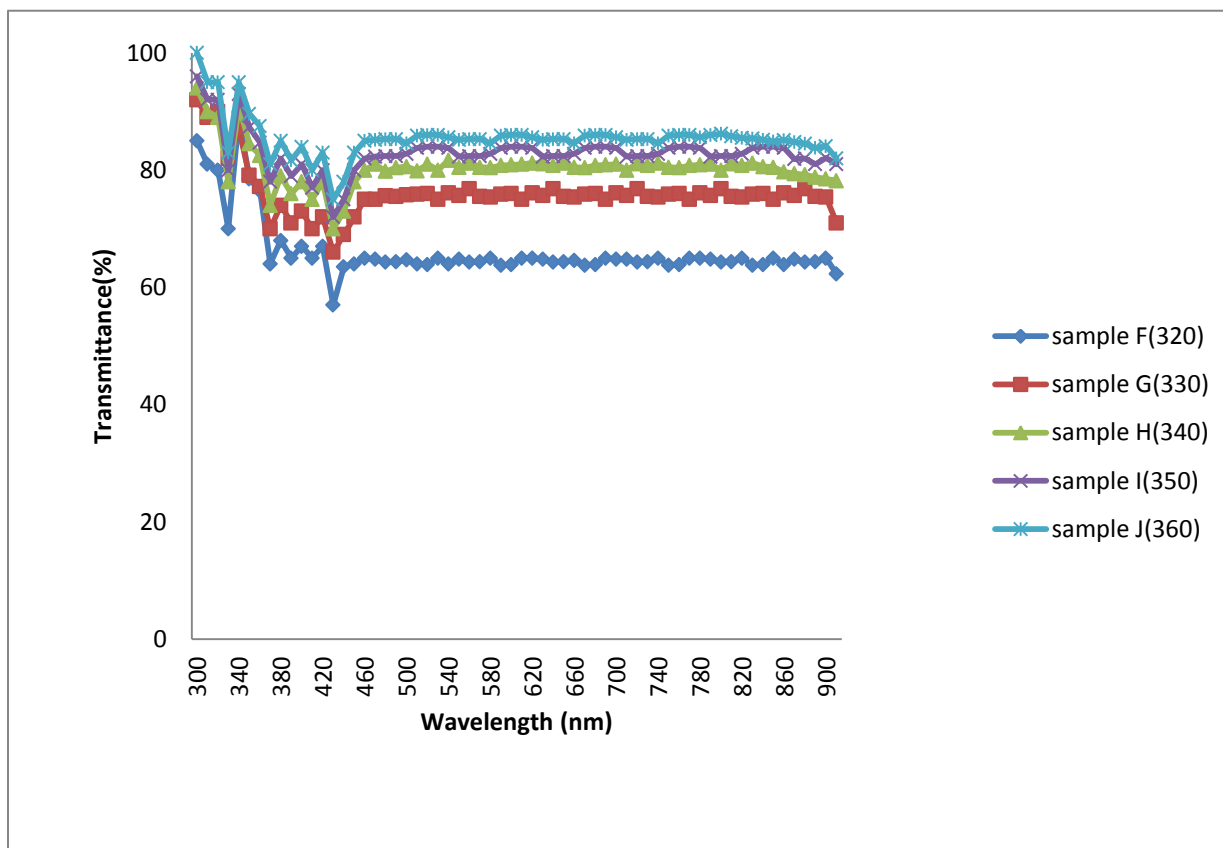


**Fig.4.4. UV-Visible light transmission of FTO films prepared at different substrate temperatures**

$$D = \frac{K\lambda}{\beta \cos\theta} \quad (4.1)$$

Where D is the grain size, K is a constant taken to be 0.94;  $\beta$  is the full width at half maximum (FWHM),  $\theta$  is the Bragg angle and  $\lambda$  is the wavelength of the x-rays. The CdS crystallite sizes have been determined from width of the x-ray diffraction to be 5.5nm to 6.8nm for the films. The peaks are not sharp, indicating that the average crystallite size is small. Due to size effect, the peaks in the diffraction pattern broaden and their widths become large as the particles become smaller.

Fig.4.5 (b) shows the surface image of the CdS thin film. A continuous film was formed from aggregation of granules as shown in Fig.4.5 (b), although a surface image of the precursor film was very smooth. The film showed larger and densely packed grains than the film reported by (Sanap and Pawar, 2009).

From the transmission  $T(\lambda)$  and reflection  $R(\lambda)$  data, the absorption coefficient was calculated using the formula by Bube (1974).

$$\alpha = \frac{1}{t} \ln \left[ \frac{(1-R(\lambda))^2}{T(\lambda)} \right] \quad (4.2)$$

where t- is the film thickness.

For direct allowed transition the values of  $\alpha$  follow the formula by Kireev (1977).

$$\alpha \sim A(h\nu - E_g)^{1/2} \quad (4.3)$$

Where  $E_g$  is the optical band gap and  $h\nu$  is the photon energy.

The optical band gap has been calculated by plotting  $(\alpha h\nu)^2$  versus  $h\nu$  (figure 4.6(a)-(d)) for films grown at different deposition speeds. As the plots show linear dependence, the optical band gap values were determined from the intercept with x-axis (energy axis). The calculated optical band gap values are found to be in the range of 2.18-2.40eV.

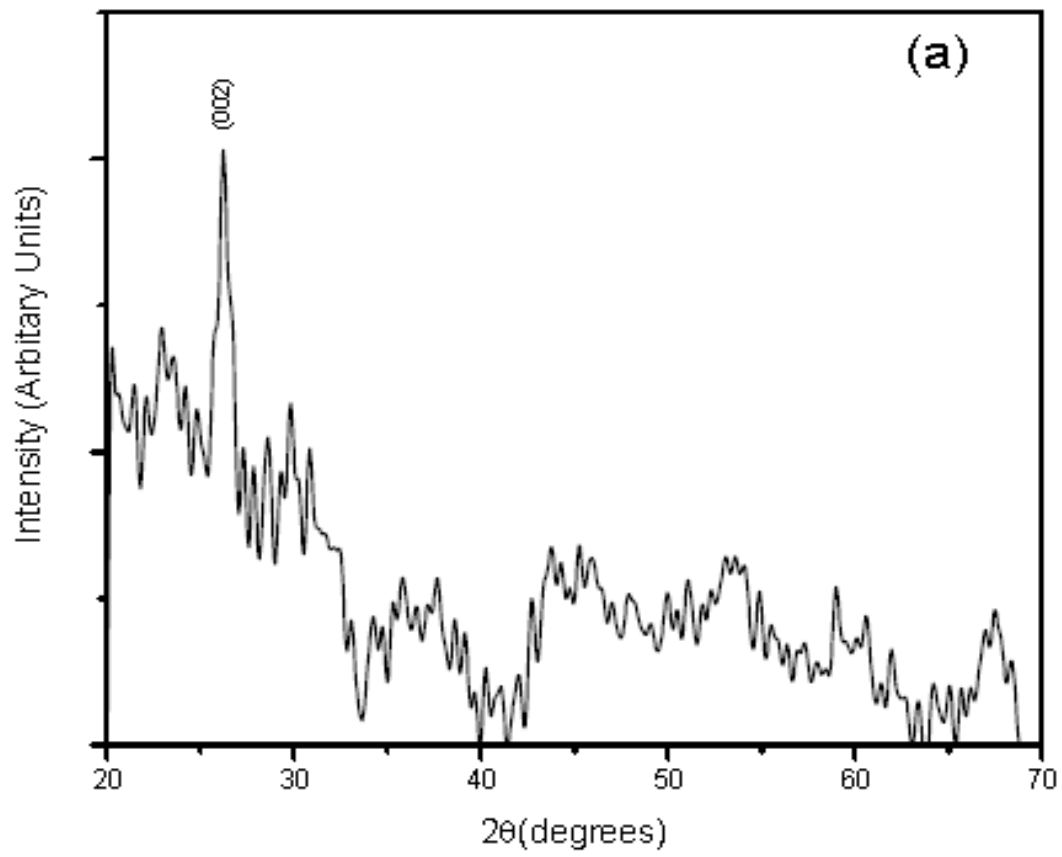


**Fig.4.5 (a): X-ray diffraction pattern of CdS film (10cycles)**

The value of energy band gap of the film obtained using the absorption spectra are closer to the bulk band gap (2.42eV) and the closest is the film deposited at 1,600 rpm which gave 2.4eV.

In conclusion, a simple and very cheap route to obtain CdS was used, starting with a precursor solution based on Cadmium acetate, Thiourea, 2- Methoxy methanol and PEG spin-coated onto glass substrates. It was found out that the film properties can be controlled by spinning speed and number of deposition cycles. The obtained films were uniform and smooth, and had a good adherence to the substrates, especially for films deposited at speed of 1,600 rpm. The films analyzed by x-ray diffraction technique indicated the presence of the (002) crystal planes corresponding to CdS hexagonal structure. Also, the films had good stoichiometry. The band gap energy values obtained for these samples were in the range between 2.18 and 2.40eV, depending on the deposition speed and the number of cycles. Nanocrystalline CdS thin film suitable for solar cell application has been prepared. This makes it easier to grow buffer layers of CdS thin film for solar cells through the spin-coating method instead of undergoing the rigours of the usual Chemical Bath deposition method.

#### **4.3. The Absorber layer ( $\text{Cu}_2\text{ZnSnS}_4$ ) optimization results:**

Also, the deposition speed of our films on the spin-coater was used to arrive at the appropriate speed for the deposition of good CZTS thin film for the absorber layer of the fabricated solar cell. The speed considered were 1000 rpm, 1200 rpm, 1400 rpm and 1600 rpm respectively. The optical, structural and morphological characterization results of the best film at 1200rpm after sulphurization is presented and discussed as well.

The analysis of samples by XRD can provide important insights in the structure of films. The identification of crystalline secondary phases is a powerful tool that is not possible with other analyzing methods used. However, the drawback of this technique is that XRD results are difficult to interpret in cases of peak overlap and multiple-phase systems. The X-ray diffraction pattern shows peaks appearing at  $28.55^\circ$  and  $48.61^\circ$ . These peaks are due to diffraction from (1 1 2) and (2 2 0). The prominent one is (1 1 2) and this indicates that the film was oriented to (1 1 2) which is similar to other reports (Katagiri *et al.*, 2001, Tanaka *et al.*, 2006). Fig.4.8. shows the surface image of the CZTS film. It shows the formation of a continuous and smooth film. The film had smaller grain size as compared to the work of Kunihiko *et al.* (2009) and there are no large voids on the surface of the film.

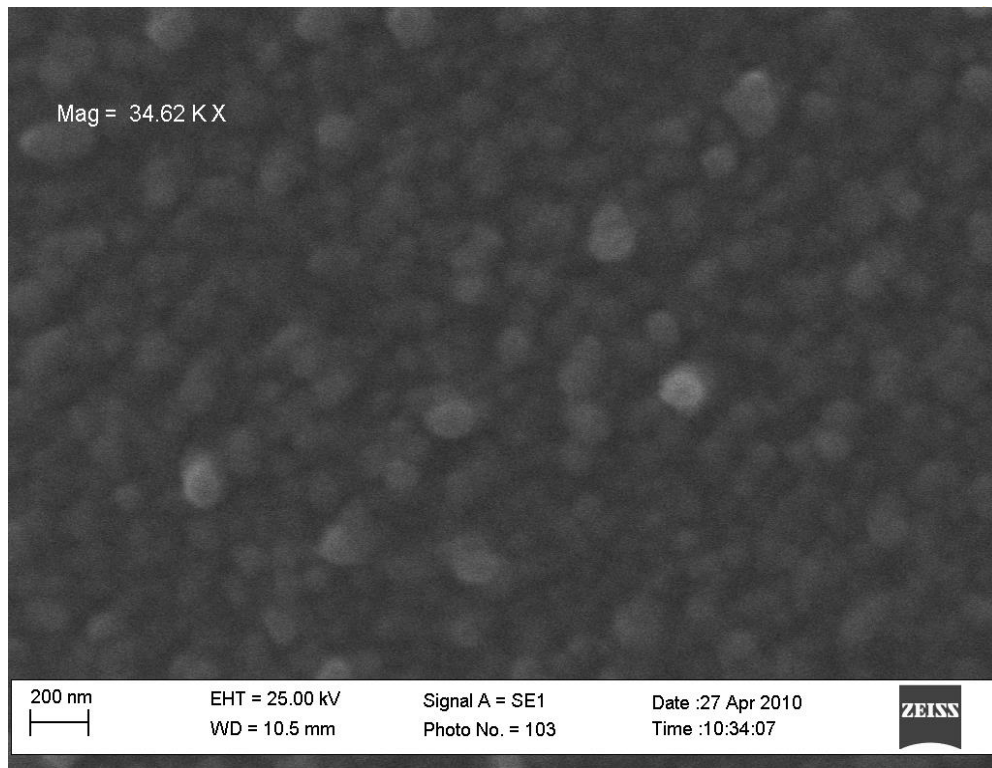


**Fig.4.5 (b) SEM micrograph of CdS thin film (10 cycles)**

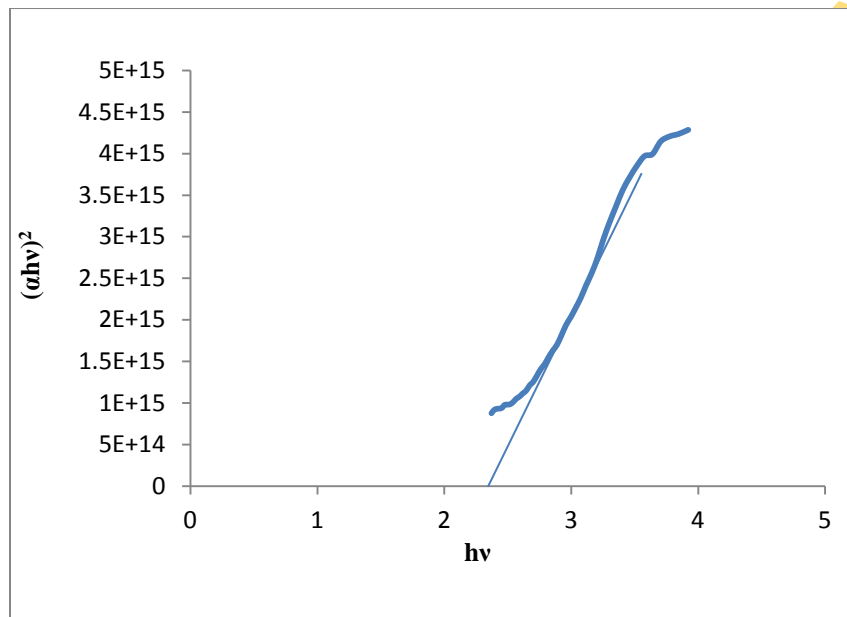


**Fig.4.6 (a)  $(\alpha h\nu)^2$  as a function of photon energy ( $h\nu$ ) for films deposited at 1600 rpm**

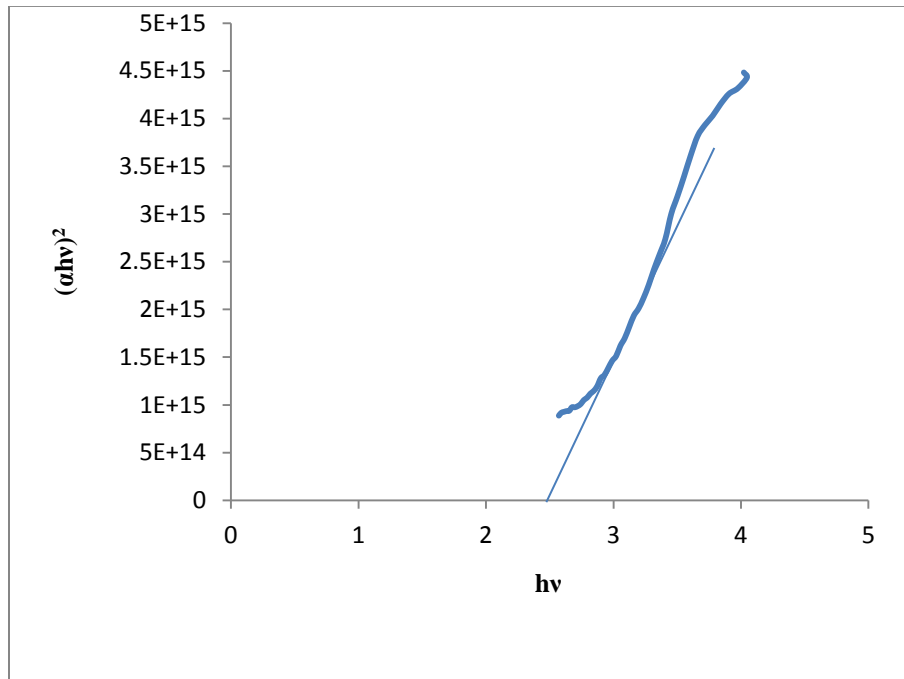
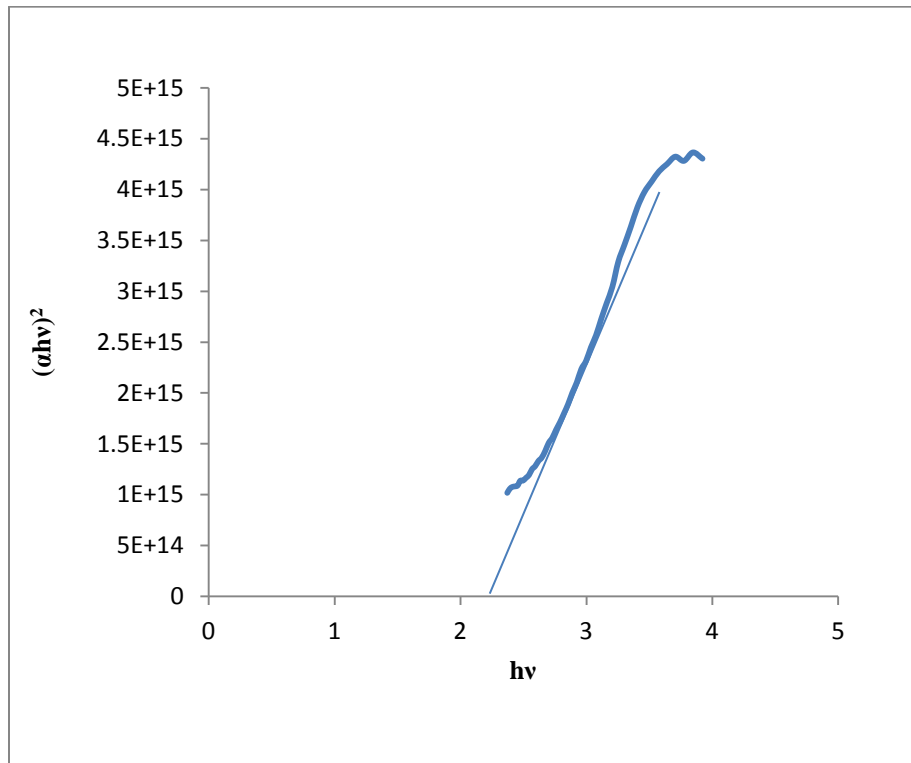


Fig.4.6 (b)  $(\alpha h\nu)^2$  as a function of photon energy ( $h\nu$ ) for films deposited at 1800 rpm



**Fig.4.6(c)  $(\alpha h\nu)^2$  as a function of photon energy ( $h\nu$ ) for films deposited at 2000 rpm**



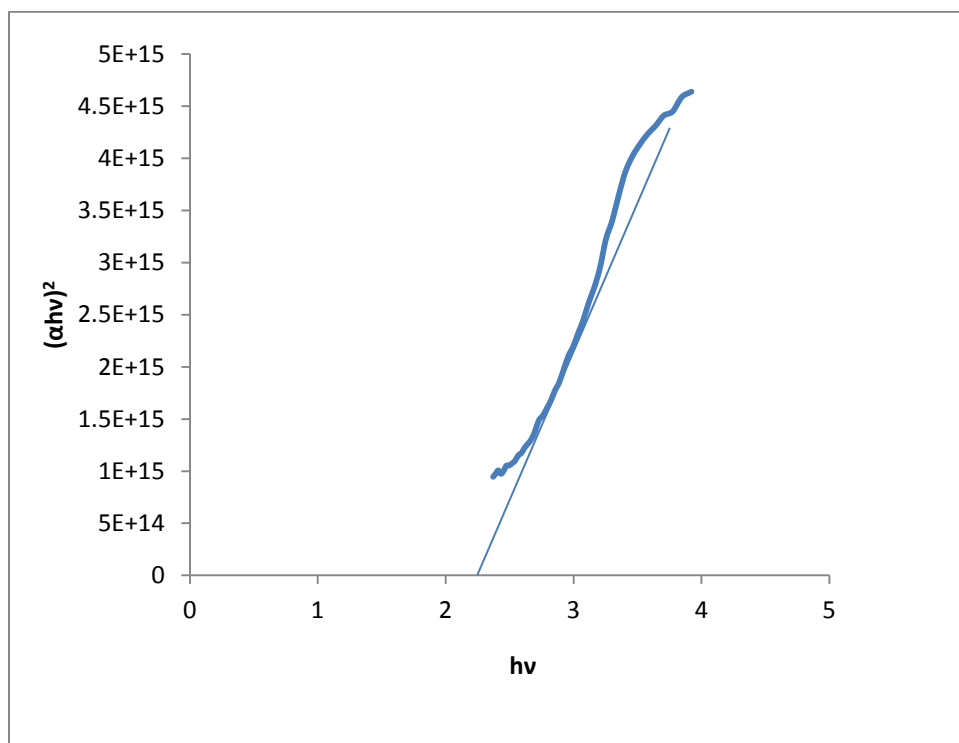


Fig.4.6 (d)  $(\alpha h\nu)^2$  as a function of photon energy ( $h\nu$ ) for films deposited at 2200 rpm

The optical band gap of the samples were deduced from the plot of  $(\alpha h\nu)^2$  vs  $h\nu$  as shown in Fig.4.10., by extrapolating the straight line portion of the graph in the high absorption regime, where  $\alpha$  and  $h\nu$  are absorption co-efficient and photon energy. It was observed that our CZTS film had a band gap of  $\sim 1.51$ eV. This band gap is comparable with result from Tooru *et al.* (2010). The absorption co-efficient in the visible region was larger than  $10^4$ cm<sup>-1</sup>. The optical properties of the CZTS thin film are suitable for absorber layer of the thin film solar cells.

EDX measurements were done for analyzing the composition of the CZTS films. The Spectrogram of the EDX is shown in Fig.4.9. and the chemical composition is as shown in Table 4.1.

The chemical composition of the CZTS thin film was almost stoichiometric but slightly S poor. It is observed from the EDX spectrogram that the sulphurised CZTS film contains other impurities such as Carbon, Oxygen, Silicon, Magnesium and Calcium. The Oxygen could have been introduced as a result of improper cleaning of the surface of the soda lime glass (SLG) while other elements found are from the glass substrate. Most of the impurities were introduced as a result of non-availability of clean room because the doors to the laboratories were being opened frequently.

In conclusion, it could be said that it was possible to control film quality only to a very limited extent. However, these results concern only the appearance of the material. The next section will shed light on the impact of these parameters on the efficiency of the fabricated solar cells.

#### **4.4. The solar cells:**

The final analysis that was performed on the solar cells was the determination of the performance of the fabricated solar cells. The most important aspect of this research used to evaluate the quality of the solar cells is the efficiency which is determined from I-V measurements. The solar cells A and B fabricated in the laboratory of different buffer thicknesses (40nm and 60nm) were placed under the solar simulator for I-V characterization. During the I-V measurements, the cells are illuminated; the current is measured while the voltage is varied. Further discussions on possible influences on the IV behaviour of the cells will be enumerated.

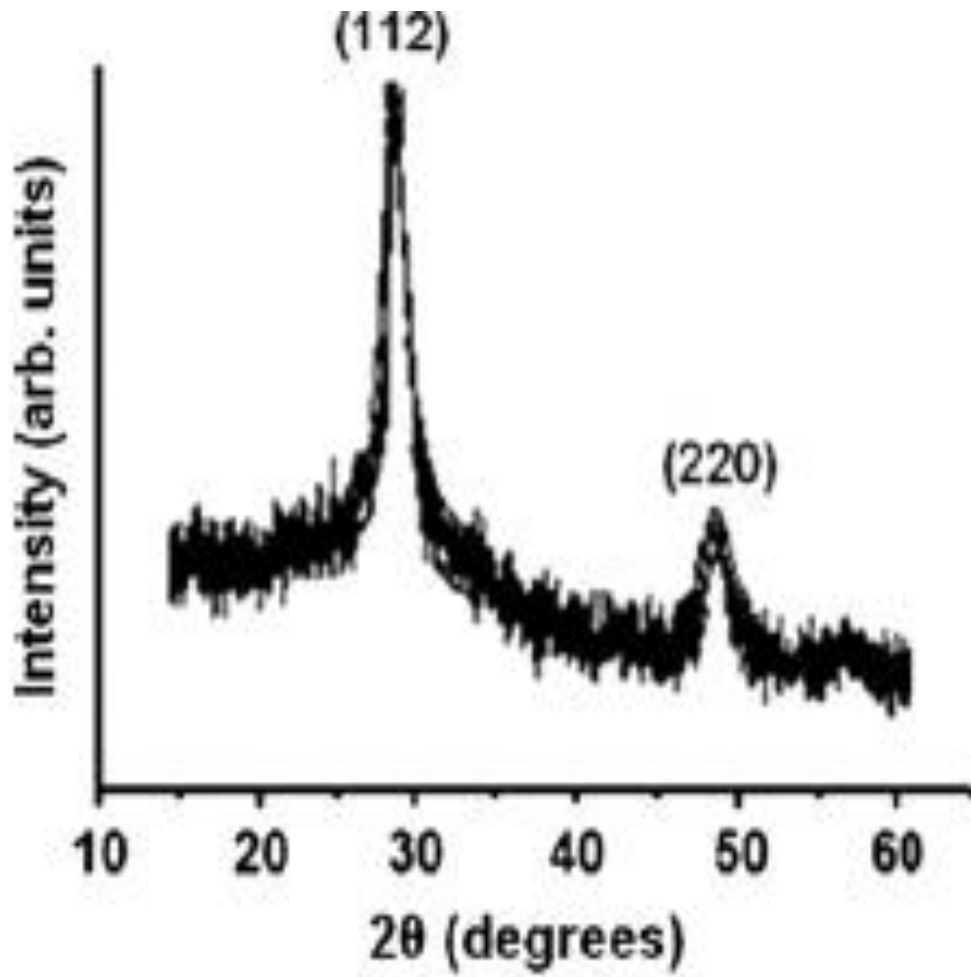
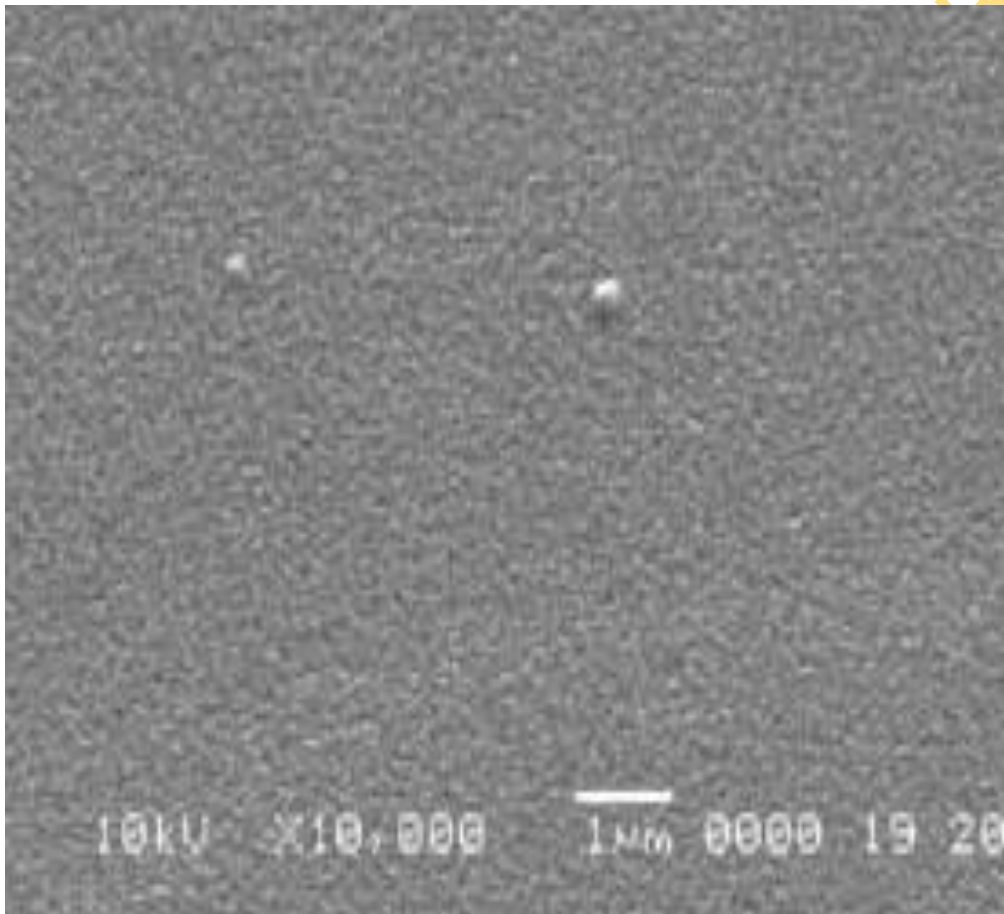
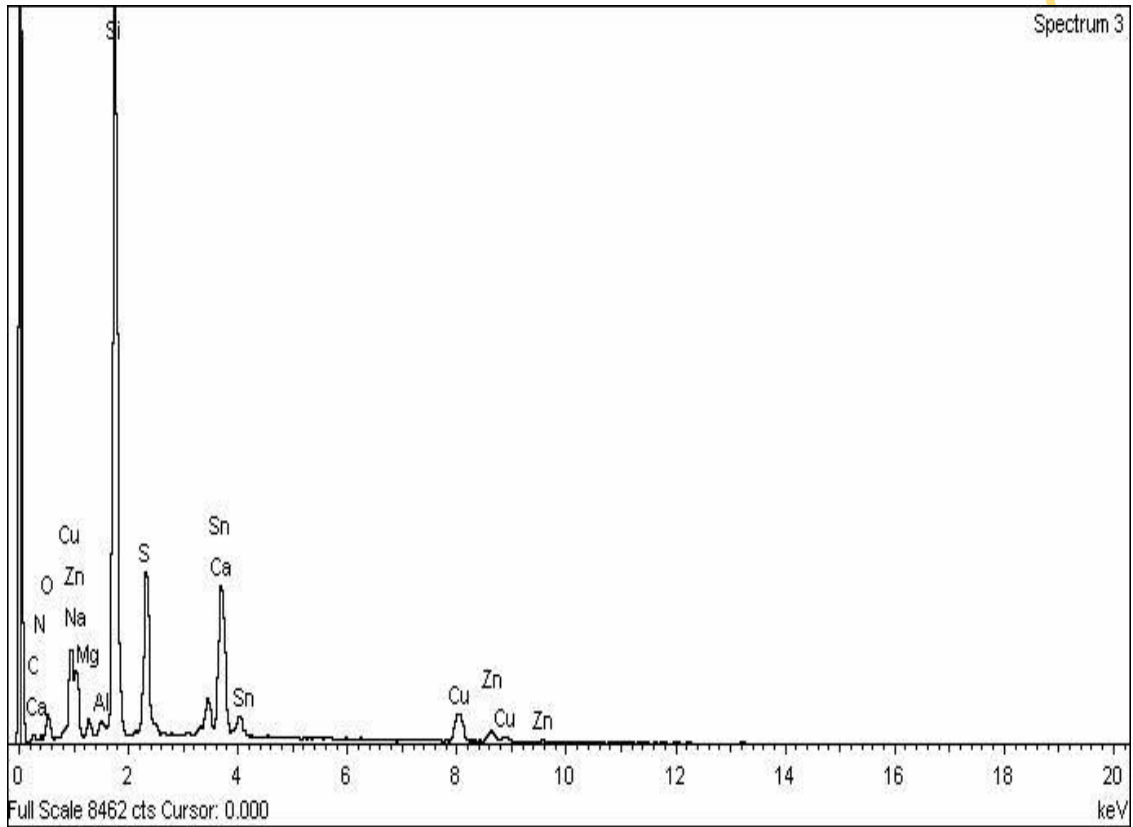


Fig.4.7 X-ray diffraction pattern of CZTS films grown on soda lime glass



**Fig.4.8 Surface morphology (SEM image) of the CZTS thin film**



**Fig.4.9. EDX Spectrogram of CZTS film**

**Table 4.1 Chemical compositions of CZTS thin films**

	Chemical composition (at %)				Ratio of Composition		
	Cu	Zn	Sn	S	Cu/(Zn+Sn)	Zn/Sn	S/metal
CZTS thin film	24	14	13	47	0.89	1.08	0.92

UNIVERSITY OF IBADAN LIBRARY

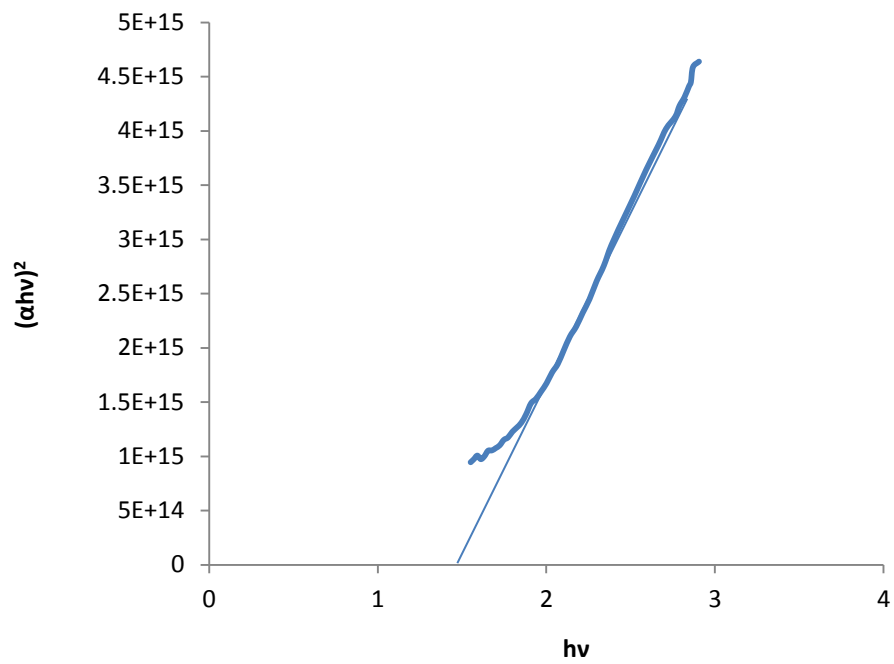


**Fig.4.10.** Absorption spectrum of CZTS thin film

UNIVERSIT

The open circuit voltages and short circuit current densities were determined from Figs 4.11 (a) & (b) as indicated on Fig.2.3. The fill factors (ff) were determined according to eq. (2.10) while the conversion efficiencies were calculated using eqn. (2.12). Fig.4.11 (a) which has a buffer layer thickness of 40nm had the best parameters (open circuit voltage of 262 mV, a short circuit current density of 3.544 mA/cm<sup>2</sup>, a fill factor of 0.30 and a conversion efficiency of 0.28%) while Fig.4.11 (b) with a buffer thickness of 60nm had an open circuit voltage of 240mV, a short circuit current density of 2.100 mA/cm<sup>2</sup>, a fill factor of 0.26 and a conversion efficiency of 0.13%.

The efficiencies of the fabricated solar cells are lesser when compared to those reported by Qin Miao Chen *et al.* (2011), which had 0.53% and 0.55% for those fabricated by Chen Qin-Miao *et al.* (2011). The transmittance of the best SnO<sub>2</sub>:F film deposited is 80% in the visible and near infra red region. Therefore the transmittance of the SnO<sub>2</sub>:F (window layer) was not the cause of the low efficiency. However, the insufficient incorporation of Na into the absorber layer as a result of the FTO (and other TCO's) acting as diffusion barrier inhibits sufficient supply of Na from the soda lime glass substrate, resulting in a low effective carrier density and low open circuit voltage (Huang *et al.*, 2003). The inclusion of sodium into the absorber layer enhances the conductivity of thin films (Su-Huai *et al.*, 1999). Also, a probable reason could be as a result of poor heterojunctions between FTO and CZTS as suggested by Huang *et al.* (2003) with CIGS which led to poor J-V characteristics. Thus, incorporation of Na into the absorber layer should be adopted to enhance the efficiency of this superstrate CZTS thin film solar cell.

The chemical composition of the CZTS thin film was almost stoichiometric but slightly sulphur poor. Therefore, the non-stoichiometry of our sol-gel and small grain size of CZTS can lead to a short diffusion length of carriers. This short diffusion length of carriers is one of the reasons for the resulting low efficiency.

The small grain size and Sulfur poor chemical composition could be improved by sulfurization at higher temperature or in higher concentration of elemental sulfur.

The CdS layer could be another possible reason for the low efficiency of our solar cell. This is due to the fact that the CdS layer was prepared by the sol-gel method and not by Chemical bath deposition method which has been recognized to be the best method for the deposition of CdS buffer layer. Also, the effect of the deposited CdS buffer layer by the sol-gel



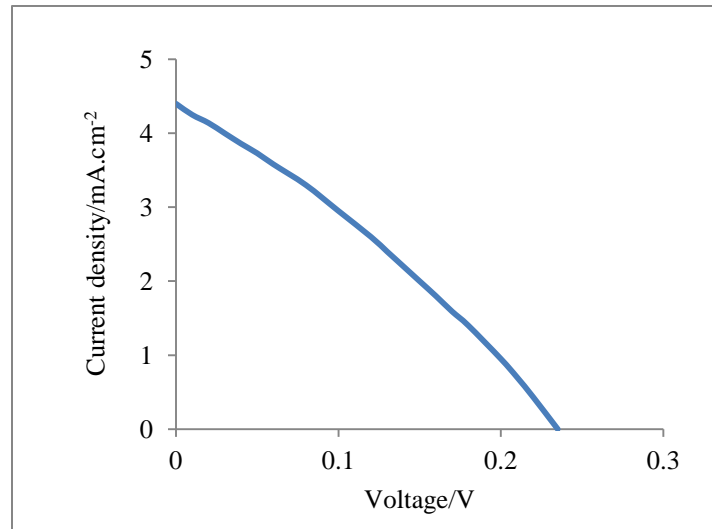


**Fig.4.11 (a) J-V characteristics of the most efficient CZTS photovoltaic cell with an active area of 2.25 cm<sup>2</sup> (buffer layer thickness of 40nm)**

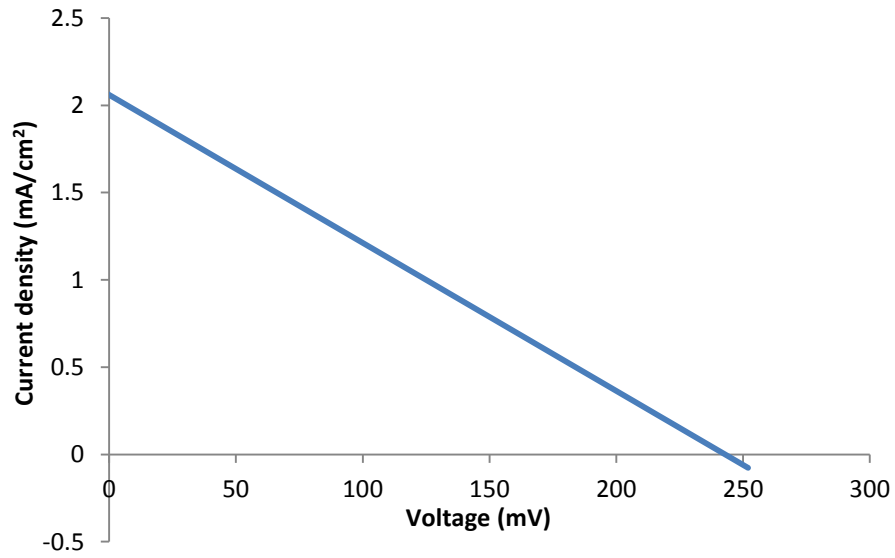


**Fig.4.11 (b) J-V characteristics of a typical CZTS photovoltaic cell with an active area of 2.25 cm<sup>2</sup> (buffer layer thickness of 60nm)**

method was not studied and it was reported that CdS buffer layers greatly affect the properties of thin film solar cells such as efficiency and rectification characteristics (Kylner, 1999).

These reductions in the performance characteristics have led to the low efficiencies of our produced cells. The low current indicates general losses for electron collection; the fill factor is reduced by parallel and series resistances in our cells. The efficiency is affected by these losses (i.e. lower than it would be possible for this material). The results show the possibility of the presence of secondary phases which leads to the loss of active area (affects  $I_{sc}$ ). Pinholes, voids and other defects could be further reasons for the described effects. For this experimental series it was not possible to correlate the observed phenomena to certain defects, it can only be stated that – like for the efficiency part – the best IV characteristic results were found for solar cell sample with a buffer layer thickness of 40nm.

In conclusion, the best solar cell fabricated in this experimental series had 0.28% efficiency and the band gap of the CZTS films were estimated as  $\sim 1.51\text{eV}$ . However, the potential for this material is much higher than what was measured for the samples. I-V measurements revealed that there were significant losses due to low values of  $I_{sc}$  which indicates general losses in charge carrier generation and collection. Also, secondary phases, voids, layering and bad adhesion can increase the series resistance while recombination as well as shunting could be responsible for these low performance characteristics.

## CHAPTER FIVE

### CONCLUSION AND RECOMMENDATIONS

#### 5.1 Conclusion

The commercial viability of solar cells is fast evolving in recent time. Recent advancements in thin-film technology have contributed significantly to the bullish expansion in the solar industry. However, the need to provide environmental friendly and low cost thin film solar cell are still being investigated. Generally, the existing challenges in conventional energy budget even on global scale have led to the shift of interest towards alternative energy sources. In the case of Nigeria, thin film solar cells may provide the required alternative energy sources.

In this research work, simple fabrication methods (non-vacuum methods) were considered for the deposition of each of the layers of the solar cells. The window layer ( $\text{SnO}_2\text{:F}$ ) was deposited using the Atmospheric Pressure Chemical Vapour Deposition method (APCVD) wherein the APCVD set up was locally fabricated at the Sheda Science and Technology Complex, the buffer layer (CdS) was deposited using the sol-gel spin coating method and the absorber layer (CZTS) was deposited using the sol-gel spin coating method as well. These methods were adopted to see to the possibility of fabricating, inorganic thin film solar cells in the country at low cost.

The optical characterization of our thin films reveals that our buffer and absorber layers have approximately 2.40eV and 1.51eV respectively as their energy bandgaps. The XRD analysis of the CZTS thin film indicates that our films were oriented to (1 1 2). Also, the SEM image of the CZTS thin film reveals the formation of a continuous, smooth, smaller grain size without large voids on the surface of the film. The EDX measurements of our CZTS thin film was almost stoichiometric but slightly sulphur poor.

The performance characteristics of our fabricated solar cells with active area of  $2.25\text{cm}^2$  and buffer thicknesses of 40nm and 60nm reveals these cells have efficiencies of 0.28% and 0.13% respectively. In conclusion, the possible reasons for the low efficiencies of our fabricated solar cells are as follows:

- (i) The non-stoichiometry of our sol-gel and small grain size of CZTS thin film can lead to a short diffusion length of carriers.
- (ii) The CdS layer is another possible reason for the low efficiency of our solar cell as reported by Kylner (1999).

- (iii) Inability to get proper masking material which resulted into poor heterojunction between the SnO<sub>2</sub>:F and the CZTS as suggested by Haug *et al.* (2003) for CIGS solar cells.
- (iv) Non-availability of a clean room.
- (v) Insufficient incorporation of Na into the absorber layer as a result of the SnO<sub>2</sub>:F (FTO) acting as diffusion barrier inhibits sufficient supply of Na from the soda- lime glass (SLG) substrate, resulting in a low effective carrier density and low open circuit voltage as reported by Su-Huai *et al.*(1999).

## 5.2 Recommendations

It is recommended that the following steps be taken for future research work to enhance the present efficiencies of the superstrate CZTS thin film solar cells which can be used as tandem cells with existing inorganic cells. They are as follows:

- (i) Investigations into the heterojunction of the semiconductor layers of the CZTS superstrate cells for bulk and interface defects.
- (ii) Investigations of ordered defect compounds existence in the CZTS layer.
- (iii) Usage of alternative buffer layers compounds to see if there will be an improvement in the overall performance characteristics of the CZTS solar cells.
- (iv) Improvement on the stoichiometry of the CZTS thin film and annealing at higher temperature in elemental sulphur to further improve on the structure and surface morphology of the films.

Finally, it is recommended that Nigerian government should endeavour to support academic research, so as to create conducive atmosphere that will support fabrication of solar cells. It is hoped that this research will assist the Federal Government of Nigeria in its drive towards improving electricity supply to cities and villages through the use of locally fabricated solar cells in hard-to-reach areas in certain regions of the country. This will assist in improving security in these rural areas as surveillance equipment can be powered using the solar cells. Also, the fabrication of these solar cells locally will make it cheaper and allow the country to pursue the global trend in trying to get alternative energy sources so as to minimize the effect of global warming.

## REFERENCES

- Adams, W. G. and Day, R. E. (1876). The action of light on selenium. *Proceedings of Royal Society, London*, vol. 25, p. 113.
- Babichuk, I. S., Yukymchuk, V. O., Dzhagan, V. M., Valkh, M., Leon, M., Yanchuk, I. B., Gule, E. G., and Greshchuk, O. M. (2013). Thin films of  $\text{Cu}_2\text{ZnSnS}_4$  for solar cells: Structural and Optical Properties. *Functional Materials*, 20, No 2, p 186-191.
- Balboul, M. R., Jasenek, A., Chernykh, O., Rau, U., and Schock, H. W. (2001).  $\text{CuGaSe}_2$ - based superstrate solar cells. *Thin Solid Films*, 387:74-76.
- Becquerel, A. E., (1839). Mémoires sur les effets électriques produits sous l'influence des rayons. *Comptes rendus de l'Academie Scientifique*, vol. 9, p. 561.
- Bube, R. H. (1974). Electronic properties of crystalline solids. *Academic Press, London*, p 152.
- Birkmire, R. W., Mc candler, B. E., and Hegedus, S. S. (1992). Effects of processing on CdTe/CdS materials and device. *International Journal of Solar Energy*, vol.12, p145.
- Carlson, D., and Wronski, C. (1976). Amorphous silicon solar cells. *Applied Physics Letters*, vol.28, pg 671.
- Chapin, D. M., Fuller, C. S., and Pearson, G. L. (1954). A new silicon p-n junction photocell for converting solar radiation into electrical power. *Journal of Applied Physics*, vol. 25, p 676.
- Chen, Q., Li, Z., Ni, Y., Cheng, S., and Dou, X. (2012). Doctor-bladed  $\text{Cu}_2\text{ZnSnS}_4$  light absorption layer for low-cost solar cell application. *Chinese Physics B*, 21(3): 384-389.
- Contreras, M. A., Romero, M. J., To, B., Hasoon, F., Noufi, R., Ward, S., and Ramanathan, K. (2002). Optimization of CBD CdS process in high-efficiency  $\text{Cu}(\text{In,Ga})\text{Se}_2$ -based solar cells. *Thin Solid Films*. (403-404):204–211.
- Devi, R., Purkayastha, P., Kalita, P.K., and Sarma, B.K. (2007). Synthesis of nanocrystalline CdS thin films in PVA matrix. *Bulletin of Material Science*, 30, p123.
- Emery, K. (2003). Handbook of photovoltaic science and engineering, Eds. A. Luque and S. Hegedus. (Wiley, New York), Chap. 16.
- Emsley, J. (1998). The elements, 3rd ed., *Oxford University Press, Oxford*. 289pp.

- Friedlmeier, T. M., Wieser, N., Walter, T., Dittrich, H., and Schock, H. W. (1997). Heterojunctions based on  $\text{Cu}_2\text{ZnSnS}_4$  and  $\text{Cu}_2\text{ZnSnSe}_4$  thin films. *Proceedings of the 14th European Conference of Photovoltaic Science and Engineering and Exhibition, Bedford*. 1242pp.
- Girtan, M., Boutiville, A., Rusu, G. G., Rusu, M. (February 2006). Preparation and properties of  $\text{SnO}_2:\text{F}$  thin films. *Journal of Optoelectronics and advanced materials*, 8 (1): 27-30.
- Gabor, A. M., Tuttle, J. R., Albin, D. S., Contreras, M. A., Noufi, R., and Hermann, A. M. (1994). High-efficiency  $\text{CuIn}_x\text{Ga}_{1-x}\text{Se}_2$  solar cells made from  $(\text{In}_x\text{Ga}_{1-x})\text{Se}_3$  precursor films. *Applied Physics Letter*. 65(2): pg. 198.
- Green, M., Emery, K., Bucher, K., King, D. L., and Igari, S. (1999). Solar cell efficiency tables (Version 13), *Progress in Photovoltaic Research Applications*, 7: 31.
- Goetzberger, A., and Hebling, C. (2000). Photovoltaic materials, past, present, future. *Solar Energy Materials and Solar Cells*, 62:1-19.
- Haug, F. J., Rudmann, D., Pomev, A., Zogy, H. and Tiwan, A.N. (2003). Electrical properties of the heterojunction in  $\text{Cu}(\text{In,Ga})\text{Se}_2$  superstrate solar cells. *Proceedings of 3<sup>rd</sup> world conference in photovoltaic solar energy conversion, Osaka*.
- Ishida, T., Katagiri, H., Ihigaki, N., and Saito, K. (2001). Characterization of  $\text{Cu}_2\text{ZnSnS}_4$  thin films prepared by vapor phase sulfurization. *Japanese Journal of Applied Physics*. 40: 500–504.
- Ito, K., and Nakazawa, T. (1988). Electrical and optical properties of stannite-type quaternary semiconductor thin films, *Japanese Journal of Applied Physics*. 27: 2094.
- Ito, K., and Nakazawa, T. (1989). Stannite type photovoltaic thin film, *Proceedings of the 4th International Conference of Photovoltaic Science and Engineering, Sydney*, 341pp.
- Jimbo, K., Kimura, R., Kamimura, T., Yamada, S., Maw, W. S., Araki, H., Oishi, K., Katagiri, H. (2007).  $\text{Cu}_2\text{ZnSnS}_4$  type thin film solar cells using abundant materials. *Thin Solid Films*. 515(15): 5997 –5999.

- Katagiri, H., Sasaguchi, N., Hando, S., Hoshino, S., Ohashi, J., and Yokota, T. (1996). *Technical digest of the 9th International Conference of Photovoltaic Science and Engineering, Miyazaki*, 745pp.
- Katagiri, H., Saito, K., Washio, T., Shinohara, H., Kurumadani, T., and Miyajima, S. (2001). Development of thin film solar cell based on  $\text{Cu}_2\text{ZnSnS}_4$  thin films. *Solar Energy Materials & Solar Cells*. 65:141–148.
- Katagiri, H., Ihigaki, N., Ishida, T., and Saito, K. (2001). Characterization of  $\text{Cu}_2\text{ZnSnS}_4$  thin films prepared by vapour phase sulfurization. *Japanese Journal of Applied Physics*. 40:500-504.
- Kelsi, B., Charles, V. S. and Adam, V. (2013). Hydropower: federal and nonfederal investment. *Bulletin on USA Congressional Research Service*.
- Kireev, P. S. (1977). Semiconductor physics (roum.). *Scientific and Encyclopedic Publishing House, Bucharest*. 706pp.
- Kunihiko, T., Masatoshi, N., and Hisao, U. (2009).  $\text{Cu}_2\text{ZnSnS}_4$  thin film solar cells prepared by non-vacuum processing. *Solar Energy Materials & Solar Cells*. 93:583– 587.
- Kylner, A. (1999). Effects of impurities in the CdS buffer layer on the performance of  $\text{Cu}(\text{In,Ga})\text{Se}_2$ . *Journal of Applied Physics*. 85: 6858-6865.
- Madara'sz, J., Bombicz, P., Okuya, M., Kaneko, S. (2001). Thermal decomposition of thiourea Complexes of  $\text{Cu}(\text{I}),\text{Zn}(\text{II})$  and  $\text{Sn}(\text{II})$ chlorides as precursors for the spray pyrolysis Deposition of sulfide thin films. *Solid State Ionics*. 141–142: 439–446.
- Moritake, N., Fukui, Y., Oonuki, M., Tanaka, K., and Uchiki, H. (2009). Preparation of  $\text{Cu}_2\text{ZnSnS}_4$  thin film solar cells under non-vacuum condition, *Physica Status Solidi C*. 6:1233-1236.
- Moriya, K., Tanaka, K., and Uchiki, H. (2005). Characterization of  $\text{Cu}_2\text{ZnSnS}_4$  thin films prepared by photo-chemical deposition, *Japanese Journal of Applied Physics*. 44:715.
- Moriya, K., Watabe, J., Tanaka, K., and Uchiki, H. (2006). Characterization of  $\text{Cu}_2\text{ZnSnS}_4$  thin films prepared by photo-chemical deposition. *Physica Status Solidi (C)* 3:2848–2852.



- Mcveigh, J., Bertraw, D., Darmstadter, J., Palmer, K. (2000). Winner, loser, or innocent victim? Has renewable energy performed as expected? *Solar Energy*. 68(3):237-255.
- Nathan S., (2009). An excerpt from “Design is the problem”, published by Rosenfeld Media.
- Nakayama, N., and Ito, K. (1996). Sprayed films of stannite  $\text{Cu}_2\text{ZnSnS}_4$ . *Applied Surface Science*. 92:171–175.
- Neaman, D. A. (2003). Semiconductor physics and devices. *McGraw-Hill Publishers*, 297pp.
- Neuberger, F. (2009). Module power evaluation report. Retrieved June 24, 2013 from <http://www.schott solar.com/global/solar-yield/long-term-study/>.
- Nozik, A. J. (2005). Exciton multiplication and relaxation dynamics in quantum dots: Application to Ultrahigh-Efficiency Solar Photon Conversion. *Inorg. Chem.* 44, 6893.
- Pankove J. I. (1971). Optical processes in semiconductors. *Dover Publication, Inc.*, p35.
- Pillai, S. O. (2010). Solid state physics. *New Age International Publishers*, 590pp.
- Qin Miao, C., Xiao, M.D., Zhen, Q. L., Shu, Y. C., and Song, L. Z. (2011). Preparation of CZTS film by printing process for low-cost solar cell. *Advanced Materials Research*. (335-336): 1406-1411.
- Romeo A., Terheggen M., Abou-Ras D., Batzner D. L., Haug F. J., Ka'lin, M., Rudmann, D., and Tiwar,i A. N. (2004). Development of Thin-film  $\text{Cu}(\text{In,Ga})\text{Se}_2$  and  $\text{CdTe}$  Solar Cells. *Progress in Photovoltaic: Research and Applications*. (12) 93-111.
- Saitoh, K., Katagiri, H., Washio, T., Shinohara, H., Kurumadani, T., and Miyajima, S. (1999). *Technical Digest of the 11th International Photovoltaic Science and Engineering Conference, Sappor*, 647pp.
- Sambo, A. S., (2008). National Workshop on the Participation of State Governments in the Power Sector: Matching Supply with Demand, Paper presented at the Ladi Kwali Hall, Sheraton Hotel and Towers, Abuja.
- Sanap, V.B. and Pawar, B.H. (2009). “Growth and characterization of nanostructured  $\text{CdS}$  thin films by chemical bath deposition technique. *Chalcogenide letters*. 6(8):415-419.
- Shadia, J., Ikhmayies and Ahmad-Bitar, R.N. (2010). Characterisation of the  $\text{SnO}_2:\text{F}/\text{CdS}:\text{In}$  structures prepared by the spray pyrolysis technique. *Solar Energy Materials & Solar Cells*. 94: 878–883.

- Schmid, D., Ruckh, M., and Schock, H. W. (1996). A comprehensive characterization of the interfaces in Mo/CIS/CdS/ZnO solar cell structures. *Solar Energy Materials and Solar Cells*. (41-42):281–294.
- Seol, J. S., Lee, S. Y., Lee, J. C., Nam, H. D., and Kim, K. H. (2003). Electrical and optical properties of  $\text{Cu}_2\text{ZnSnS}_4$  thin films prepared by rf- magnetron sputtering process, *Solar Energy Materials and Solar Cells*. 75:155.
- Sheel, D. W., Yates, H. M., Evans, P., Dagkaldiran, V., Gordijn, A., Finger, F., Remes, Z., and Vanecek, M. (2009). Atmospheric pressure chemical vapour deposition of F doped  $\text{SnO}_2$  for optimum performance solar cells. *Thin Solid Films*. 517: 3061.
- Shell renewable energy information brochure (1997).
- Shockley, W. and Queisser, H. J. (1961). Detailed balance limit of efficiency of p-n. junction Solar Cells. *Journal of Applied Physics*. 32, pp. 510-519.
- Silverman T.J., Michael G. D., Bill M., Sam C., Brendan K., and Sarah K. (2013). Thin film photovoltaic. *Proceedings of the 39<sup>th</sup> IEEE Photovoltaic Specialist Conference*, 520pp.
- Sweet, W. (2001). Restructuring the thin-stretched grid. *Article on the Electric Power Research Institute*. pp 43-49.
- Sze, S. M. (1981). *Physics of Semiconductor Devices*, Wiley Eastern Limited, 211pp.
- Su-Huai, Z. W., Alex, S. B., and Zunger. (1999). Effects of Na on the electrical and structural properties of  $\text{CuInSe}_2$ . *Journal of Applied Physics*. 85:7214-7218.
- Tanaka, K., Moritake, N., and Uchiki, H. (2007). Preparation of  $\text{Cu}_2\text{ZnSnS}_4$  thin films by sulphurizing sol-gel deposited precursors. *Solar Energy Materials and Solar Cells*. 91:1199–1201.
- Tanaka, T., Kawasaki, D., Nishio, M., Guo, Q., and Ogawa, H. (2006). Fabrication of  $\text{Cu}_2\text{ZnSnS}_4$  thin films by co-evaporation, *Physica Status Solidi*. C3:2844-2847.
- Tooru, T., Akihiro, Y., Daisuke, S., Katsuhiko, S., Qixin, G., Mitsuhiro, N., and Toshiyuki, Y. (2010). Influence of composition ratio on properties of  $\text{Cu}_2\text{ZnSnS}_4$  thin films fabricated by co-evaporation. *Thin Solid Films*. Retrieved on the 17 January, 2011 from doi:10.1016/j.tsf.2010.03.026.

- Tsuchida, K., Katagiri, H., Jimbo, K., and Moriya, K. (2003). Solar cells without environmental pollution by using CZTS film, *Proceedings of the 3<sup>rd</sup> World Conference on Photovoltaic Solar Energy Conversion, Osaka*, 2874pp.
- Tsukagoshi, T., Chiba, Y., Miyazaki, H., Wada, T., Yamada, A., and Konagai, M. (2006). Grain size enlargement of CuInGaSe<sub>2</sub> thin films by hot filament melting process, *Physica Status Solidi*. A203:2559–2563.
- Tsur, Y., and Zemel, A., (2000). Long-term perspective on the development of solar energy. *Solar Energy*. 68(5):379-392.
- Prabhakar, T., and Jampana, N. (2010). Effect of Na diffusion on the structural and electrical properties of CZTS thin films. *Solar Energy Materials and Solar Cells*. 95, 1001-1004.
- Zdenek, R., Vanecek, M., Yates, H. M., Evans, P. and Sheel, D.W. (2009). Optical properties of SnO<sub>2</sub>:F films deposited by APCVD, *Thin Solid Films*, 517:6287-6289.
- Zihua, Z., Yanyan, W., Dong, X., and Yafei, Z. (2010). Fabrication of Cu<sub>2</sub>ZnSnS<sub>4</sub> screen printed layers for solar cells, *Solar Energy Materials and Solar Cells*. 94:2042-2045.

**APPENDIX A**  
**(PUBLICATIONS)**

UNIVERSITY OF IBADAN LIBRARY

UNIVERSITY OF IBADAN LIBRARY